THE PROCEEDINGS OF
THE PHYSICAL SOCIETY
Section B

VOL. 63, PART 8 1 August 1950 No. 368 B

New Localized Multiple-Beam Interference Fringes formed with Curved Thin Sheets

BY S. TOLANSKY AND N. BARAKAT
Royal Holloway College, University of London

MS. received 25th October 1949, and in amended form 7th February 1950

ABSTRACT. A description is given of the mode of formation and optical properties of some new sharp localized multiple-beam fringes produced by cylindrically curved thin sheets which are silvered upon both sides. Illumination with strictly parallel monochromatic light leads to sharp line fringes lying in a plane passing through the centre of curvature and perpendicular to the direction of incidence. An approximate theory is developed and checked by observation. The use of mica as the film leads to interesting birefringent doubling effects. These are complicated by differential phase change effects occurring on reflection at the silver surfaces. Fringe systems have been examined both in reflection and in transmission and related systems obtained with white light used together with a spectrograph. Cleavage step phenomena are revealed by the mica with high precision and high dispersion. It is proposed to name the monochromatic system ' fringes of equal tangential inclination '.

§1. ORIGIN OF THE FRINGES

In this paper a description is given of the mode of formation and general properties of some new localized multiple-beam interference fringes which are formed by thin sheets of parallel-sided transparent material silvered on both sides and then bent into cylindrical curvature.

A suitable material is a thin cleavage sheet of muscovite mica, and since the use of such material leads in addition to some interesting complex birefringent effects, most of the experiments reported here have been made with varieties of mica.

The fringes in their simplest form are produced in transmission with monochromatic light, but variants, such as reflection fringes and white light modifications both in transmission and in reflection, have also been studied. The selected thin sheet of material is coated on both sides with high reflectivity silverings of the type generally adopted for multiple-beam interferometry (Tolansky 1948 a) and viewed with the simple optical arrangement shown in Figure 1. S is the source, C a condenser and F a filter.

A parallel beam of monochromatic light is incident on the convex face of the mica. Related but different effects result if mica is turned so that the light falls on the concave face. A suitable thickness, t, of mica is some 1/50 mm. and a suitable cylindrical curvature has a radius, R, of perhaps 2 cm. Fringes can also be obtained over relatively wide ranges of both t and R. An example taken with the green mercury line is shown in Plate I (a).

The origin of formation of the fringes is shown by Figure 2, where for simplicity refraction effects within the interference film have been disregarded. To a close approximation both faces can be considered to have the same radius of curvature. Parallel incident light at any specific point A is incident on the film at an angle θ which is determined by the distance XY above the axis of symmetry XO. Providing t is small compared with R (in the case quoted the ratio is 1 : 1,000) then for any particular incident ray, YA, the successive multiple reflections meet at a point M and there interfere. This can be demonstrated either by ray tracing or by calculation. If θ, R and t are such that the optical path difference between successive beams (including phase change effects) is an integral number of waves $n\lambda$, then reinforcement occurs at M and a bright fringe results. Clearly at a further distance from XO there is another ray with a suitable angle of incidence leading to another fringe with path difference $(n-1)\lambda$. Hence a succession of localized fringes form and owing to the multiple-beam effect these are very sharp.

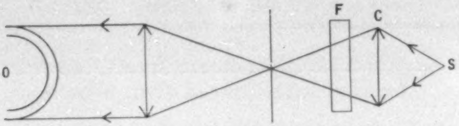

Figure 1.

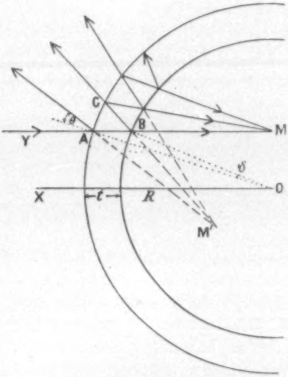

Figure 2.

In this introductory report in which it is intended to survey the subject only, a simplified geometrical theory will be developed, justifiable approximations being used, and in a later communication the theory will be treated fully and applications to birefringent films examined critically. A preliminary notice has already been communicated elsewhere (Tolansky and Barakat 1948).

§ 2. FRINGE LOCALIZATION

It is readily demonstrated by the following simple geometrical construction that to a close approximation, when t is small, successive fringes are localized on a plane passing through O, the centre of curvature, and perpendicular to the symmetry axis XO. From Figure 2 it follows that

$$\mathrm{BM}=\mathrm{BC}\frac{\sin 2\theta}{\sin 2\delta}; \qquad \mathrm{BC}=\mathrm{AB}=R\frac{\sin\delta}{\sin\theta};$$

therefore

$$\mathrm{BM}=R\frac{\cos\theta}{\cos\delta}.$$

Since the angle δ is very small, BM is approximately equal to $R\cos\theta$ and the angle OMB is very nearly $\frac{1}{2}\pi$. Thus the locus of the point M for various angles of incidence is the straight line passing through the centre of curvature O at right angles to the axis XO.

It may be pointed out that the strict condition of incident parallel light, with resulting plane localization, extreme sharpness and linear shape, makes the fringes described here completely different from the broad, non-localized fringes of shape varying with the observer's position, found with unsilvered curved mica plates by Raman and Rajagopalan (1939). The source we have used is a pinhole of diameter $\frac{1}{2}$ mm. at the focus of well-corrected lens of focal length 15 cm. and diameter 6 cm.

If chromatic dispersion effects be disregarded then to a close approximation the condition of interference is controlled by the relation $n\lambda=2\mu t\cos\theta$. Strictly speaking this should be replaced by the modified refraction expression which holds for either a Fabry–Perot with a dispersing medium or for a Lummer plate. This more exact treatment leads to corrections of but a few per cent. Furthermore, a detailed analysis shows that one should write $n\lambda=2\mu t\cos\theta+\Delta$ in which Δ is a correcting term which is primarily a function of θ and δ where δ is the small angle between the radii for successively reflected rays (see Figure 2), but this too can be shown to be a secondary matter.

Measurement shows that up to angles of 60° the fringes are critically localized in the predicted plane, but beyond this up to the limiting 90° value there are slight deviations. The following table shows a comparison between the predicted linear localization and that observed for a particular mica sample with $t=1/50$ mm., $\mu=1{\cdot}59$ and θ in the neighbourhood of 30°. The value of R was varied and the distance between the film surface and fringe localization measured. All figures are in centimetres.

R	Localization	
	Predicted	Observed
1·5	1·30	1·32
2	1·73	1·68
3	2·60	2·60
4	3·46	3·4
5	4·33	4·2

The observed localizations agree with prediction to within a fraction of a millimetre. The larger the R value the broader is the fringe and then some small experimental uncertainty in localization arises.

§ 3. PROPERTIES OF THE FRINGES

The fringes obtained with a selected piece of high quality muscovite are shown in Plate I (*a*). Attention may be drawn to the following features: (i) the fringes are sharply localized in the predicted plane; (ii) they are very narrow, the outer orders becoming progressively sharper; (iii) successive orders clearly follow some simple geometrical law of separation; (iv) the fringes are double and the doubling exhibits an unexpected variation with order. These features will now be discussed in turn, the consideration of the doubling being left until later.

(i) The localization in the predicted plane is as exact as can be measured with a microscope having a small depth of focus.

(ii) A striking characteristic is the unusual sharpness of the fringes for a given silvering. The reason lies in the increased reflectivity resulting from the large values of the angles of incidence θ which vary over the whole range from 0 to 90°. It is this increase in θ which is directly responsible for the marked sharpening up of the outer orders by producing high effective Fresnel reflecting coefficients at the metallic surfaces. To appreciate the sharpness fully one must focus on the true surface of localization, not on the approximate plane. It will be shown later that the two components are plane polarized mutually perpendicularly, hence the doublets can be made to appear as single fringes with a polarizing device. Figure 3 shows a microphotometer trace across a sequence of single fringes. The outer orders are not only sharper, but fall off in intensity too. This is due to several causes, the major ones being the rapid increase in absorption by the silver films and by the mica itself with increase in θ.

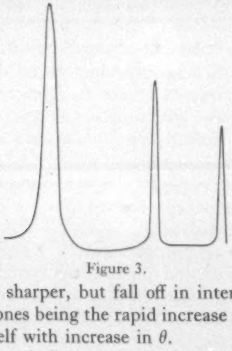

Figure 3.

(iii) It will suffice here to indicate a simple derivation of the fringe separation law for successive orders, dispersion effects being disregarded.

The order of interference, n_0, at the centre of the system is a maximum and is given by $n_0\lambda = 2\mu t$. Consider a symmetrical system with fringes on either side of the axis XO, then the distance between a pair of symmetrically situated fringes on either side of this axis will be called 2ρ, the 'diameter' of the fringes. If n is the order of interference for the pth fringe, counting from the centre outwards, then by analogy from the well-known corresponding Fabry–Perot theory one obtains the following: Refraction can no longer be disregarded. Let r be the angle of refraction within the film; then as $n_0 = 2\mu t/\lambda$, the order of interference at the centre, the order n for the refracting angle is $n = n_0 \cos r$; $\sin\theta = \rho/R$ so that

$$\frac{n}{n_0} = \left[1 - \frac{\rho^2}{\mu^2 R^2}\right]^{1/2}.$$

PROC. PHYS. SOC. VOL. 63, PT. 8—B (S. TOLANSKY AND N. BARAKAT)

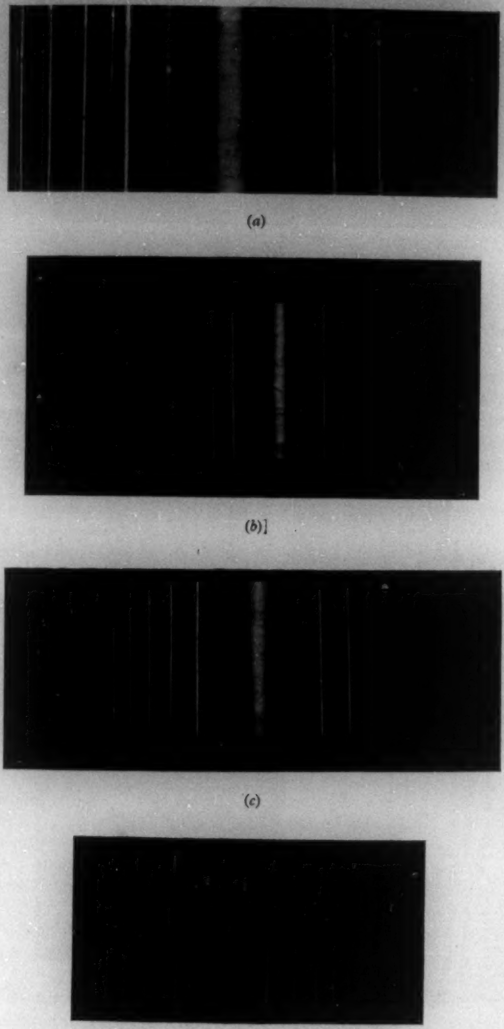

(a)

(b)]

(c)

(d)

PLATE I.

To face page 548

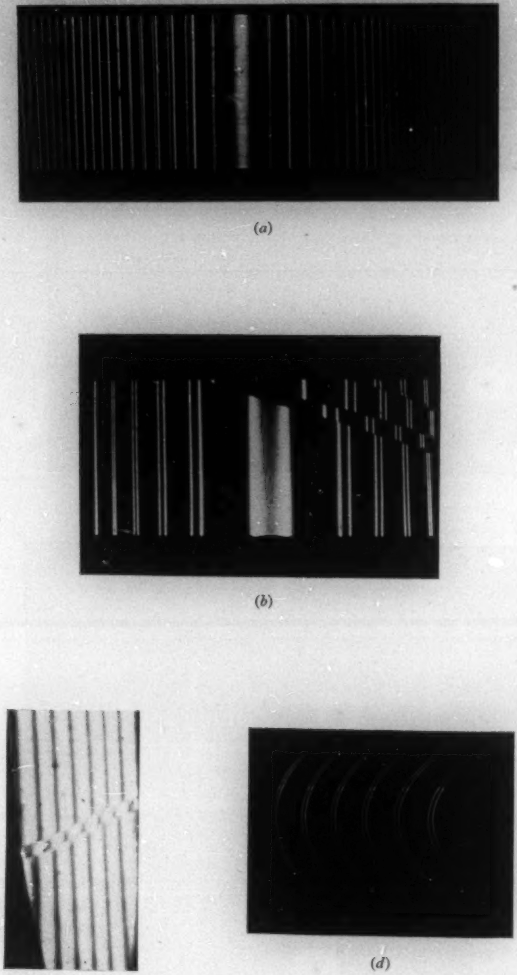

(a)

(b)

(c)

(d)

PLATE II.

In general the order of interference n_0 at the centre will be non-integral; let it therefore be written $n_0 = n_1 + \epsilon$, where ϵ is a fraction and n_1 the order of the first fringe. The order of the pth fringe will thus be $n = n_0 - (p + \epsilon - 1)$.

Hence

$$\left(1 - \frac{p + \epsilon - 1}{n_0}\right)^2 = 1 - \frac{\rho^2}{\mu^2 R^2}.$$

As p is small compared with n_0, then sufficiently closely

$$\frac{2}{n_0}(p + \epsilon - 1) = \frac{\rho^2}{\mu^2 R^2}$$

giving

$$\rho = R\left[\frac{\mu\lambda}{t}(p + \epsilon - 1)\right]^{1/2}.$$

The scale of the fringe pattern is therefore directly proportional to R and inversely proportional to $t^{1/2}$.

This formula has been confirmed by measurement and shown to hold closely. Plates I (*b*) and I(*c*) illustrate the fringes given by a piece of mica acting as isotropic in which R has the respective values 1·5 and 2 cm. By assuming for simplicity that n_0 is integral (i.e. $\epsilon = 0$) the scale of the pattern can be readily calculated. Thus for example for $R = 5$ cm. and $t = 1/50$ mm. the diameter of the fifth fringe ($\lambda = 5460$ A.) is almost exactly 4 cm.

The fringes are therefore very easy to see with the naked eye if they are allowed to fall on a ground-glass screen placed in the plane of localization. They can of course be projected and enlarged if so required for demonstration purposes.

§ 4. NOMENCLATURE

It is clear that these fringes are intimately related to the two classical types of multiple-beam interference fringes, namely fringes of *equal thickness* and fringes of *equal inclination*; it is desirable to classify them so as to retain this relationship, and several such methods of classification could reasonably be adopted.

Since one way of regarding them is the recognition of the fact that each fringe is formed as the locus of rays which on entering the system make the same angle of inclination with the tangent at the point of entry, we propose that these fringes be called 'fringes of *equal tangential inclination*'.

This terminology fits all cases and if, for example, a spherical shell replaces the cylindrical film (e.g. a blown thin curved film of glass of uniform thickness) then ring-shaped localized fringes arise, since the equal tangential loci then lie on rings.

The relationship to fringes of equal inclination is clear, for the fringes under discussion move off to infinity and become identical with fringes of equal inclination when R becomes infinite, i.e. when the sheet is *plane* parallel.

§ 5. CLEAVAGE EFFECTS

The use of mica as the material leads to an interesting application linked with the cleavage properties: it has already been established that mica sheets usually cleave in steps which are integral multiples of the crystal lattice spacing (20 A.). If the selected mica exhibits cleavage steps the result on flexing is the production of fringes as shown in Plate I (*d*) in which the cleavage discontinuities are immediately evident. For let the mica thickness in a given region suffer an increment dt due to a cleavage step. Then near the centre of the system

$dt = (\lambda/2\mu)\,dn$, where dn is the fractional change of order produced by the step dt at a certain angle of incidence. With monochromatic light the direction of displacement and any integers of fringe overlapping cannot be easily decided, but if several distinct wavelengths are used the direction and exact number of orders can both be determined.

It is clear that the fringes offer a new precision method for the measurement of cleavage steps because a change of a whole order ($dn = 1$) requires a change of thickness of $\lambda/2\mu\cos r$, i.e. about 1700 A. near the centre (in the green). Since the fringe sharpness permits the detection of one-hundredth of an order displacement, then steps of 17 A. can be detected.

This property does not depend on the absolute value of t except in so far as the latter affects the whole scale. This is a marked advantage over the fringes of equal chromatic order. Attention is drawn to the possibility of applying this technique to the study of small steps in thin films, such as, for example, organic films, or metal films deposited on a base such as mica.

Particularly valuable features in this connection are: (*a*) the high fringe dispersion available without any costly auxiliary equipment and (*b*) the flexibility in dispersion which is controllable by varying R. The latter can be adapted to the value of t. For example sharp fringes have been obtained with a thin film of MgF_2 less than a light wavelength thick, deposited by evaporation between two silver films.

§ 6. DIFFERENTIAL PHASE CHANGE EFFECT

It has been shown in former studies (Tolansky 1948 b) that when the localized multiple-beam fringes given by an air wedge are formed with non-normal incidence, the fringes split into doublets, the two components being plane polarized mutually perpendicularly. Both become sharper with increasing incidence but one much more rapidly than the other, and at the same time the sharper fringe weakens rapidly relative to its slightly broader companion. It has been fully established that this is due to the differential phase change which takes place when mutually perpendicular vibrations of light are reflected at non-normal incidence from a metal, and is in fact the same effect that leads to the elliptic polarization of such reflected light.

Because of the severe bending of the silvered mica sheet, considerable angles of incidence are involved and thus inevitably the outer orders must show the differential phase change doubling. This is an effect which increases at such a rate that it becomes perceptible at $\theta = 25°$ and increases to about half an order for higher values of θ.

§ 7. BIREFRINGENCE DOUBLING

When using muscovite mica interesting complex effects arising from the biaxial crystal make their appearance, as for example in Plate II (*a*). The fringes are double, mutually perpendicularly plane polarized. This fringe doubling diminishes to a small value as the order increases and then begins to increase once more. Over the whole range the outer component becomes progressively sharper and weaker and then effectively vanishes. A further example, Plate II (*b*) shows a piece of mica which exhibits both the complex doubling and also marked cleavage steps. In the discussion that follows it will be seen that the observations are completely accounted for in that they represent a combination of birefringent doubling due to the crystal, on which is superposed differential change doubling due to the silver.

In general the splitting of any incident ray by the crystal into two mutually perpendicularly polarized rays travelling with different velocities leads to two systems of interference fringes. Leaving out for the moment the phase change effect, then the separation between any pair of members belonging to the two systems, but of the same order of interference, is due to the difference in the refractive indices of the two vibrations. Thus for a biaxial crystal there will be two directions in which the difference in refractive indices is zero. These are in the neighbourhood of the positions indicated on Plate II (*a*) where the separation is reduced to a minimum. It is obvious that the actual angular location of the zero positions within the fringe system are decided by the direction of flexure of cylindrical curvature. Plate II (*a*) refers to a specimen bent along the direction of intersection of the optical axial plane with the cleavage plane.

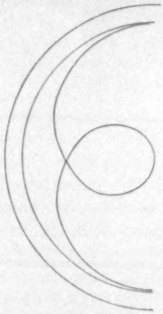

Figure 4.

Thus the angular separation between the two positions of minimum separation will give double the apparent optic angle of the mica if the differential change of phase at reflection mica–silver is allowed for. Measurements show this to be in fact the case, but will be reserved for the later more detailed discussion on birefringence.

§ 8. THE REFLECTED SYSTEM

As in all multiple-beam interference phenomena the transmitted fringes have an associated ‘complementary’ reflected system in which the fringes appear as fine dark lines on a bright broad background. However, the fringes under discussion are unique in that the localization of the reflected system is different in type from that of the transmitted system. Figure 2 shows that the reflected fringes which form are virtual arising from diverging beams and appear to be localized in a different position from the transmitted system. Figure 4 shows the localization derived from ray tracing. Because of the shape of the surface of localization it is difficult experimentally to confirm this localization with the exactness possible for the transmitted system.

It is of interest to note that reasonably sharp fringes can be obtained in reflection *without* silvering owing to the high Fresnel reflecting coefficients of the uncoated mica consequent on the high angles involved; Plate II (*c*) is an example. The fringes are relatively sharp for a 'two-beam' interference phenomenon. Actually of course there must be several effective beams to each fringe.

§ 9. FRINGES OF EQUAL CHROMATIC ORDER

In conclusion a brief indication will be given of the possibilities of investigation opened up by a study of the associated phenomena using white light, thus producing fringes analogous to the white light fringes of equal chromatic order. The system is illuminated with parallel white light and an image of the plane of localization projected on to the slit of the spectrograph. A typical result is shown in Plate II (*d*) in which a doubly silvered mica sheet was used. This shows the birefringence of the fringes which has several advantages over the monochromatic system. Any existing chromatic variations can be obtained over a more extensive wavelength range from a single photograph. More useful still is the ease with which order allocations can be made and the angular positions of intersections of the birefringence components established. In the case of the monochromatic fringes this may require a series of observations with different wavelengths if ambiguities are to be avoided; the white light fringes supplying inherently a continuous number of wavelengths do not suffer from this defect.

§ 10. OTHER APPLICATIONS

The experiments described here have been made with muscovite mica but there are many other distinct possibilities. Already some preliminary studies have been made on thin evaporated magnesium fluoride films. When uniform thin films of such materials are used as interference films the Fizeau fringe system is simply a field of uniform tint and this is the basis of interferometric colour filters. Thus it is difficult to obtain any numerical information from any local tint variations of such a film arising from changes in thickness, and furthermore, a determination of the thickness itself is a difficult matter unless the film growth from zero thickness has been observed. If such a thin film is built up on silvered mica, and then again silvered, flexing leads to the localized fringes even if the thickness of the film is appreciably less than half a light wavelength. With such a film we have obtained both excellent monochromatic and white light fringes, and in view of the sensitivity of fringe position to thickness, this result offers a further means of studying such films.

Another possible field of application is to the study of the organic layers which it is possible to put down on a silvered mica surface.

Since the fringes can be formed in reflection it should be possible to apply the technique to the examination of the surfaces of metallic foils either by coating these with a thick transparent film, which is then silvered, or alternatively, by pressing into contact with a silvered glass cylinder. It is of course certain that t will vary considerably in the latter case, hence we are already exploring the nature of the fringes formed by flexion of slightly wedged film instead of a parallel-sided film.

REFERENCES

Raman, C. V., and Rajagopalan, V. S., 1939, *J. Opt. Soc. Amer.*, **29**, 413.

Tolansky, S., 1948 a, *Multiple-beam Interferometry of Surfaces and Films* (Oxford: Clarendon Press), p. 26; 1948 b, *Ibid.*, p. 38.

Tolansky, S., and Barakat, N., 1948, *Nature, Lond.*, **162**, 816.

The Monocentric Schmidt–Cassegrain Cameras

By P. A. WAYMAN
The Observatory, Cambridge University

MS. received 23rd September 1949

ABSTRACT. Formulae are obtained for the leading coefficents in the plate-profile expansion of the monocentric Schmidt–Cassegrain cameras. These are used to derive expressions for the monochromatic and chromatic aberrations of the general monocentric system, and spot-diagrams are included to illustrate the image quality in a typical case. A comparison is made with an ordinary Schmidt camera, which has the same aperture and the same depth of figuring on the aspheric plate.

---

§ 1. INTRODUCTION

In the classical Schmidt camera the focal length is never more than half the total tube-length, and in large astronomical systems this will increase the cost of mounting and dome. Among other advantages, more compactness is obtained by the use of a convex secondary mirror, as was originally suggested by Baker (1940) and Burch (1942), to form the so-called Schmidt–Cassegrain systems. Linfoot (1944) has carried out a general discussion of such systems, either aplanats or anastigmats, and with flat or curved field-surfaces, using the method of plate-diagram analysis.

In a practical design the best results may be obtained by retaining or introducing small controlled amounts of Seidel error in order to balance the higher aberrations. This balance can be made experimentally with the help of suitable optical tests or can be predicted by extensive ray-tracing. In any case a knowledge of the higher aberrations of the unbalanced design in a general analytical form is a valuable pointer towards the selection of a particular type of Schmidt system.

An expression for the leading aberrations of the ordinary Schmidt camera can be obtained explicitly in a relatively simple way by a method originally due to Carathéodory (1940).* Use is made of the fact that the mirror and the field-surface are parts of concentric spheres whose centre in the case when the aspheric surface of the corrector plate is turned towards the mirror is the pole of that surface. The angular aberrations are then, to a first approximation, the same as the deviations from parallelism of a pencil of rays issuing from a point of the image surface, after reflection at the mirror and refraction at the corrector plate. These deviations can be calculated if assumptions are made of axial stigmatism in the light of a particular wavelength and of the monocentric property of mirror and field-surface about the pole of the aspheric surface.

A corresponding procedure cannot be adopted for the general Schmidt–Cassegrain system because the simplifying condition of concentric mirrors and field-surface no longer exists. The special case of the monocentric Schmidt–Cassegrain cameras can however be dealt with in an analogous way because here the two spherical mirrors have a common centre through which the aspheric surface of the corrector plate passes (see Figure 3). The field-surface, which, if it is to be fully accessible, must lie well behind the front surface of the primary mirror, is a sphere of radius equal to the focal length of the system and is concentric with the mirrors. The ratio of the radii of the two mirrors is, in practice, limited to a rather small range by consideration on the one hand of accessibility of image-surface and on the other of the obstruction which the secondary mirror causes to pencils entering the system.

---

* Linfoot (1949) has developed this method fully in an elegant and comprehensive treatment of the classical Schmidt camera.

In § 2 the equation of the plate-profile is obtained in the form of a power series in r, the zonal radius in the aperture. This expansion is carried up to the sixth-power terms, which is far enough to give a high degree of axial stigmatism, and in § 3 use is made of the leading terms of this expansion to obtain an expression for the monochromatic and chromatic aberrations of the system. In § 4 spot diagrams of the image points are given for an f/3·5 system covering a five-degree field in light of different wavelengths. In addition, a comparison is made with an ordinary Schmidt camera which, using the same aperture diameter but different focal ratio, would produce the same image spreads, measured in seconds of arc.

§ 2. THE PLATE-PROFILE EXPANSION

Following the notation of the previous papers, we choose as our unit of length the radius of the primary mirror R and denote by ξ the ratio of the radius of the secondary mirror to that of the primary. Thus, if f_1, f_2 denote the paraxial focal lengths of the primary and secondary mirrors respectively,

$$f_1=\tfrac{1}{2},\quad f_2=\xi/2 \quad \text{with} \quad R=1.$$

We write $\mu=H/R$ where H is the radius of the aperture stop, and suppose that μ^2 is small compared with unity. For example, in the case of an f/3·5 system $\mu^2=1/36$, very nearly. Consequently the occurrence of an error-factor $[1+\mathrm{O}(\mu^2)]$ in an equation implies an inaccuracy of only a few per cent.

If we set up coordinate axes (x, y) with centre C (Figure 1) in the aperture stop and write $x^2+y^2=H^2r^2$, then r denotes any zone-radius in the aperture and runs from O at the centre to 1 at the marginal zone.

Then if $T(r)\equiv T(x,y)$ denotes the plate thickness we can write the profile of the corrector plate in the form,

$$S(r)=\frac{T(r)-T(0)}{R}=a_1\mu^2r^2+a_2\mu^4r^4+a_3\mu^6r^6+\mathrm{O}(\mu^8). \qquad \ldots\ldots(1)$$

If, in (1), we take $a_1=0$, a_2 and a_3 can still be chosen to give a plate which produces axial stigmatism in the light of one wavelength to the same degree of approximation. This first term in the expansion is introduced in order that the steepest plate slope occurring over the aperture may be reduced. This facilitates figuring, and in practice a_1 may be chosen to lessen both monochromatic and chromatic aberrations. Because of this term the plate possesses a positive paraxial focal length f_p given by

$$f_p=-\frac{1}{2(n_0-1)}\cdot\frac{1}{a_1}, \qquad \ldots\ldots(2)$$

where n_0 is the refractive index of the corrector plate.

In the equation of the plate profile the steepest plate slope can be minimized by equating the slope at the marginal zone to the maximum slope occurring over the rest of the aperture. In between there is a ‘neutral zone’ whose radius will be denoted by $r=r_0$, at which the plate slope is zero and through which the rays pass undeflected.

In Figure 1 a ray QP_1 parallel to the axis of the system is shown to pass through the neutral zone at Q and, after reflection at the two mirrors, to cut the axis in F. If, using Gaussian optics, we image F backwards through the system to infinity by adjusting f_p, we can find a relation between f_p and r_0 which expresses the fact that F is then the paraxial focus of the system.

In Figure 1

$$\sin\theta_0 = \mu r_0/R = \mu r_0 \qquad \ldots\ldots(3)$$

and

$$CL = \mu r_0 \operatorname{cosec} 2\theta_0 \quad \text{and} \quad CP_2 = \xi.$$

Therefore, from the triangle CLP_2,

$$\frac{\sin\psi_0}{\sin 2\theta_0} = \frac{\mu r_0 \operatorname{cosec} 2\theta_0}{\xi},$$

so that

$$\sin\psi_0 = \mu r_0/\xi. \qquad \ldots\ldots(4)$$

An application of the sine rule to triangle CFP_2 gives $CF = \xi \sin\psi_0/\sin 2(\psi_0-\theta_0)$, and thus

$$BF = \xi[\sin\psi_0/\sin 2(\psi_0-\theta_0)] - \xi. \qquad \ldots\ldots(5)$$

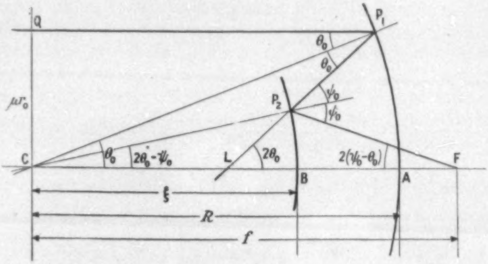

Figure 1.
The radius, R=AC, of the primary mirror is taken as unit of length.

If now we find G, the Gaussian image of F after reflection at the two mirrors, by making $f_p = 1 + AG$, we image G through the corrector plate paraxially to infinity. Using (5) we obtain

$$\frac{1}{f_p} = 2\frac{\xi-1}{\xi} + \frac{1}{\xi}\,\frac{\sin 2(\psi_0-\theta_0)}{\sin\psi_0}. \qquad \ldots\ldots(6)$$

ψ_0 and θ_0 are directly related to r_0 by (3) and (4), and so we may write (6) as

$$\frac{1}{f_p} = A(r_0). \qquad \ldots\ldots(7)$$

Equations (2) and (7) relate a_1 and r_0. We now obtain two more equations involving a_1, a_2, a_3 and r_0, enabling us to find expressions for these three plate-profile coefficients in terms of the parameter r_0 of the neutral zone.

We make use of the two following facts to obtain the required equations: (*a*) that the plate slope vanishes at $r = r_0$; (*b*) that under perfect axial stigmatism the optical paths from a wave-front entering the system to the focus is the same along the axial ray and along the ray through the neutral zone.

Because of (*a*) we have, by differentiating (1),

$$2a_1\mu^2 r_0 + 4a_2\mu^4 r_0^3 + 6a_3\mu^6 r_0^5 = \mathrm{O}(\mu^8)$$

or

$$2a_2\mu^4 r_0^4 + 3a_3\mu^6 r_0^6 = -a_1\mu^2 r_0^2 + \mathrm{O}(\mu^8). \qquad \ldots\ldots(8)$$

Because of (*b*) the path lengths $FP_2 + P_2P_1 + P_1Q$ and $FB + BA + AC$ must differ by an amount equal to the difference of retardation imposed by the plate, parallel to the axis, at the neutral zone and at the pole, i.e.

$$(FP_2 + P_2P_1 + P_1Q) - (FB + BA + AC) = -(n_0 - 1)S(r_0). \qquad \ldots\ldots(9)$$

From Figure 1, $\quad FP_2 = \xi \sin(2\theta_0 - \psi_0)/\sin 2(\psi_0 - \theta_0),$

$$LP_2 = \xi \sin(2\theta_0 - \psi_0)/\sin 2\theta_0,$$

and $\quad LP_1 = \mu r_0 \operatorname{cosec} 2\theta_0 = \tfrac{1}{2}\sec\theta_0.$

Therefore $\quad P_1P_2 = LP_1 - LP_2 = \tfrac{1}{2}\sec\theta_0 - \xi\sin(2\theta_0 - \psi_0)/\sin 2\theta_0.$

Also $\quad P_1Q = \cos\theta_0,$

$$FB = \xi\left[\frac{\sin\psi_0}{\sin 2(\psi_0 - \theta_0)} - 1\right],$$

$$BA = 1 - \xi; \qquad AC = 1.$$

Then

$$(FP_2 + P_2P_1 + P_1Q) - (FB + BA + AC)$$

$$= \xi\left[\frac{\sin(2\theta_0 - \psi_0) - \sin\psi_0}{\sin 2(\psi_0 - \theta_0)} - \frac{\sin(2\theta_0 - \psi_0)}{\sin 2\theta_0} + 2\right] + \tfrac{1}{2}\sec\theta_0 + \cos\theta_0 - 2 \qquad \ldots\ldots(10)$$

$$= B(r_0), \text{ say.}$$

Then, from (9) and (10),

$$a_1\mu^2 r_0^2 + a_2\mu^4 r_0^4 + a_3\mu^6 r_0^6 = -\frac{1}{n_0 - 1}B(r_0) + \mathrm{O}(\mu^8)$$

or

$$a_2\mu^4 r_0^4 + a_3\mu^6 r_0^6 = -a_1\mu^2 r_0^2 - \frac{1}{n_0 - 1}B(r_0) + \mathrm{O}(\mu^8). \qquad \ldots\ldots(11)$$

Using (2), (7), (8) and (11) we find

$$\left.\begin{aligned} a_1 &= \frac{-1}{n_0 - 1}A(r_0), \\ a_2\mu^4 r_0^4 &= \frac{1}{n_0 - 1}A(r_0)\mu^2 r_0^2 - \frac{3}{n_0 - 1}B(r_0), \\ a_3\mu^6 r_0^6 &= \frac{-1}{2(n_0 - 1)}A(r_0)\mu^2 r_0^2 + \frac{2}{n_0 - 1}B(r_0). \end{aligned}\right\} \qquad \ldots\ldots(12)$$

We now need power series expansions for $A(r_0)$ and $B(r_0)$.

From (3) and (4) $\sin\theta_0 = \mu r_0$ and $\sin\psi_0 = \mu r_0/\xi$, whence we can obtain

$$\left.\begin{aligned} A(r_0) &= \frac{\xi^3 - 4\xi^2 + 4\xi - 1}{\xi^3}\mu^2 r_0^2 + \frac{\xi^5 - 8\xi^3 + 8\xi^2 - 1}{4\xi^5}\mu^4 r_0^4 + \mathrm{O}(\mu^6), \\ B(r_0) &= \frac{\xi^3 - 4\xi^2 + 4\xi - 1}{\xi^3}\mu^4 r_0^4 + \frac{\xi^3 - 4\xi^4 + 6\xi^3 - 6\xi^2 + 4\xi - 1}{4\xi^5}\mu^6 r_0^6 + \mathrm{O}(\mu^8). \end{aligned}\right\} \qquad \ldots\ldots(13)$$

Substituting into (12) we finally obtain for the plate-profile coefficients:

$$\left.\begin{aligned}(n_0-1)a_1&=-\frac{\xi^3-4\xi^2+4\xi-1}{2\xi^3}\mu^2r_0{}^2-\frac{\xi^5-8\xi^3+8\xi^2-1}{8\xi^5}\mu^4r_0{}^4+\mathrm{O}(\mu^6),\\(n_0-1)a_2&=\frac{\xi^3-4\xi^2+4\xi-1}{4\xi^3}-\frac{\xi^5-6\xi^4+13\xi^3-13\xi^2+6\xi-1}{2\xi^5}\mu^2r_0{}^2+\mathrm{O}(\mu^4),\\(n_0-1)a_3&=\frac{3\xi^5-16\xi^4+32\xi^3-32\xi^2+16\xi-3}{8\xi^5}+\mathrm{O}(\mu^2).\end{aligned}\right\}\qquad\ldots\ldots(14)$$

Combining (14) with (1), the plate-profile expansion can be written as*

$$S(r)=\frac{\xi^3-4\xi^2+4\xi-1}{4(n_0-1)\xi^3}\mu^4(r^4-ar^2)+\mathrm{O}(\mu^6),\qquad\ldots\ldots(15)$$

where $a=2r_0{}^2$.

If we take $a=3/2$, $\partial^2S/\partial r^2=0$ at $r=\frac{1}{2}$ and then

$$\left|\frac{\partial S}{\partial r}\right|_{r=1}=\left|\frac{\partial S}{\partial r}\right|_{r=1/2}$$

so that the maximum plate slope occurring over the aperture is minimized. This is the condition for minimum axial colour spread (Stroemgren 1935). The radius of the neutral zone is then given by $r_0=\sqrt{3}/2\simeq 0{\cdot}866$, and the shape of the plate profile is the same as in the colour-minimized classical Schmidt camera.

If, using the sixth-power terms in the plate-profile expansion as well, a more exact value of r_0 for axial colour minimization is obtained, the departure from the $\sqrt{3}/2$ value is negligible even in wide-aperture systems ($\mu=\frac{1}{4}$), and no appreciable improvement in performance could result.

The focal length of the system, represented by CF in Figure 1, is given by

$$\begin{aligned}\mathrm{CF}&=\xi\sin\psi_0/\sin 2(\psi_0-\theta_0)=\mu r_0\operatorname{cosec}2(\psi_0-\theta_0)\\&=\frac{\xi}{2(1-\xi)}\left\{1+\frac{\xi^2-3\xi+1}{2\xi^2}\mu^2r_0{}^2+\frac{3\xi^4-11\xi^3+15\xi^2-11\xi+3}{8\xi^4}\mu^4r_0{}^4+\mathrm{O}(\mu^6)\right\}.\end{aligned}\qquad\ldots\ldots(16)$$

The nominal aperture ratio of the system is therefore

$$\mathrm{F}=f/2\mu=\frac{\xi}{4\mu(1-\xi)}\left\{1+\frac{\xi^2-3\xi+1}{\xi^2}\frac{3}{8}\mu^2+\mathrm{O}(\mu^4)\right\}$$

and

$$\left.\begin{aligned}\lambda&=\frac{1}{4F}=\mu\frac{(1-\xi)}{\xi}\left\{1-\frac{\xi^2-3\xi+1}{\xi^2}\frac{3}{8}\mu^2+\mathrm{O}(\mu^4)\right\},\end{aligned}\right.$$

while conversely,

$$\mu=\lambda\frac{\xi}{(1-\xi)}\left\{1+\frac{\xi^2-3\xi+1}{\xi^2}\frac{3}{8}\lambda^2+\mathrm{O}(\mu^4)\right\}:\qquad\ldots\ldots(17)$$

§ 3. THE ABERRATION-DISPLACEMENTS

Using the argument of Hawkins and Linfoot (1945), we can, as explained above, obtain from equation (3.4) of that paper an expression for the leading monochromatic terms in the components of angular aberration for a monocentric system:

$$\delta X+i\delta Y=(n-1)\sin^2\phi\left(\frac{n+1}{2n}\frac{\partial T}{\partial x}+\frac{x}{2}\frac{\partial^2T}{\partial x^2}+\frac{i}{2n}\frac{\partial T}{\partial y}+\frac{ix}{2}\frac{\partial^2T}{\partial x\partial y}\right).\qquad\ldots\ldots(18)$$

---

* The 'plate-strength' is given by the term in r^4 in equation (15). This result agrees with equation (15) in Linfoot (1944), obtained by plate diagram analysis.

As before, $T(x,y)$ is the thickness of the corrector plate which has refractive index n. ϕ is the off-axis angle of an image point in the plane containing Cx and the axis of the system.

We take coordinates (u, v) in the aspheric surface such that $x = \mu uR$, $y = \mu vR$. Then u and v each lie in the range $[-1, +1]$ and the marginal zone of the corrector plate is represented by $r^2 \equiv u^2 + v^2 = 1$. To keep the obstruction caused by the secondary mirror, which is partly dependent on ϕ, reasonably small, we must have the semi-angle ϕ_0 of the order of μ.

Now $T(x,y) - T(0,0) = SR$, so that $\dfrac{\partial T}{\partial x} = \dfrac{1}{\mu}\dfrac{\partial S}{\partial v}$, etc.

Then from (15) and (18) we find apparent angular aberrations $(\delta X, \delta Y)$, in seconds of arc, to be

$$\partial X + i\delta Y = \frac{\xi^3 - 4\xi^2 + 4\xi - 1}{4\xi^3} K\mu^3\phi^2 \left[\frac{n_0+1}{2n_0}\frac{\partial}{\partial \mu} + \frac{1}{2}u\frac{\partial^2}{\partial u^2} + \frac{i}{2n_0}\frac{\partial}{\partial v} + \frac{1}{2}iu\frac{\partial^2}{\partial u\,\partial v}\right] (r^4 - ar^2) + \mathrm{O}(K\mu^7), \qquad \ldots\ldots(19)$$

where $K = 648{,}000/\pi$.

Effects of plate tilt other than those represented in (18), together with the effect of the terms of the order of μ^6 in the plate-profile expansion, are included in the error term $\mathrm{O}(K\mu^7)$ in (19). This equation then represents the leading monochromatic aberrations of the monocentric Schmidt–Cassegrain camera, and these are seen to be dependent, to a first approximation, only on the second- and fourth-power terms of the plate-profile expansion.

In practice the corrector plate is usually figured to give as good axial stigmatism as possible under an autocollimation test. Before polishing, the plate is ground to the profile given by equation (1), which represents this final form with the stated accuracy. The sixth-power terms are included in the explicit formulae because in wide-aperture systems their neglect may cause errors in the figuring depth greater than can easily be corrected in polishing (see Linfoot 1948, p. 285).

If we take n_0 to be the refractive index for the light in which the system is axially stigmatic, equation (19) represents the aberrations in light of that wavelength completely. In light of other wavelengths the refractive index of the plate is in practice $n = n_0 + \mathrm{O}(\mu^2)$.

We can write the chromatic aberrations as the angular change with wavelength in deviation by the plate. This deviation, for any ray meeting the plate in a point (u, v), inclined to the axis at an angle not greater than the order of μ, is given by*

$$\frac{n-1}{\mu}\left(\frac{\partial S}{\partial u} + i\frac{\partial S}{\partial v}\right)(1 + \mathrm{O}(\mu^2)).$$

Therefore we can write, for the angular chromatic aberrations, in seconds of arc,

$$\delta X + i\delta Y = \frac{K}{\mu}(n - n_0)\left(\frac{\partial S}{\partial u} + i\frac{\partial S}{\partial v}\right)(1 + \mathrm{O}(\mu^2))$$

$$= \frac{\xi^3 - 4\xi^2 + 4\xi - 1}{4\xi^3} K\mu^3 \frac{n - n_0}{n_0 - 1}\left(\frac{\partial}{\partial u} + i\frac{\partial}{\partial v}\right)(r^4 - ar^2)(1 + \mathrm{O}(\mu^2)). \qquad \ldots\ldots(20)$$

Since $n - n_0$ is of the order of μ^2, the error term in (20) is

$$\mathrm{O}(K\mu^3)\mathrm{O}(\mu^2)\mathrm{O}(\mu^2) = \mathrm{O}(K\mu^7),$$

---

* See Hawkins and Linfoot (1945), equation (3.1).

and thus (20) represents the chromatic aberrations to the same degree of accuracy as (19) represents the monochromatic aberrations.*

The total components of angular aberration for an off-axis image point in light for which the refractive index of the corrector plate is n are represented by the addition of (19) and (20), the cross terms involved being of the order of $K\mu^7$.

§4. A TYPICAL SYSTEM

Choice of a value for the parameter ξ is restricted to a small range, for while it is desirable that it should be as low as possible, so that the obstruction caused by the secondary mirror shall not be too great, the focal surface must lie behind the primary mirror if we are to obtain the advantage of a fully accessible image-surface which a Schmidt–Cassegrain system permits. Thus we must have f greater than 1 or, from (17), to a first approximation, $\xi/2(1-\xi)>1$, i.e. $\xi>\frac{2}{3}$.

Allowing for the thickness of the mirror, $\xi=0{\cdot}69$ seems to be the lowest permissible value.

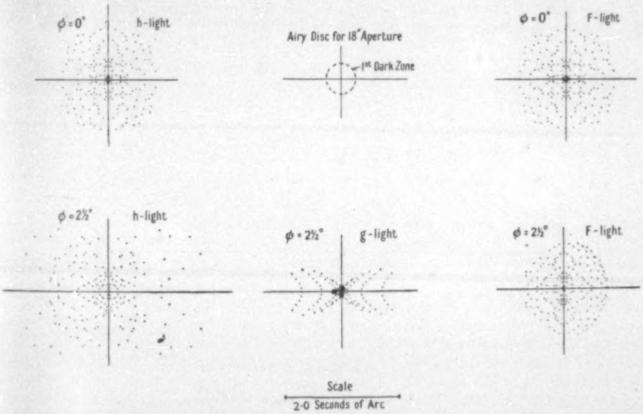

Figure 2. Spot-diagrams of the image-points of an f/3·5 monocentric Schmidt–Cassegrain camera at the centre and edge of a five-degree field in F, g and h-light and the Airy disc of an 18-inch system.

Because of the curvature of the image-surface, the system cannot conveniently be used over a greater field diameter than five degrees, corresponding to $\phi_0=2\frac{1}{2}°=0{\cdot}0436$ radian. For such off-axis angles the chromatic aberrations are more important than the monochromatic aberrations, and if, over a spectral range F–h, which includes the brightest part of an ordinary photographic spectrum, the geometrical images are not to have an effective diameter greater than about two seconds of arc, the lowest nominal aperture-ratio permissible is about f = 3·5.

Figure 2 shows spot diagrams of the geometrical images of an axially colour-minimized f/3·5 system at the centre and at the edge of a five-degree field, in F, g and h light. Each diagram is obtained by plotting as spots the $(\delta X, \delta Y)$ which correspond to the rays from a single object point passing through the points $u, v=0,\ \pm 0{\cdot}1,\ \pm 0{\cdot}2,\ \ldots\ ;\ u^2+v^2 \leqslant 1$ of a lattice of small squares filling the entry-pupil. The spot density may be taken as an indication of the light intensity in the aberrated image. Rays which are intercepted by the secondary mirror have been excluded; hence there is asymmetry in the off-axis image points. A quantitative picture of the part played by diffraction in image formation is not easily to be obtained from the size of the Airy disc (see Figure 2) because the wave fronts entering the system suffer continual small distortions due to atmospheric disturbances. Under average 'seeing' conditions the size of this 'tremor disc' will be as much as two seconds of arc in diameter.

---

* It is evident that the diameter of the chromatic disc in the light of any wavelength is directly proportional to the change in the refractive index of the corrector plate.

It seems that the ordinary Schmidt system, which might best be compared with the above system, would be that having the same diameter of aperture and a focal ratio of f/1·9. The depth of figuring on the plate would then, to a first approximation, be the same as on the f/3·5 monocentric Schmidt–Cassegrain system. Because of this similarity the two systems will, over a five-degree field, have practically the same angular aberrations. Moreover, because their apertures are of equal size, the angular diameter of the diffraction discs will be the same in the two systems. Both from the geometrical standpoint, therefore, and from the more precise diffraction theory of image formation, a given star-field will be rendered in very much the same way in the two systems but on a smaller plate and with greater speed on the f/1·9 ordinary Schmidt camera. If allowance is made for the smaller light loss within the latter system, partly through the reduced obstruction and partly through the elimination of a second reflection, the difference in exposure times with the same aperture diameter might amount to a factor of five-thirds.

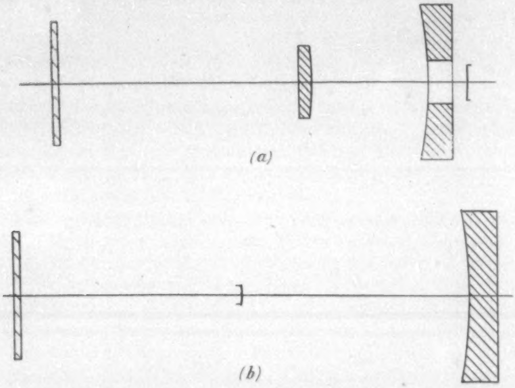

Figure 3.

(*a*) f/3·5 monocentric Schmidt–Cassegrain camera.

(*b*) f/1·9 ordinary Schmidt camera with the same aperture diameter.

The larger plates used on the Schmidt–Cassegrain system would exhibit the defects of grain size and sky-blackening to a lesser extent than would the plates of half the size used on the ordinary Schmidt camera. This would be an advantage of some importance except in systems where the focal length is already greater than about 100 inches. Figure 3 shows the two systems drawn to the same scale; their external dimensions are seen to be comparable.

ACKNOWLEDGMENTS

The author wishes to express his gratitude to Dr. E. H. Linfoot and Dr. E. Wolf for their interest and encouragement in the preparation of this paper, and to the former for the loan of his paper (1949) in advance of publication.

REFERENCES

Baker, J. G., 1940, *J. Amer. Phil. Soc.*, **83**, 3, 339.
Burch, C. R., 1942, *Mon. Not. R. Astr. Soc.*, **102**, 159.
Carathéodory, C., 1940, *Hamburger Mathematische Einzelschrift*, **28**, 36.
Hawkins, D. G., and Linfoot, E. H., 1945, *Mon. Not. R. Astr. Soc.*, **105**, 334.
Linfoot, E. H., 1944, *Mon. Not. R. Astr. Soc.*, **104**, 48; 1949, *Ibid.*, **109**, 279.
Stroemgren, B., 1935, *Vierteljahresschrift der Astr. Ges.*, **70**, 65.

The Operation and Photographic Characteristics of a Kerr-cell Type of Electro-optical Shutter

By A. E. J. HOLTHAM and H. A. PRIME
Electronics Department, University of Liverpool

MS. received 13*th December* 1949

ABSTRACT. A Kerr-cell electro-optical shutter is described, the shutter action being controlled by a high voltage pulse applied to the cell electrodes. The exposure time used is 2×10^{-8} second, and provision is made for obtaining ' delayed ' exposures up to times of the order of 10^{-4} second. The photographic limitations of the shutter are discussed and the formation of the image considered in some detail. The assumptions necessary for a quantitative photometric analysis of Kerr-cell exposures are stated and an approximate limit is set on the magnitude of errors resulting from such assumptions. The applications of the Kerr-cell technique to the measurement of particular spark channel characteristics are also described.

§ 1. INTRODUCTION

CERTAIN isotropic liquids, such as nitrobenzene, become doubly refracting when subjected to a high electrical stress. This property, first observed by Kerr in 1875, and subsequently known as the 'Kerr effect', has been used by various investigators in the development of electrically controlled light shutters, by which the transmission of light can be controlled down to times of the order of 10^{-8} second or less. The time lag between the occurrence of the 'Kerr effect', and the application of the stress (to two electrodes immersed in the nitrobenzene or similar liquid) is not greater than 10^{-8} second, and hence the rate of opening or closing the shutter depends mainly on the rate of rise or fall of the voltage applied to the electrodes.

Some workers (Abraham and Lemoine 1900, Dunnington and Lawrence 1930, Dunnington 1931) have used the 'open-to-closed' type of shutter, in which the shutter, a Kerr cell placed between 'crossed' polarizing Nicol prisms, is initially kept open by the application of a steady D.C. voltage to the cell plates. The shutter is then closed by the removal of the applied voltage at some instant subsequent to the initiation of the event being observed. A 'closed-to-open-to-closed' shutter, employing two cells between crossed Nicols, has also been developed (Beams 1926), in which both cells are initially under stress, the directions of the two electric fields being mutually perpendicular, thus giving an optically 'closed' shutter. To obtain the exposure, the voltage on one cell is removed an instant before that on the other. This permits a light pulse to be transmitted, the intensity depending on the difference in the voltages on the two cells at any given instant.

An alternative method of obtaining a 'closed-to-open-to-closed' shutter action, using only a single cell, is by the application of a voltage pulse to the cell electrodes. The duration of the pulse determines the exposure time, and the steepness of the leading and trailing edges of the pulse determines the rates of opening and closing of the shutter. An advantage of this technique is that the pulse may be applied at any instant relative to the initiation of the phenomenon, but a limitation is that the exposure times are not as short as those obtainable with the previous techniques. Nevertheless, the method appears to be the one mainly used at the present time (Lapsley, Snoddy and Beams 1948, Rawcliffe 1942, Froome 1948, Zarem, Marshall and Poole 1949). A recent feature of these single cell pulse techniques is the use of Polaroid film in place of Nicol prisms as the polarizing elements in order to improve the aperture of the optical system. A description of a Kerr-cell equipment based on this technique is given in §2 of the paper.

Although several of the papers quoted, and also others, consider the electro-optical characteristics of the various types of shutter in some detail (Dunnington 1931, Washburn 1932, Zarem *et al.* 1949), there has been practically no discussion of the photographic characteristics of the shutter from the point of view of image formation and the photometric analysis of results obtained. This aspect of the shutter mechanism is considered in §3 of the paper. Since the equipment described has been primarily used for investigations concerned with the growth of a spark channel, the results quoted in the text refer to this type of optical transient (Prime and Saxe 1949). In the final section of the paper consideration is given to the application of the technique to the determination of the channel diameter and the variation of radial intensity across a spark.

§2. DESCRIPTION OF THE EQUIPMENT

(i) *Electronic Equipment*

A schematic diagram of the apparatus is shown in Figure 1. A hydrogen thyratron modulator circuit is used to generate a pulse, the amplitude of which can be adjusted by varying the H.T. supply voltage to the hydrogen thyratron from almost zero to 4 kv. The pulse is subsequently stepped up to a maximum of 10 kv. by means of a pulse transformer for direct application to the cell electrodes. The duration of the pulse is determined by the characteristics of the artificial line forming the pulse, and is approximately 2 μsec. A trigger circuit, for tripping the hydrogen thyratron at any time relative to the initiation of the event under observation, and associated power units are contained in a single unit with the modulator. In addition, a 3-in. cathode-ray tube is incorporated for monitoring the performance of the equipment.

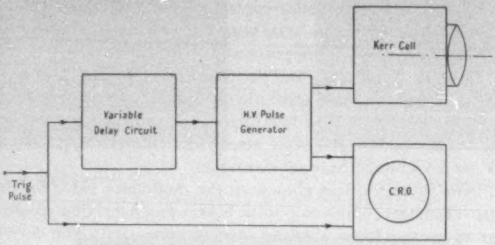
Kerr Cell
Variable Delay Circuit
H.V. Pulse Generator
Trig Pulse
C.R.O.

Figure 1. Schematic diagram of apparatus.

A diagram of the trigger, delay and modulator circuits is shown in Figure 2. Facilities are provided for triggering the system by means of a positive or negative external pulse or by a recurrent pulse generated internally in the multivibrator stage V_1. V_2 serves to reverse the phase of the external negative pulse so that a positive pulse is always applied to the first grid of V_3. This positive pulse can be monitored on the oscillograph. The switch S_1 controls the operation of V_1; V_3 and V_4 comprise the delay stages enabling a variable delay from 0–250 μsec.

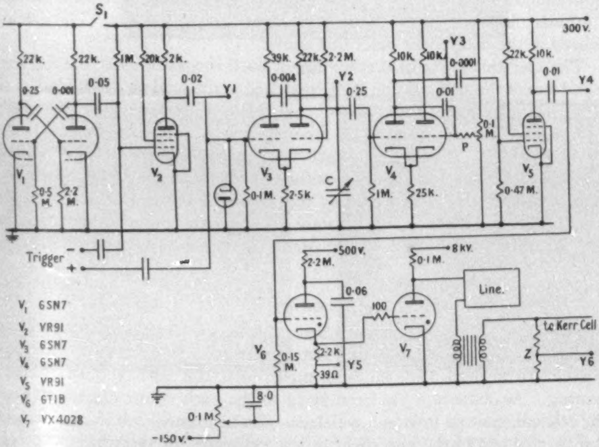
S1
300 V.
22k.
22k.
1M.
20k.
2k.
0·25
0·001
0·05
0·02
Y1
39k.
22k.
2·2M.
0·004
Y2
0·25
10k.
10k.
Y3
0·0001
0·01
22k.
10k.
0·01
Y4
0·1 M.
P
V1
0·5 M.
2·2 M.
V2
V3
0·1M.
2·5k.
C
1M.
V4
25k.
V5
0·47 M.
Trigger
–
+
500 V.
2·2M.
8 kV.
0·1 M.
Line.
0·06
100
to Kerr Cell
V6
0·15 M.
2·2K.
Y5
39Ω
V7
Z
Y6
8·0
0·1M.
–150 V.
V1 6SN7
V2 VR91
V3 6SN7
V4 6SN7
V5 VR91
V6 6T1B
V7 VX4028

Figure 2. Circuit diagram of delay and pulsed modulator unit.

to be obtained. The output from the right-hand anode of V_3 is a positive-going saw-tooth wave which is fed to the grid of the voltage comparator stage V_4. The rate of rise of the saw-tooth can be controlled by variation of the capacitor C, between the output anode and earth. The comparator stage V_4 operates when the instantaneous voltage of the saw-tooth is equal to the potential set by the potentiometer connected to the right-hand grid. Variation of C, by switching a bank of condensers, provides a coarse delay control while variation of the potentiometer P enables a fine control of delay to be obtained on any given range. The output from the comparator stage is a negative square pulse generated at the left-hand anode. The pulse is amplified, and the phase reversed in the following valve V_5 which, in turn, triggers a small argon thyratron V_6. The hydrogen thyratron V_7 requires to be triggered from a low impedance source and by a positive-going pulse of the order of 100–200 volts amplitude; the use of an argon thyratron between V_5 and V_7 fulfils these requirements.

A hydrogen thyratron was chosen as the modulator valve for the following reasons: (i) The trigger-pulse amplitude is very much less than would be required by a triggered spark gap or trigatron type of valve. (ii) The current-handling capacity ($\sim$90 amp.) greatly exceeds that of a hard valve. In addition, the operation of the thyratron is independent of the shape of the trigger pulse subsequent to the valve 'firing'. (iii) The hydrogen thyratron is not temperature dependent as would be a mercury thyratron, and the ionization and de-ionization times are very much less than would obtain for a mercury thyratron, due to the higher ion mobility. Also, the hydrogen thyratron has a positive grid control characteristic which avoids the necessity of a bias supply for the grid circuit.

A detailed description of the operation of hydrogen thyratrons has been given by Germeshausen (1948), and it has been shown that the delay between the application of the grid pulse and the 'firing' of the anode circuit, is of the order of 0·2 μsec. for a rate of rise of grid voltage of 1,500 volts/μsec. This condition is realized in the equipment described above.

The operation of the modulator circuit itself is conventional, the characteristic impedance of the artificial line being matched to the load on the secondary side of the pulse transformer.

Points indicated Y1–Y5 on the circuit diagram can be monitored by the oscillograph, the circuit diagram of which is shown in Figure 3. The wave-forms shown in Figure 5 (photograph) show the shape of the pulse applied to the Kerr-cell electrodes, and were obtained using the internal trigger pulse and a delay of the order of $\frac{1}{2}$ μsec. The delay is constant from pulse to pulse within approximately 10^{-7} sec., thus permitting a steady oscillogram to be obtained under recurrent pulse conditions.

(ii) *Optical Equipment and Method of Adjustment*

An aerial camera was modified to take the two Polaroid discs and the cell. The lens of the camera is a Kodak 'Ektar' f/2·5 of 7 in. focal length. The polarizer is fixed into the focal-plane shutter compartment, and can be rotated by a reduction gearing. An extension has been fitted to the back of the camera and contains the cell and analyser Polaroid, which can also be rotated. A 35-mm. film adaptor can be attached to the end cover of the extension for recording purposes. An overall magnification of unity is obtained with the above system.

The preparation of the copper electrodes for the Kerr cell was carried out in the following manner: the surfaces were first milled, then rubbed with emery cloth, cleaned and finally coated with black cupric oxide in order to minimize internal reflections from the electrodes. The oxide deposit was obtained

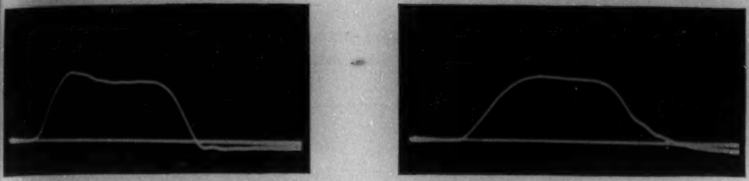

(*a*) Cell unconnected.

(*b*) Cell connected to modulator.

Figure 5. Oscillograms of Kerr-cell exposure pulse.

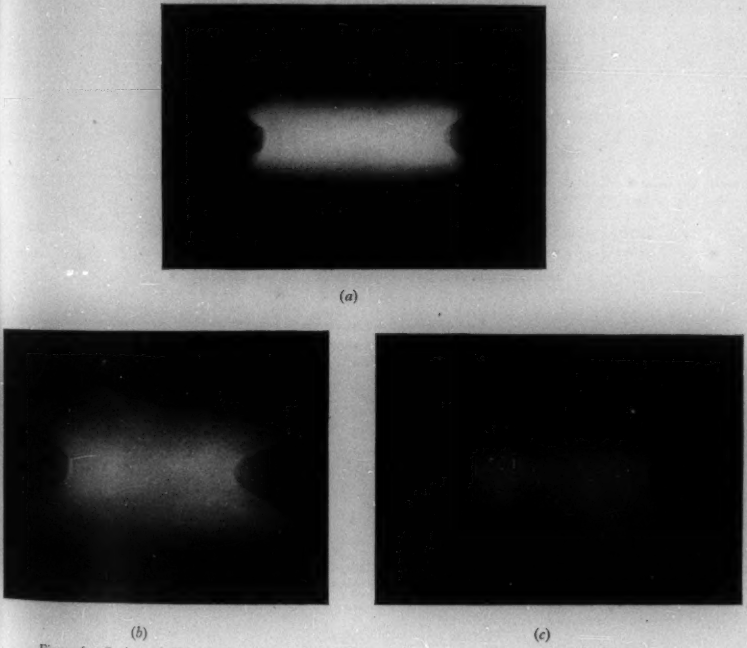

Figure 6. Series of Kerr-cell records for 2,000-amp. spark in air at atmospheric pressure. Exposure time 2 μsec. at (*a*) 0–2 μsec.; (*b*) 3–5 μsec.; (*c*) 5·5–7·5 μsec. Duration of current pulse 15 μsec.

electrolytically in a chemically normal solution of caustic soda as the electrolyte. The size of the electrodes and their spacing is arranged to give maximum light transmission for a 10 kv. pulse; the length of the electrodes along the optic axis is 1·5 cm., the separation 0·34 cm., and the height 5 cm. The nitrobenzene is distilled into the cell, which is then sealed using water-glass as a cement.

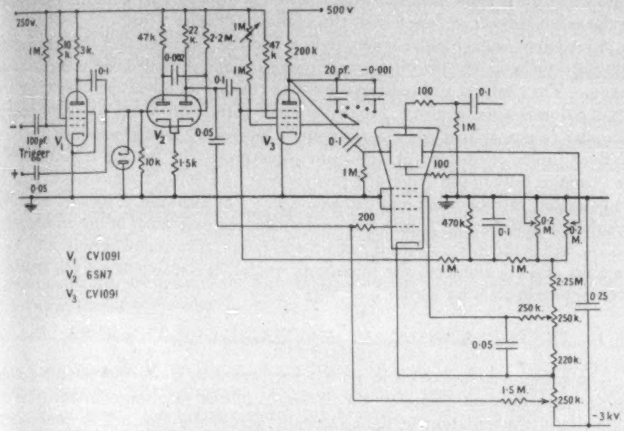
250v.
500 v
1M.
10 k.
3k.
0·1
47k
22 K.
2·2M.
0·002
1M.
1M.
47 k
200 k
0·1
20 pf. -0·001
100
0·1
1M
100pf.
Trigger
V_1
V_2
V_3
0·05
0·1
10k
1·5k
1M.
100
0·05
200
470k
0·1
0·2 M.
0·2 M.
V_1 CV1091
V_2 6SN7
V_3 CV1091
1M.
1M.
2·25M.
0 25
250 k.
250 k.
0·05
220k.
1·5 M.
250 k.
-3 kV

Figure 3. Circuit diagram of cathode-ray oscillograph monitor unit.

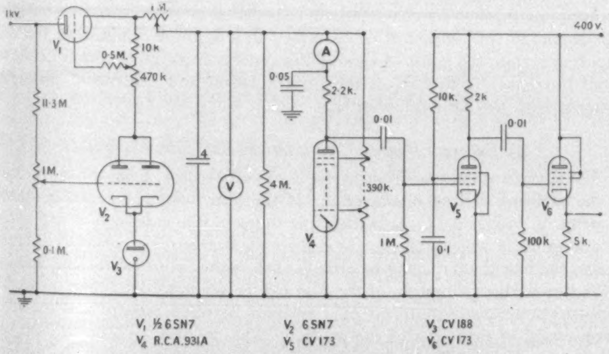
1kv.
1M.
400 v.
V_1
0·5M.
10k
470 k
A
0·05
2·2k.
11·3 M
0·01
10k.
2k
0·01
1M.
4
V
4 M.
390k.
V_2
V_5
V_6
V_4
1M.
0·1
100k
5 k.
0·1 M.
V_3
V_1 ½6SN7
V_4 R.C.A.931A
V_2 6SN7
V_5 CV173
V_3 CV188
V_6 CV173

Figure 4. Circuit diagram of photo-multiplier and amplifier unit.

In order to adjust and check the performance of the equipment, a photo-multiplier cell and amplifier together with the necessary rectifier circuits was developed for use with the monitoring oscilloscope to record the light transmitted through the Kerr-cell unit. The circuit diagram of this unit is shown in Figure 4.

For optimum conditions of light transmission, the polarizer and analyser should be crossed and their planes of polarization should be at 45° to the plane of the cell electrodes (Kingsbury 1930). This adjustment is made using a steady light source. For a given orientation of the analyser, the polarizer is slowly rotated by the reduction gearing until the light transmission to the photo-multiplier tube is a minimum. This position is indicated by a minimum reading on the milliammeter in series with the photo-multiplier tube.

A recurrent voltage pulse is next applied to the Kerr cell and the transmitted light pulse picked up by the photo-multiplier tube and recorded on the oscillograph screen. The analyser and polarizer are then rotated together until the amplitude of the pulses is a maximum. Finally, a small correction of the polarizer may be necessary to ensure that the polarizer and analyser are still crossed.

Even under conditions of optimum adjustment, the overall transmission of the system is only of the order of a few percent due to the attenuation of light by the polarizer, nitrobenzene and the analyser. For example, Zarem *et al.* (1949) give the transmission of 'J' film Polaroid within the pass-band of the nitrobenzene as 32%, and as the Kerr cell itself has a theoretical transmission of only 50% when the Kerr effect is induced, the maximum overall transmission for the system is given approximately by $\frac{1}{3} \times \frac{1}{2} \times \frac{1}{3}$ or 5%.

§ 3. PHOTOGRAPHIC CHARACTERISTICS OF THE KERR-CELL SHUTTER

The equipment described in § 2 has been used to study the variation of the visible spark channel diameter, the variation of the maximum intensity of the channel and the variation of light intensity across the channel, as functions of time, gas, pressure and current. A typical series of results is shown in Figure 6. These were obtained for a 15 kv. spark in air, generated by the discharge of an artificial line through its characteristic impedance to give 2,000 amp. for 15 μsec. The results of this work will be described in a separate publication, but it is of importance from the point of view of the general technique, to consider in some detail those factors that affect the interpretation and analysis of photographs obtained with the Kerr-cell shutter.

(i) *Exposure Density Characteristic and Film Calibration*

For any quantitative analysis of the Kerr-cell records, a knowledge is required of the exposure density characteristic of the film, which is normally expressed in terms of $\log E$ and D. It is desirable to use a film emulsion having a characteristic as linear as possible, and to restrict the exposure by means of an aperture so that the maximum density recorded is below the 'knee' of the characteristic.

A step-wedge calibration of the film can be made to determine the exposure density characteristic in terms of a relation between density and the relative transmission of each step of the wedge. The calibration is carried out under conditions which, as far as possible, are the same as those applying at the instant of normal spark recording. Thus a spark is used as the source of illumination in order to ensure that the spectral response of the emulsion introduces no additional complication, and the Kerr-cell exposure is maintained at the same value of 2 μsec. The step-wedge is placed immediately in front of the film and a series of records is made of a given spark through successive steps of the wedge. Then, knowing the percentage transmission of each step of the wedge (see below), a relation can be obtained between density (measured at a fixed arbitrary point on each record) and percentage transmission, taking the density recorded with no step-wedge to be 100%. By adjustment of the lens aperture, the maximum density recorded is arranged to be greater than that of any spark to be analysed.

The percentage transmission of the step-wedge must also be measured as far as possible under the same operating conditions in order to eliminate variations due to light scatter at the step-wedge surface. This is carried out by replacing the film by a photo-multiplier tube and using a uniformly illuminated slit at the focus of the lens, in place of the spark electrodes. By partial 'uncrossing' of the Polaroids, and adjustment of the voltage per stage of the photo-multiplier tube, a maximum anode current of about $250\,\mu$a. for 100% transmission is obtained. For each step, the corresponding current is noted and hence the percentage transmission recorded. Within experimental error, a linear relation exists between light intensity and anode current up to 1 ma. (Engstrom 1947). Each individual reading has to be taken quickly to avoid fatigue of the tube and care has to be exercised to obtain steady D.C. potentials for both the photo-multiplier tube H.T. and the light source. This method does however neglect inter-reflections between the step-wedge and the photocell, which might be different from the inter-reflections between the step-wedge and the film, thus giving rise to an inaccurate transmission characteristic for the wedge.

(ii) *Formation of the Kerr-cell Image*

The Polaroids of the Kerr cell are imperfect is so far as a small percentage of the incident light is transmitted even when the two discs are 'crossed'. For the type of material used for this work, the manufacturers state that the degree of polarization for each element is approximately 99% (Polaroid Products Bulletin). This limitation results in the formation of a spurious image of the phenomenon on the photographic plate or film in the following manner. Assume that the duration of the optical transient being recorded is T sec. and that the duration of the Kerr-cell exposure is ΔT sec. and occurs at time t'; in addition, denote the transmission of the cell when the Polaroids are 'crossed' by the fraction p, and the transmission during the exposure by q. Then, if the intensity of the phenomenon is I_t, a function of time, the three components contributing to the exposure of the film are given by the integrands

$$\int_0^{t'} I_t p\,dt, \quad \int_{t'}^{t'+\Delta T} I_t q\,dt, \quad \text{and} \quad \int_{t'+\Delta T}^{T} I_t p\,dt,$$

of which the second is the significant exposure, the first and third being unwanted.

The resultant exposure of the image may not necessarily be proportional to the sum of these integrands owing to the existence of reciprocity-law failure and the Clayden effect. The latter effect (Mees 1945) relates to the resultant density of an image produced by a very brief exposure to light of extremely high intensity and a subsequent exposure to light of moderate intensity. Under such conditions the separate exposures do not add in a simple manner. Failure of the reciprocity law is due to the fact that the density D depends not only on the exposure E (=intensity × time), but also on the actual values of these two factors. Failure of the law has been investigated by Webb (1933) and Berg (1940, 1946). Berg claims in his second paper that reciprocity failure is negligible providing the times involved are less than 5×10^{-5} sec.

These photographic considerations lead to the conclusion that the density of the recorded or 'normal' image may not necessarily be given by a function of the form

$$D_N = f\left\{\int_0^{t'} I_t p\,dt + \int_{t'}^{t'+\Delta T} I_t q\,dt + \int_{t'+\Delta T}^{T} I_t p\,dt\right\}, \qquad \ldots\ldots(1)$$

where f is determined by the exposure–density characteristic of the film.

For the purpose of analysis however, it is convenient to assume that equation (1) is in fact, exact. Accordingly, by the definition of exposure, we have

$$E_N = \int_0^{t'} I_t p\,dt + \int_{t'}^{t'+\Delta T} I_t q\,dt + \int_{t'+\Delta T}^{T} I_t p\,dt$$

$$= \int_0^{t'} I_t p\,dt + \int_{t'}^{t'+\Delta T} I_t(q-p)\,dt + \int_{t'}^{t'+\Delta T} I_t p\,dt + \int_{t'+\Delta T}^{T} I_t p\,dt.$$

Similarly, the spurious image exposure is defined by the equation

$$E_{sp} = \int_0^{T} I_t p\,dt = \int_0^{t'} I_t p\,dt + \int_{t'}^{t'+\Delta T} I_t p\,dt + \int_{t'+\Delta T}^{T} I_t p\,dt,$$

so that

$$\int_{\Delta T} I_t(q-p)\,dt = E_N - E_{sp}.$$

Further, if I_t is approximately constant at the value $I_{t'}$ during the interval ΔT, then

$$I_{t'} = \frac{E_N - E_{sp}}{(q-p)\Delta T}. \qquad \ldots\ldots(2)$$

Now the units of exposure and intensity are arbitrary and since by the previous definition, E_{sp} is a constant for the event it is convenient to use the ratio, $E_{sp}/E_N = \phi$ and hence obtain a general solution

$$I_t = k\frac{1-\phi_t}{\phi_t}, \qquad \ldots\ldots(2\,a)$$

where k is some constant having the dimensions of intensity. The assumption that equation (1) is exact, which was necessary for the derivation of equation (2), is also implicit in the experimental determination of E_N and E_{sp} for the following two reasons. Firstly, the density transmission curve, referred to in the preceding section, is prepared under conditions almost similar to those obtaining during normal recording. There is, therefore, a spurious image contribution to the recorded density. The calibration curve so obtained is thus particular to the time t' at which the exposure is made and should strictly only be used to analyse normal recordings for which the exposure is likewise made at time t'. Secondly, the transmission scale of the calibration curve can only be interpreted as an exposure scale provided that there is no reciprocity-law failure. It is clear, therefore, that the use of a common calibration curve for the determination of E_N from D_N over all t' and the determination of E_{sp} from D_{sp} is only justified when equation (1) is exact.

A comparison of calibration curves obtained for different values of the exposure time t' showed that the spread of separation of these curves (which were obtained from the records on a number of films) was comparable with the spread due to processing the films separately. A separate experiment had shown that the agreement between curves obtained from different films, but for constant t', was of the order of 20%. This discrepancy due to processing errors therefore sets an approximate limit on the errors likely to result from the assumptions made in the previous analysis.

§4. THE EXPERIMENTAL DETERMINATION OF SPARK CHANNEL CHARACTERISTICS

(i) *Determination of Intensity as a Function of Time*

In order to illustrate the considerations of the preceding section, the determination of the variation of intensity as a function of time is described for the case of the 2,000 amp. air spark previously mentioned. A series of photographs are taken on a single film of: (*a*) the normal image for various delays from the time of initiation, (*b*) the normal image, at time $t=0$, through a step-wedge, and (*c*) the spurious image (i.e. no pulse applied to the Kerr cell). The lateral density profiles (i.e. variation of density across the images) are then determined using a microphotometer and the density–transmission calibration curve is constructed from the recorded images detailed under (*b*). The lateral exposure values are then tabulated for the records detailed (*a*) and (*c*) by reference to the calibration curve, and hence the ratio $E_{\mathrm{sp}}/E_{\mathrm{N}}$ can be determined for corresponding points on the profiles. The table shows the values of E_{N}, ϕ_t and I_t in arbitrary units tabulated as functions of t', the mid-time of the exposure.

t' ($\times 10^{-6}$ sec.)	1·5	5·5	7	10	12·5	16·5
E_{N}	48	16	6·2	3·4	1·8	1·5
ϕ_t ($E_{\mathrm{sp}}=0{\cdot}6$)	0·013	0·037	0·093	0·18	0·33	0·40
I_t (arbitrary units)	76	26	9·8	4·6	2·0	1·5

It is to be noted that the spurious image contribution increases from approximately 1% of the total exposure at the initial stage, to approximately 30% at the end of the phenomenon. It is essential therefore to correct for the contribution at low intensities.

(ii) *Spark Channel Diameter and the Radial Variation of Intensity*

Knowing the spurious image contribution and the film characteristic, the intensity profile is readily determined from the density profile; it is therefore possible to investigate variations in spark channel 'diameter' as a function of the discharge parameters such as current, gas, gas pressure, etc. For this purpose some arbitrary definition of channel diameter must be proposed and it is convenient to use the distance between points on the intensity profile for which the intensity is half the maximum value. The definition is not altogether satisfactory as it depends on the recording sensitivity (i.e. the ratio of maximum recorded density to the density of the 'fog' which forms the background for the image). However, since the 'skirts' of the profile are relatively steep, the dependence of the diameter, as defined above, on the maximum density is not critical; in fact, a change in aperture (which is equivalent to a change in maximum recorded density) by a factor of 3 results in an apparent change in diameter of only 20%.

The intensity profile, from which the channel diameter is determined as described above, only shows the lateral variations of intensity. If it is assumed that the channel is of circular cross section and radius R, and if the axis of the channel is taken along Oz, see Figure 7 (a), then the lateral intensity profile shows the variation of intensity I_x, as a function of x, when the channel is viewed along a direction parallel to the plane Oyz. Now the intensity I_x is related to the more fundamental quantity, radial intensity I_r, which is the intensity at a point distance r from the Oz axis, by the relationship:

$$I_x = k\int_x^R rI_r(r^2-x^2)^{-1/2}\,dr, \qquad \text{......(3)}$$

where k is a numerical constant which can be neglected since the units are arbitrary.

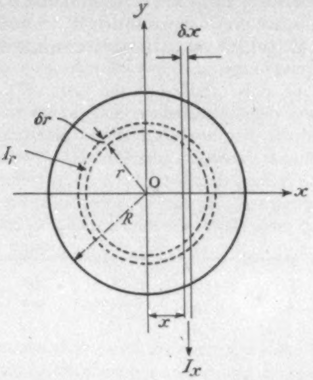

Figure 7 (a). Relation between lateral intensity I_x and radial intensity I_r.

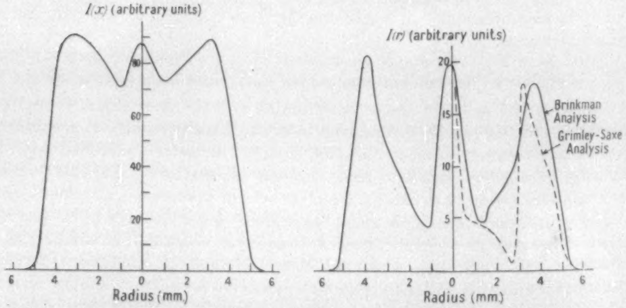

Figure 7 (b). (i) Lateral intensity profile; (ii) radial intensity profile.

Solutions of equation (3), giving I_r as a function of I_x have been obtained by Hörmann (1935), Brinkman (1937) and Grimley and Saxe (1949). Brinkman obtains

$$I_r = \frac{1}{\pi}\frac{d}{dr}\int_r^R I'x(x^2-r^2)^{-1/2}\,dx \qquad \text{......(4)}$$

and an equivalent expression, in slightly different form, is obtained by Grimley and Saxe. Numerical integrations have been carried out to determine the radial intensity profiles for the case of a 2,000 amp. spark in hydrogen at a pressure of 1 atmosphere. For comparison the I_x profile is shown with the I_r profiles in Figure 7 (*b*). The channel diameter as determined from the I_r profile according to the same definition is approximately 7% more than the diameter determined from the I_x profile.

§ 5. CONCLUSIONS

The conclusions that can be drawn from the work described in the paper relate to the photographic aspects of the shutter mechanism rather than to the electro-optical characteristics. Nevertheless, the technique described in § 2 illustrates in some detail the operation of the shutter by pulse control, and the type of results obtained using an exposure time of 2×10^{-6} sec. A reduction of the exposure pulse duration to approximately 10^{-7} sec. could probably be effected if necessary by eliminating the pulse transformer, but a limit of this order is set by the stray capacities associated with the cell and the current rating of the switching valve in the modulator unit.

A reduction of the exposure time would, however, increase the spurious image contribution to the exposure in relation to the normal image contribution and hence the photographic considerations outlined in § 3 would be of even greater significance. Clearly any step which can be taken to reduce the contribution of the spurious image is desirable and three possible methods are now proposed. Primarily, an improvement in the 'cut-off' characteristics of the Polaroid elements would contribute towards a reduction of the spurious image component, but whether this could be achieved using the existing type of element material is not known. The use of Nicol prisms as the polarizing elements would also give an improved cut-off, but the difficulty in that case arises in obtaining Nicols of sufficient aperture. A second method for the reduction of the spurious image component is based on the observation that the spectral distribution of the light producing this image is different from the distribution of the light producing the normal image (this observation may not be true for all sources). This difference immediately suggests the introduction of a filter which would reduce the spurious image intensity. (The authors have recently been informed that this technique has been adopted with considerable success by workers of another laboratory.) The third and most involved method depends on the use of a rotating mirror system between the phenomena and the Kerr cell for the purpose of selecting a portion of the emitted light (say over a period of 10 μsec.), and directing this light towards the Kerr cell, the latter being shielded from direct light from the source. The attendant problems of mirror synchronization and the delay of the selected portion by the required time would require investigation.

Apart from spurious image considerations however, the work has shown that there are at present insufficient data concerning reciprocity-law failure and the Clayden effect for the conditions obtaining in the recording of optical transients by techniques such as described in the paper. Such data are required before the quantitative aspects of recording can be put on a rigorous basis, and further work along these lines would be of value.

ACKNOWLEDGMENTS

In conclusion, the authors wish to express appreciation of the advice given by members of the Ilford and Kodak organizations during the course of the work. Acknowledgment is also due to Professor J. M. Meek and Dr. J. D. Craggs of this Department, who have assisted the authors by discussing the work and this paper on many occasions. Finally, one of us (A. E. J. H.) desires to acknowledge the award of a grant from the Department of Scientific and Industrial Research which enabled the work to be undertaken.

REFERENCES

ABRAHAM, H., and LEMOINE, J., 1900, *C. R. Acad. Sci., Paris*, **130,** 245.
BEAMS, J. W., 1926, *J. Opt. Soc. Amer.*, **13,** 597.
BERG, W. F., 1940, *Proc. Roy. Soc.* A, **174,** 559; 1946, *Photogr. J.*, **86B,** 154.
BRINKMAN, H., 1937, *Dissertation*, Utrecht.
DUNNINGTON, F. G., 1931, *Phys. Rev.*, **38,** 1535.
DUNNINGTON, F. G., and LAWRENCE, E. O., 1930, *Phys. Rev.*, **35,** 396.
ENGSTROM, R. W., 1947, *J. Opt. Soc. Amer.*, **37,** 420.
FROOME, K. D., 1948, *J. Sci. Instrum.*, **25,** 371.
GERMESHAUSEN, K. J., 1948, *Pulse Generators*, Vol. 5 (New York : McGraw-Hill).
GRIMLEY, T. B., and SAXE, R. F., 1949, *E.R.A. Report* L/T211.
HÖRMANN, H., 1935, *Z. Phys.*, **97,** 539.
KINGSBURY, E. F., 1930, *Rev. Sci. Instrum.*, **1,** 22.
LAPSLEY, A. C., SNODDY, L. B., and BEAMS, J. W., 1948, *J. Appl. Phys.*, **19,** 111.
MEES, C. E. K., 1945, *Theory of the Photographic Process* (New York : Macmillan).
POLAROID LABORATORY PRODUCTS (*Bulletin*), Polaroid, Corporation, Cambridge, Mass.
PRIME, H. A., and SAXE, R. F., 1949, *Proc. Instn. Elect. Engrs.*, Pt. II, **96,** 662.
RAWCLIFFE, R. D., 1942, *Rev. Sci. Instrum.*, **13,** 413.
WASHBURN, H. W., 1932, *Phys. Rev.*, **39,** 688.
WEBB, J. H., 1933, *J. Opt. Soc. Amer.*, **23,** 316; 1935, *Ibid.*, **25,** 4.
ZAREM, A. M., MARSHALL, F. R., and POOLE, F. L., 1949, *Elect. Engng.*, **68,** 282.

The Optical Emissivity of Titanium and Zirconium

By F. J. BRADSHAW *
Royal Aircraft Establishment, Farnborough

MS. received 11th January 1950

ABSTRACT. A method of measuring the optical emissivity of titanium and zirconium using eddy current heating is described. The specimen consisted of a cylinder of metal drilled with a small black-body hole, and its real and apparent temperatures were measured with an optical pyrometer at a mean wavelength of $0{\cdot}652\,\mu$. The variation of emissivity with temperature was investigated and the precautions taken to avoid errors are described.

As part of a programme of work at the Royal Aircraft Establishment, Farnborough, it was decided to measure the optical emissivities of titanium and zirconium. Existing data consisted only of unpublished work quoted by Van Arkel (1939). Measurements of the variation of vapour pressure with temperature of these metals were also being carried out at Farnborough and for this reason it was felt necessary to check the emissivities.

§ 1. METHOD

Of the various possible ways of measuring emissivity, the direct temperature comparison 'bore hole' method was chosen. That is, a block of material of which the surface emissivity is to be measured has a small cavity of a certain depth made in it and is then heated. If the radiation emerging from the cavity has suffered many internal reflections then it approximates closely to black-body radiation. Measurements of the temperature of the surface and of the cavity with an optical pyrometer lead to the emissivity by

$$\ln \epsilon_\lambda = 1{\cdot}432/\lambda \left(\frac{1}{T_{\mathrm{H}}} - \frac{1}{T_{\mathrm{S}}}\right),$$

where ϵ_λ is the spectral emissivity, λ the mean effective pyrometer wavelength, T_{H} the cavity temperature and T_{S} the surface temperature.

The main difficulties of this method are in producing a uniformly heated specimen and at the same time having it in surroundings the temperatures of which are low enough not to interfere, by reflection, with the specimen's inherent surface brightness. This makes indirect furnace heating unsatisfactory. With electrical resistance heating of the specimen it is still difficult to get a uniform temperature throughout and true black-body radiation from the cavity (Price 1947). However, by using high-frequency eddy current heating these difficulties were overcome. The specimen was a solid cylindrical block of material and was mounted inside an H.F. coil. The circulating currents flowed round the curved surface so that the heat was put in effectively only at the surface. Calculation showed the mean current depth of penetration to be sufficiently small for the cross section temperature gradients to be negligible. Thus the centre temperature was the same as that of the outside, and a bore hole which was drilled down a diameter had a uniform wall temperature throughout its whole length. The only source of non-uniformity was at the ends of the cylinder, where there was nothing but loss by radiation. This non-uniformity was reduced to a negligible amount by the use of a sufficiently long specimen.

---

* Now at the British Iron and Steel Research Association, London.

§2. APPARATUS

The apparatus is shown in the Figure. The metals were obtained in powder form, sintered *in vacuo* (Bickerdike and Sutcliffe 1949) and then suitably worked into fully dense bars. Care was taken to keep the material as pure as possible (for analyses, see §5). Specimens were turned out of the bars in the form of cylinders 2·0 cm. long and 7·3 mm. in diameter. These dimensions allowed the central portion of the specimen, where the bore hole was drilled, to reach a uniform temperature when heated. The surface of the specimen was polished by normal metallographic methods, magnesia being used in the final stages.

The specimen was held in a molybdenum mount on the top of an alumina rod and the rod was tapered to fit a brass plate which was waxed (Apiezon W 100) into the vacuum tube. The specimen was aligned and centred with the wax still soft by three adjusting screws mounted rigidly to the vacuum tube and bearing on the base plate.

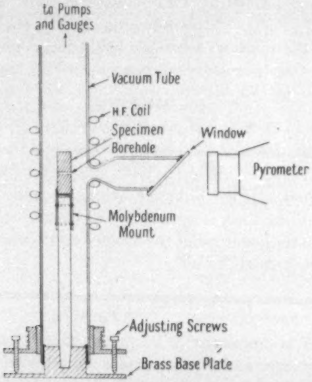

Emissivity furnace.

The vacuum tube was made in Pyrex and fitted inside the H.F. coil. A side arm was let into the tube just opposite the intended bore hole position and a plane glass window was waxed on to the end of an angle of 45° to the side arm axis. The pyrometer was then sighted through the window, down the arm at the bore hole. With this arrangement radiation was not reflected back by the concentric walls of the vacuum tube on to the specimen, which would have raised the apparent surface temperature without affecting the bore hole temperature. (These radiation reflection errors could have amounted to as much as 5° c.)

A Metrovic ionization vacuum gauge was mounted directly over the specimen. Pumping was by rotary and oil diffusion pumps with a liquid air trap between them and the vacuum tube.

A G.E.C. 1 kw. portable eddy current heating set, with variable power control, operating at approximately 10 Mc/s. was used, with a heating coil about 5 cm. long, 2·5 cm. diameter and of 5 turns.

A Leeds and Northrup optical pyrometer was used. The transmission curves of the red and neutral filters were measured and the mean effective wavelength was then calculated to be 0·652 μ for the temperature ranges used. The pyrometer was checked at intervals against standard lamps calibrated by the National Physical Laboratory.

§ 3. PROCEDURE

The following preliminary points were investigated using titanium specimens, suitable zirconium being very scarce (in view of the similarity between the two metals, it is unlikely that the conclusions with zirconium would have been different).

To check that the heated specimen was at a uniform temperature, readings were taken at various points on its surface. No change in temperature was detectable at any point on circles perpendicular to the axis of the specimen. A slight temperature gradient parallel to the axis of about ½° c. per mm. was noted, due probably to differences in coupling between coil and specimen. To avoid any error, measurements of surface temperature were taken on the circle containing the bore hole and close to it. The experimental readings were corrected for pyrometer errors and window absorption errors with the aid of standard lamps. Increased window absorption due to deposit of metallic vapour at higher temperatures was allowed for where necessary.

Buckley (1934) has calculated the theoretical minimum ratio of bore hole length to diameter necessary for the radiation to approximate to that of a black body. His figure was taken as a guide, but confirmatory experiments on holes of various dimensions were also carried out to check it. The final dimensions were: depth 6·0 mm., diameter 0·85 mm. As an added precaution, the inside of the hole was etched with hydrofluoric acid so as to give a pitted roughened surface.

A certain amount of surface thermal etching occurred, and to test its effect, an etched specimen was measured for emissivity, removed, repolished, remounted and again measured. No change was found. Similarly, although all specimens showed grain growth after a run, no change in emissivity with crystal orientation was observed.

§ 4. OBSERVATIONS

Pure titanium and zirconium change from hexagonal to body-centred cubic form at 880° c. and 865° c. respectively (Van Arkel 1939). Work done on zirconium indicated that the change point is spread over a temperature range when impurities such as oxygen are present (Fast 1938). From the analysis of the metal and Fast's work, it was thought that the transition of the zirconium used would not spread over more than 865–925° c. Similarly it was assumed that the titanium transition was between 880 and 940° c. Figures for emissivity inside these regions were thus rejected. Readings were taken at successively increasing temperatures, the whole run lasting 1½ to 2 hours. Mean pressures were normally about 2×10^{-5} mm. Hg at the start of a run and fell to about 8×10^{-6} mm. at the end. The temperature range was limited at the lower end by the increasing errors due to poor visibility and at the higher end by the power available and the rapid deposition of metallic vapour on the window.

Titanium. From the mean of three runs:

Hexagonal. Temperature range 810–870° c.

$\epsilon_\lambda = 0{\cdot}459$ at a mean temperature of 840° c.

No significant variation with temperature was detected.

Body-centred cubic. Temperature range 950–1,380° c.

Temp. (° c.)	950	1000	1100	1200	1300	1350
ϵ_λ	0·484	0·482	0·479	0·476	0·473	0·471

These figures were taken from the mean regression line, that is, the line best fitting the experimental points, of the three runs. Observational errors arose mainly in the readings and in power supply fluctuations. The standard deviation of the absolute value of ϵ_λ was 0·01 (corresponding to about 1·5° c. in temperature).

Zirconium. Work on this was limited by scarcity of material. From the mean of two runs :

Hexagonal. Temperature range 820–840° c.
$\epsilon_\lambda = 0{\cdot}436$ at a mean temperature of 825° c.
No variation with temperature was detected.

Body-centred cubic. Temperature range 1,020–1,540° c.
$\epsilon_\lambda = 0{\cdot}426$ at a mean temperature of 1,308° c.
No variation with temperature was detected.

The standard deviation of ϵ_λ was 0·013.

§ 5. SUMMARY AND ANALYSES

The following analyses for likely impurities were made by Messrs. Johnson Matthey and Co. Ltd.

Titanium bar sample :	Iron	0·096%	Magnesium	<0·002%
	Nickel	<0·002%	Oxygen	0·073%
	Silicon	0·056%	Nitrogen	0·19%
	Carbon	0·059%		
Zirconium bar sample :	Iron	0·36%	Magnesium	Nil
	Nickel	0·02%	Oxygen	0·075%
	Silicon	0·13%	Nitrogen	0·17%
	Carbon	0·048%		

The zirconium also contained hafnium, and a recent analysis of material from the same source gave the proportion as 3·0%.

It was known that both metals would adsorb gases during the experiment and one specimen each of titanium and zirconium was analysed for oxygen and nitrogen after a typical run. There was no detectable increase in oxygen or nitrogen in either case. The emissivity of a specimen held at 1,150° c. for 2½ hours (longer than any normal run) showed in the first 25 minutes a barely detectable rise (<0·008) and then remained at a steady value.

These emissivity results are different from those quoted by Van Arkel, who gives:

Titanium at $\lambda = 0{\cdot}655\,\mu$.

Temp. (° c.)	880	980	1080	1180	1280	1380
Emissivity	0·533	0·523	0·502	0·480	0·450	0·419

Zirconium at $\lambda = 0{\cdot}652\,\mu$.

Hexagonal emissivity	0·48
Body-centred emissivity	0·43

The purity of material and conditions of experiment were not given. However, evidence for the correctness of the present results at least for titanium is given by the work of Carpenter and Mair on the vapour pressure of titanium, shortly to be published. It is found that, using Van Arkel's figures to convert from brightness to true temperature, the latent heat of sublimation deduced from the temperature coefficient of the vapour pressure is inconsistent with that derived from the value of the free energy together with the known difference between the entropy of solid and gas. If the values of emissivity reported here are used to convert from brightness to true temperature the discrepancy disappears.

Michels and Wilford (1949) have recently given a minimum value for titanium emissivity of 0·59 (at 0·665 μ). The figure is certainly high compared with any of the above, but the material was of commercial purity.

ACKNOWLEDGMENTS

I wish to thank my colleagues at the Royal Aircraft Establishment, Farnborough, for their help in this work, and in particular Mr. L. G. Carpenter for his guidance throughout.

This paper is published with the permission of the Chief Scientist, Ministry of Supply, and of the Controller, H.M. Stationery Office.

REFERENCES

Bickerdike, R. L., and Sutcliffe, D. A., 1949, *Metallurgia, Manchr.*, **39**, 303.
Buckley, H., 1934, *Phil. Mag.*, **17**, 576.
Fast, J. D., 1938, *Metallwirtschaft*, **17**, 641.
Michels, W. C., and Wilford, S., 1949, *J. Appl. Phys.*, **20**, 1223.
Price, D. J., 1947, *Proc. Phys. Soc.*, **59**, 118.
Van Arkel, A. E., 1939, *Rein Metalle* (Berlin : Julius Springer), pp. 187 and 202.

Determination of the Elastic and Piezoelectric Coefficients of Monoclinic Crystals, with particular Reference to Ethylene Diamine Tartrate

By R. BECHMANN
Post Office Research Station, Dollis Hill, London

MS. received 14*th November* 1949

ABSTRACT. The dynamic determination of elastic and piezoelectric coefficients of crystals belonging to the monoclinic sphenoidal class is discussed using the longitudinal mode of vibration for narrow bars, low-frequency longitudinal and face-shear modes for square plates containing the axis of symmetry, coupled modes for square plates perpendicular to the axis of symmetry and the thickness-shear mode for plates containing the axis of symmetry. A new set of values for the elastic and piezoelectric coefficients and their temperature coefficients for ethylene diamine tartrate is given based on this method. Some properties are considered of face-shear vibrating square plates of ethylene diamine tartrate rotated about the axis of symmetry as functions of the orientation, and of Y-cut plates as functions of the breadth–length ratio.

§ 1. INTRODUCTION

The investigation of the performance of piezoelectric crystals involves the determination of their elastic and piezoelectric coefficients and this becomes more difficult with decreasing symmetry of the crystal. For instance, no example of the determination of the 21 elastic and 18 piezoelectric coefficients of a triclinic crystal (triclinic pedial class) has yet been published. However, the piezoelectric coefficients of several crystals representing the monoclinic sphenoidal class have been determined; e.g. tartaric acid (Tamaru 1905), cane sugar (Holman 1909), rhamnose (Meyer 1937), lithium sulphate (Spitzer 1938), di-ammonium tartrate (Spitzer 1938), dipotassium tartrate (DKT) (Spitzer 1938, Mason 1946, Jaffe 1948), ethylene diamine tartrate (EDT) (Mason 1947, Jaffe 1948, Bechmann and Lynch 1949). Of these crystals the elastic coefficients are known only for DKT and EDT; they were determined by Mason (1946, 1947), and this was the first determination of these coefficients for monoclinic crystals. The elastic and piezoelectric coefficients have been determined for numerous crystals belonging to classes of higher symmetry.

The method of determining the required coefficients should be the simplest and most reliable for the size and quantity of crystal available. New synthetic materials are usually available at first in small quantities only and this can impose severe limitations on the experimental technique employed. In the following, none of these limitations are assumed, and rough determinations on small crystals are not taken into consideration.

To determine the elastic coefficients of crystals of low symmetry, the simplest method is the dynamic one, in which the constants are deduced from observations of the natural frequencies, dimensions and density of piezoelectrically excited bars and plates made of the material to be tested. The piezoelectric coefficients can be measured statically and can also be determined from dynamic measurements on piezoelectrically excited bars and plates. The piezoelectric coefficients of a number of crystals have been measured by Spitzer (1938) by an improved static method, in which periodically varying stresses were used and for which accuracy within 1% was claimed.

Recently the dynamic methods have been more widely used. Mason (1946) has shown how both the elastic and piezoelectric coefficients can be determined dynamically, the elastic coefficients from measurements of resonance frequencies, and the piezoelectric coefficients by measurements of frequencies of resonance and anti-resonance. All the measurements were to be made on bars.

This paper describes a dynamic method in which the elastic and piezoelectric shear coefficients are deduced from the properties of square plates. This has the advantage of determining these constants more accurately and with greater reliability. The formulae for determination of the piezoelectric coefficients are given in terms of the dynamic capacitance in the equivalent circuit of the resonator, because the magnitude of this circuit element can be measured with satisfactory accuracy in several ways.

The following considerations are quite general for the monoclinic sphenoidal class. In accordance with the conventions for piezoelectric crystals the binary axis is taken as the *b* axis and as Y axis for the rectangular coordinate system used for the physical properties. The schemes of elastic, s_{ik}, and piezoelectric, d_{ik}, coefficients and permittivities, ϵ_{ik}, referred to this coordinate system, the Y axis being the axis of symmetry, are:

$$\begin{array}{cccccc}
s_{11} & s_{12} & s_{13} & 0 & s_{15} & 0 \\
 & s_{22} & s_{23} & 0 & s_{25} & 0 \\
 & & s_{33} & 0 & s_{35} & 0 \\
 & & & s_{44} & 0 & s_{46} \\
 & & & & s_{55} & 0 \\
 & & & & & s_{66}
\end{array}
\qquad
\begin{array}{cccccc}
0 & 0 & 0 & d_{14} & 0 & d_{16} \\
d_{21} & d_{22} & d_{23} & 0 & d_{25} & 0 \\
0 & 0 & 0 & d_{34} & 0 & d_{36}
\end{array}$$

$$\begin{array}{cccccc}
\epsilon_{11} & \epsilon_{22} & \epsilon_{33} & 0 & \epsilon_{13} & 0
\end{array} \qquad \ldots\ldots(1)$$

The scheme of coefficients of linear expansion a_{ik} corresponds to that of the permittivities ϵ_{ik}.

For the determination of all elastic and piezoelectric coefficients using the dynamic method, the following modes of vibration are used and the formulae for these modes are given in detail: longitudinal mode for narrow bars, low-frequency longitudinal and face-shear modes for square plates containing the axis of symmetry (Y axis), coupled modes for square plates perpendicular to the axis of symmetry, and thickness-shear mode for plates containing the axis of symmetry. For definitions of these modes see Cady (1946).

For crystals with higher symmetry, in general similar considerations hold good, but there are fewer coefficients, and the formulae are simpler on this account.

§2. LONGITUDINAL MODE FOR NARROW BARS

Some of the elastic and piezoelectric coefficients can be determined from measurements of the longitudinal mode of vibration of small bars. Provided that the surfaces perpendicular to the electric field, which is in the direction of the thickness, are fully covered with very thin conducting layers as electrodes, the other surfaces being free from conducting layers, the frequency of series resonance for a bar parallel to the Y′ axis is given by

$$\nu = \frac{1}{2l}\left(\frac{1}{\rho s_{22}'}\right)^{1/2}\left(1 + \frac{2\pi}{\epsilon_{22}'}\cdot\frac{d_{22}'^{2}}{s_{2}'} + \frac{2\pi}{\epsilon_{11}'}\frac{d_{12}'^{2}}{s_{22}'}\right), \qquad \ldots\ldots(2)$$

where l is the length of the bar and ρ its density, s_{22}' is the elastic coefficient in the direction of the length of the bar, d_{12}', d_{22}' are piezoelectric coefficients, ϵ_{22}', ϵ_{11}' are permittivities. The dashed symbols refer to any chosen direction of the orientation of the axis of the bar.

The frequency equation (2) contains two correction terms; first, if d_{22}' is not zero, space charges distributed along the length of the bar appear, and thus the elastic coefficient is changed; second, if the piezoelectric coefficient d_{12}' in the direction of the breadth of the bar is not zero, there is another term due to the boundary conditions caused by the surface charges on these faces.

The piezoelectric coefficient d_{32}' is given in terms of the frequency ν and the dynamic capacitance C_{k} of the equivalent electric circuit (in E.S.U.)

$$d_{32}' = \left(\frac{\pi^2}{32\rho}\cdot\frac{C_{\mathrm{k}}}{\nu^2}\cdot\frac{t}{bl^3}\right)^{1/2}, \qquad \ldots\ldots(3)$$

where b and t are the breadth and thickness of the bar.

To define the orientation of the bar in the coordinate system given, a polar coordinate system is used as shown in Figure 1, the Y axis (binary axis) being polar axis. A plane containing the Y axis, rotated from the positive Z axis to the positive X axis, is determined by the angle ϕ. For a bar with its length in this plane, the axis of the bar is defined by the angle θ, measured from the positive Y axis. The angle ψ describes a rotation of the bar about its own axis. It gives the direction of the piezoelectric excitation. $\psi = 0$ means that the direction of the electric field falls in the plane considered containing the Y axis. For $\psi = 90°$ the electric field is perpendicular to this plane. The angle ψ therefore indicates the particular surface intended to carry the electrodes. In the above formulae the direction of the electric field corresponds to the thickness of the bar.

The well-known general expressions for s_{ik}' and d_{ik}' as functions of the direction cosines are simplified for the particular case of monoclinic sphenoidal class with the scheme (1) of s_{ik} and d_{ik}. Using the above-mentioned polar coordinate system with the Y axis as the polar axis, the following equations for the coefficients s_{22}', d_{32}', d_{22}' and the permittivities ϵ_{22}', ϵ_{11}' are obtained:

$$\begin{aligned} s_{22}' = {} & [s_{33}\cos^4\phi + s_{11}\sin^4\phi + (s_{55}+2s_{13})\sin^2\phi\cos^2\phi \\ & + 2s_{15}\sin^3\phi\cos\phi + 2s_{35}\sin\phi\cos^3\phi]\sin^4\theta \\ & + [(s_{44}+2s_{23})\cos^2\phi + (s_{66}+2s_{12})\sin^2\phi \\ & + 2(s_{25}+s_{46})\sin\phi\cos\phi]\sin^2\theta\cos^2\theta + s_{22}\cos^4\theta \qquad \ldots\ldots(4) \end{aligned}$$

$$\begin{aligned} d_{32}' = {} & \cos\psi[\{d_{23}\cos^2\phi + d_{21}\sin^2\phi + d_{25}\sin\phi\cos\phi\}\sin^3\theta \\ & + \{(d_{22}-d_{34})\cos^2\phi + (d_{22}-d_{16})\sin^2\phi \\ & - (d_{14}+d_{36})\sin\phi\cos\phi\}\sin\theta\cos^2\theta] \\ & - \sin\psi[d_{14}\cos^2\phi - d_{36}\sin^2\phi + (d_{16}-d_{34})\sin\phi\cos\phi]\sin\theta\cos\theta \\ & \qquad \ldots\ldots(5) \end{aligned}$$

$$\begin{aligned} d_{22}' = {} & [(d_{23}+d_{34})\cos^2\phi + (d_{21}+d_{16})\sin^2\phi + (d_{14}+d_{25}+d_{36})\sin\phi\cos\phi] \\ & \times \sin^2\theta\cos\theta + d_{22}\cos^3\theta \qquad \ldots\ldots(5\,a) \end{aligned}$$

$$\begin{aligned} \epsilon_{11}' = {} & \cos^2\psi[\epsilon_{11}\cos^2\phi + \epsilon_{33}\sin^2\phi - 2\epsilon_{13}\sin\phi\cos\phi] \\ & + \sin^2\psi[\{\epsilon_{33}\cos^2\phi + \epsilon_{11}\sin^2\phi + 2\epsilon_{13}\sin\phi\cos\phi\}\cos^2\theta + \epsilon_{22}\sin^2\theta] \\ & - \sin\psi\cos\psi[(\epsilon_{11}-\epsilon_{33})\sin 2\phi + 2\epsilon_{13}\cos 2\phi]\cos\theta \qquad \ldots\ldots(6) \end{aligned}$$

$$\epsilon_{22}' = [\epsilon_{33}\cos^2\phi + \epsilon_{11}\sin^2\phi + 2\epsilon_{13}\sin\phi\cos\phi]\sin^2\theta + \epsilon_{22}\cos^2\theta. \qquad \ldots\ldots(6\,a)$$

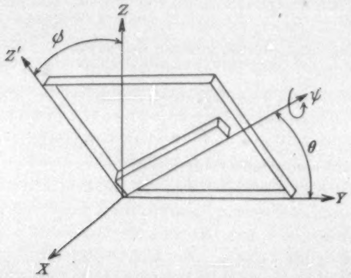

Figure 1. Diagram illustrating the coordinates used to define the orientation of bars.

The formulae (4), (5 *a*) and (6 *a*) for s_{22}', d_{22}' and ϵ_{22}' are independent of ψ. The coefficient d_{12}' appearing in equation (2) is obtained from d_{32}' (equation (5)) by writing $\pi/2+\psi$ for ψ.

For bars in various coordinate and inclined planes the formulae simplify to

(i) bars in the YZ plane: $\phi = 0$

$$
\begin{aligned}
& s_{22}' = s_{22}\cos^4\theta + s_{33}\sin^4\theta + (s_{44} + 2s_{23})\sin^2\theta\cos^2\theta, \\
\psi = 0: \quad & d_{32}' = d_{23}\sin^3\theta + (d_{22} - d_{34})\sin\theta\cos^2\theta, \\
\psi = 90^\circ: \quad & d_{32}' = -d_{14}\sin\theta\cos\theta;
\end{aligned}
$$

(ii) bars in the XY plane: $\phi = 90^\circ$

$$
\begin{aligned}
& s_{22}' = s_{22}\cos^4\theta + s_{11}\sin^4\theta + (s_{66} + 2s_{12})\sin^2\theta\cos^2\theta, \\
\psi = 0: \quad & d_{32}' = d_{21}\sin^3\theta + (d_{22} - d_{16})\sin\theta\cos^2\theta, \\
\psi = 90^\circ: \quad & d_{32}' = d_{36}\sin\theta\cos\theta;
\end{aligned}
$$

(iii) bars in the XZ plane: $\theta = 90^\circ$

$$
\begin{aligned}
& s_{22}' = s_{33}\cos^4\phi + s_{11}\sin^4\phi + (s_{55} + 2s_{13})\sin^2\phi\cos^2\phi \\
& \qquad + 2s_{15}\sin^3\phi\cos\phi + 2s_{35}\sin\phi\cos^3\phi, \\
\psi = 0: \quad & d_{32}' = d_{23}\cos^2\phi + d_{21}\sin^2\phi + d_{15}\sin\phi\cos\phi, \\
\psi = 90^\circ: \quad & d_{32}' = 0;
\end{aligned}
$$

(iv) bars in the plane: $\phi = 45^\circ$

$$
\begin{aligned}
& s_{22}' = \tfrac{1}{4}[s_{11} + s_{33} + s_{55} + 2s_{13} + 2s_{15} + 2s_{35}]\sin^4\theta \\
& \qquad + \tfrac{1}{2}[s_{44} + 2s_{23} + s_{66} + 2s_{12} + 2(s_{25} + s_{46})]\sin^2\theta\cos^2\theta \\
& \qquad + s_{22}\cos^4\theta, \\
\psi = 0: \quad & d_{32}' = \tfrac{1}{2}[(d_{21} + d_{23} + d_{25})\sin^3\theta + \{(d_{22} - d_{34}) + (d_{22} - d_{16}) \\
& \qquad - (d_{14} + d_{36})\}\sin\theta\cos^2\theta], \\
\psi = 90^\circ: \quad & d_{32}' = -\tfrac{1}{2}[(d_{14} - d_{36}) + (d_{16} - d_{34})]\sin\theta\cos\theta.
\end{aligned}
$$

Using the measurements of frequency, capacitance and dimensions of an adequate number * of suitably orientated bars in the planes considered above and solving the appropriate equations it is possible to determine: 5 elastic coefficients: s_{11}, s_{22}, s_{33}, s_{15}, s_{35}; 4 combinations of elastic coefficients: $s_{44} + 2s_{23}$, $s_{55} + 2s_{13}$, $s_{66} + 2s_{12}$, $s_{25} + s_{46}$; 5 piezoelectric coefficients: d_{21}, d_{23}, d_{25}, d_{14}, d_{36}; 3 combinations of piezoelectric coefficients: $d_{22} - d_{16}$, $d_{22} - d_{34}$, $d_{16} - d_{34}$.

§3. LOW-FREQUENCY LONGITUDINAL AND FACE-SHEAR MODES OF SQUARE PLATES CONTAINING THE AXIS OF SYMMETRY (Y AXIS)

Generally, square and rectangular plates of any orientation can be excited by an electric field normal to the plates in modes dependent on the contour, and these are modified by the coupling of longitudinal and shear modes (Bechmann 1941, 1942). In particular, square plates having their major planes and one edge parallel to the axis of symmetry can only be excited in a pure shear mode given by the elastic coefficient s_{44}' because s_{24}' and s_{34}', which cause the coupling between longitudinal and shear modes, both vanish. If one edge is inclined at 45° to the

---

* The signs of the piezoelectric coefficients must be regarded as an additional unknown quantity, see § 6.

axis of symmetry, then $s_{22}'=s_{33}'$ and $s_{24}'=s_{34}'$ and the plate can be excited in a longitudinal mode *, the resultant elastic coefficient being $s_{22}'-s_{23}'$. For two square plates in the same plane, one inclined 45° to the axis of symmetry and the other parallel to this axis (0°), there is the relation

$$(s_{22}'-s_{23}')_{45^\circ}=\tfrac{1}{2}(s_{44}')_{0^\circ} \quad \text{and} \quad (d_{12}')_{45^\circ}=-(d_{13}')_{45^\circ}=\tfrac{1}{2}(d_{14}')_{0^\circ}.$$

Using the above-mentioned polar coordinate system the plate parallel to the Y axis is defined by the angle Θ between the normal of the plate and the X axis. The angle Θ is measured from the positive direction of the X axis towards the negative direction of the Z axis. The elastic and piezoelectric coefficients s_{44}' and d_{14}' as functions of the angle Θ are

$$\left.\begin{aligned} s_{44}'&=s_{44}\cos^2\Theta+s_{66}\sin^2\Theta+2s_{46}\sin\Theta\cos\Theta,\\ d_{14}'&=d_{14}\cos^2\Theta-d_{36}\sin^2\Theta+(d_{16}-d_{34})\sin\Theta\cos\Theta.\end{aligned}\right\} \qquad \ldots\ldots.(7)$$

The expression for the series resonance frequency for the longitudinal and shear modes of square plates can be written in the same form:

$$\nu=\frac{a\sqrt{2}}{2l}\sqrt{\left(\frac{1}{\rho s_{44}'}\right)}, \qquad \ldots\ldots(8)$$

where l is the length of the square. The factor a is equal to 1 for the longitudinally vibrating plates inclined at 45° to the axis of symmetry ; formula (8) is an exact solution for this case. The factor a for the shear mode in equation (8) was first determined empirically from quartz (Hight and Willard 1937, Bechmann 1942). For an isotropic plate Ekstein (1944) gives the value $a=a_0=0{\cdot}9132$; Mähly and Trösch (1947) give $a_0=x\sqrt{2}/\pi$ where x is root of equation

$$\tan x+x=0. \qquad \ldots\ldots(9)$$

$x=2{\cdot}0288$ is the first root and therefore $a_0=0{\cdot}9132$. An improved theory of shear vibration of square plates by Mähly and Trösch (1947) taking into consideration longitudinal effects gives a corrected value $a=a_0(1-A\sqrt{\sigma})$ and A becomes

$$A=\frac{1}{2x}\left(\frac{x^2-2}{x^2+2}\right)^{3/2}=0{\cdot}0501_2,$$

where for an isotropic plate $(s_{22}=s_{33}')$, $\sigma=s_{22}/s_{44}$. In the case considered where $s_{22}\neq s_{33}'$ an average value between σ formed with s_{22} and s_{33}' can be used. This value for a is only an approximation, but it has been shown experimentally to be reliable. If both kinds of plates are used and N_{0° means the frequency constant (i.e. the product of frequency and length) for the plate with one edge parallel to the Y axis, and N_{45° the frequency constant for the plate at the same angle Θ but inclined at 45° to the Y axis, then

$$\left(\frac{N_{0^\circ}}{N_{45^\circ}}\right)_{\Theta}=a. \qquad \ldots\ldots(10)$$

---

* This longitudinal mode agrees with one of the longitudinal modes (mode 1) derived by Ekstein (1944) whose equation (48) for a Z-cut quartz plate, or an isotropic plate, is $\rho\omega^2=k^2(\gamma_{11}-\gamma_{12})$ with

$$\gamma_{11}=\frac{s_{11}}{s_{11}^2-s_{12}^2}, \qquad \gamma_{12}=\frac{-s_{12}}{s_{11}^2-s_{12}^2}, \qquad \text{that is} \qquad \gamma_{11}-\gamma_{12}=\frac{1}{s_{11}-s_{12}}=\frac{1}{\frac{1}{2}s_{66}}.$$

Another mode can also be excited in a plate rotated about 45° to the axis of symmetry which corresponds with Ekstein's longitudinal mode 2.

According to the above expressions, a is slightly dependent on the direction of the particular orientation Θ and also on the material.

For the longitudinally vibrating square plate inclined at 45° to the axis of symmetry the piezoelectric coefficient d_{14}' expressed in terms of series resonance frequency ν and the capacitance C_k is given by*

$$d_{14}' = \left(\frac{\pi^4}{128\rho}\cdot\frac{C_k}{\nu^2}\cdot\frac{t}{l^4}\right)^{1/2}, \qquad \ldots\ldots(11)$$

where t is the thickness of the plate. In the case of the shear vibrating square plate parallel to the axis the expression for d_{14}' becomes

$$d_{14}' = \left(\frac{(x^2+2)x^2}{4\pi^2\rho}\cdot\frac{C_k}{\nu^2}\cdot\frac{t}{l^4}\right)^{1/2}; \qquad \ldots\ldots(12)$$

x means the root of equation (9).

Summarizing, from measurements of these plates, the following coefficients can be obtained: 3 elastic coefficients s_{44}, s_{66}, s_{46}, 2 piezoelectric coefficients d_{14}, d_{36}, and the combination of the piezoelectric coefficients $d_{16}-d_{34}$.

§ 4. SQUARE PLATES WITH COUPLED MODES PERPENDICULAR TO THE AXIS OF SYMMETRY (Y AXIS)

For the determination of s_{55} and s_{13} which are known from § 2 as a combination $s_{55}+2s_{13}$ it is necessary to use bars or plates vibrating in a coupled mode. A simple case is a square plate perpendicular to the axis of symmetry (Y axis), having edges parallel to the X and Z axes. An approximate frequency equation recently given for three of the main modes of a square plate (Bechmann 1942) is

$$\begin{vmatrix} s_{11}-s & s_{13} & s_{15} \\ s_{13} & s_{33}-s & s_{35} \\ s_{15} & s_{35} & s_{55}-2a^2s \end{vmatrix} = 0, \qquad \ldots\ldots(13)$$

where $s=1/4\rho\nu^2l^2$, l is the edge-length of the square and a the factor already mentioned in § 3. The only unknown elastic coefficients in this equation are s_{55} and s_{13}. From measurements of the three frequencies the elastic coefficients $s_i (i=1, 2, 3)$ can be found, and these should agree with the roots of the equation (13). There are then two equations containing s_{55} and s_{13} and the solution can be obtained as a cubic in either one. On the other hand the expression $s_{11}+s_{33}+s_{55}/2a^2$ is an invariant of the cubic equation (13), and since this equals the sum of $s_1+s_2+s_3$ the elastic coefficient s_{55} can be obtained. It must be checked, however, that s_1, s_2 and s_3 equal the roots of the frequency equation (13). Therefore, to be quite sure, both forms of determination should be used. The errors in s_{55} and s_{13} include any error of the value a.

Hence all the elastic coefficients can be determined.

§ 5. THICKNESS SHEAR MODE FOR PLATES CONTAINING THE AXIS OF SYMMETRY

The piezoelectric coefficients d_{16}, d_{22} and d_{34} are combined with each other in all the above formulae. To solve these combinations, at least one of them must be determined. This can be done by means of longitudinally vibrating bars parallel to the Y axis, excited by a field along their length; the piezoelectric coefficient is then d_{22}. The value for the capacitance becomes very small for narrow bars. A more convenient method uses plates mentioned before (§3), rotated about the Y axis and excited in a thickness mode. Only one mode, the thickness-shear mode, is excitable. The formulae for frequency and capacitance are expressed in terms of elastic and piezoelectric moduli, c_{ik} and e_{ik}, instead of s_{ik} and d_{ik}.

---

* Details of derivation of the equations (11) and (12) will be given in a later paper.

For the thickness-shear mode of the plate *

$$\nu = \frac{1}{2t}\left(\frac{c_{66}'}{\rho}\right)^{1/2}\left(1+\frac{2\pi e_{16}'^2}{\epsilon_{11}'c_{66}'}-\frac{16e_{16}'^2}{\pi\epsilon_{11}'c_{66}'}\right). \qquad \ldots\ldots(14)$$

The piezoelectric modulus e_{16}', given in terms of series resonance frequency ν and capacitance C_k is:

$$e_{16}' = \left(\frac{\pi^2\rho}{2}.C_k\nu^2.\frac{t^3}{A}\right)^{1/2}, \qquad \ldots\ldots(15)$$

where A is the area of the plate covered with a thin conducting layer, and t the thickness. In the case of the plates referred to, rotated about the Y axis at the angle Θ,

$$\left.\begin{aligned} c_{66}' &= c_{66}\cos^2\Theta + c_{44}\sin^2\Theta - 2c_{46}\sin\Theta\cos\Theta,\\ e_{16}' &= e_{16}\cos^2\Theta + e_{34}\sin^2\Theta - (e_{14}+e_{36})\sin\Theta\cos\Theta,\\ \epsilon_{11}' &= \epsilon_{33}\cos^2\Theta + \epsilon_{11}\sin^2\Theta - 2\epsilon_{13}\sin\Theta\cos\Theta.\end{aligned}\right\} \qquad \ldots\ldots(16)$$

Between the elastic moduli c_{44}, c_{66}, c_{46} and the elastic coefficients s_{44}, s_{66}, s_{46}, and the piezoelectric moluli e_{14}, e_{16}, e_{34}, e_{36} and the piezoelectric coefficients d_{14}, d_{16}, d_{34}, d_{36}, there are the relations

$$\left.\begin{aligned} c_{44} &= s_{66}\Delta & \qquad s_{44} &= c_{66}\Delta'\\ c_{66} &= s_{44}\Delta & s_{66} &= c_{44}\Delta'\\ c_{46} &= -s_{46}\Delta & s_{46} &= -c_{46}\Delta'\\ \frac{1}{\Delta} &= s_{44}s_{66}-s_{46}^2 & \frac{1}{\Delta'} &= c_{44}c_{66}-c_{46}^2\end{aligned}\right\} \qquad \ldots\ldots(17)$$

and

$$e_{14}+e_{36} = d_{14}c_{44}+d_{36}c_{66}+(d_{16}+d_{34})c_{46} \qquad d_{16}+d_{34} = e_{34}s_{44}+e_{16}s_{66}+(e_{14}+e_{36})s_{46}. \qquad \ldots\ldots(18)$$

These results combined with those already obtained give the piezoelectric coefficients d_{16}, d_{22}, d_{34}. Hence all the piezoelectric coefficients can be determined. There can also be found 3 elastic moduli: c_{44}, c_{66}, c_{46}, and 4 piezoelectric moduli: e_{14}, e_{16}, e_{34}, e_{36}.

---

* Cady (1946, p. 315) quotes an error in the author's former publication (1940) where the additional term for the elastic modulus produced by the piezoelectric effect in formulae (30) and (32 *a*) is given as $c+8\pi e^2/\epsilon$. As Cady points out, this term should read $c+4\pi e^2/\epsilon$. The electric field is not independent and cannot therefore be regarded as an independent variable. This introduces the additional factor 2.

§6. MEASUREMENTS AND ACCURACY OF THE DYNAMICALLY DETERMINED COEFFICIENTS

For an exact determination of the coefficients, various influences must be taken into account. The first question is whether the condition in which the bars and plates were measured agrees with the condition on which the formulae were based. For example, bars must be small enough for errors due to the influence of the breadth–length or thickness–length ratio to be unimportant. It must be checked carefully that no disturbing frequencies are present which might influence the results. In particular, when bars having certain dimensional ratios are vibrating longitudinally, flexural modes can be excited by coupling. For example, in a bar of any material of which the width is about 0·21 times the length (see §7(ii)), the frequency of the second flexural mode coincides with that of the longitudinal mode. If the coupling coefficient between the longitudinal and shear modes is not zero, the properties of the coupled vibration differ from those of the longitudinal vibration, and ratios near this critical value should therefore be avoided. To avoid disturbances due to coupling with other modes, it may occasionally be necessary to alter the dimensions of the specimens.

Using bars and plates belonging to any group considered above more than the minimum number of differently orientated specimens should be measured, so that average values can be determined and an estimate made of the accuracy of the resulting values. Some of the coefficients can be determined independently from different modes of vibration. The values for piezoelectric coefficients determined from measurement on crystals vibrating in different modes show a slight systematic discrepancy which seems due to the fundamental equations of vibration on which the formulae were based. The maximum variation, assuming perfect measurements, is in the order of 1 to 3%. It is thought that the correct value is most likely to correspond with results obtained from longitudinally vibrating square plates. This will be discussed in a later paper already mentioned.

The dynamic method for the determination of piezoelectric coefficients, which only gives the square of these coefficients and in general the square of a combination of such values, results in an ambiguity in the sign which must be taken into account. The sign of one of the coefficients d_{ik} must be chosen according to an arbitrary definition in terms of static effect.

In all formulae for the determination of s_{ik} and d_{ik}, the expresssions ρs_{ik} and $\sqrt{\rho}\, d_{ik}$ occur, so that all values have systematic errors equal to those of ρ and $\sqrt{\rho}$ respectively. The following errors and uncertainties should be taken into consideration: specimens prepared from unsatisfactory material, errors in orientation, inaccuracy of dimensions, inaccuracy of the shapes of bars and plates, influence of silver layer and of mounting, and perhaps influence of the atmospheric pressure and humidity. These inaccuracies relate to values of s_{ik}' and d_{ik}'. The inaccuracy may become numerically greater for values s_{ik} and d_{ik} obtained from combinations of s_{ik}' and d_{ik}'.

The temperature coefficients $T(s_{ik}')$ of the elastic coefficients can be determined from the measured temperature coefficients $T(\nu)$ of frequency by the formula

$$T(s_{ik}') = \frac{1}{s_{ik}'}\frac{\partial s_{ik}'}{\partial T} = -2T(\nu) + \beta_1. \qquad \ldots\ldots(19)$$

Similarly the temperature coefficients $T(d_{ik}')$ of the piezoelectric coefficients can be obtained from measured temperature coefficients $T(C_k)$ and $T(\nu)$ of the capacitance and frequency respectively from the equation

$$T(d_{ik}') = \frac{1}{d_{ik}'}\frac{\partial d_{ik}'}{\partial T} = \tfrac{1}{2}T(C_k) - T(\nu) + \beta_2, \qquad \ldots\ldots(20)$$

where β_1 and β_2 are functions of the coefficients of linear expansion which depend on the mode of vibration and the orientation of the bars or plates. The temperature coefficients $T(s_{ik})$ and $T(d_{ik})$ can be found from the $T(s_{ik}')$ and $T(d_{ik}')$ by solving the appropriate equations in the same way as s_{ik} and d_{ik} were obtained from the observed values s_{ik}' and d_{ik}'.

§ 7. RESULTS ON ETHYLENE DIAMINE TARTRATE

A new determination of elastic and piezoelectric coefficients and their temperature coefficients was made on anhydrous ethylene diamine tartrate. The values for the capacitance of the specimens were obtained from measurements of the effective capacitance near resonance. This method has been described by Lynch (1950).* Table 1 contains the values for the adiabatic elastic coefficients.

Table 1. Elastic Coefficients for EDT in 10^{-13} cm^2 dyne^{-1}

s_{ik}	Mason	New values	s_{ik}	Mason	New values	s_{ik}	Mason	New values
s_{11}	38·8	33·4	s_{23}	−19	−18	s_{15}	− 5	−17
s_{22}	37·6	36·5	s_{44}	187	$191\cdot_{8}$	s_{25}	1	15
s_{33}	98	$100\cdot_{2}$	s_{55}	171·5	$116\cdot_{5}$	s_{35}	−25	−26·5
s_{12}	3	− 3	s_{66}	173	$191\cdot_{4}$	s_{46}	− 2	3·8
s_{13}	−52	−30						

The error in the values of the main coefficients is of the order of 0·5 to 2% and that of the other coefficients does not exceed 5%. Table 1 also contains values given previously by Mason (1947) which agree substantially, but there are differences for s_{55}, s_{12}, s_{13}, s_{15} and s_{25}. Table 2 shows the values for the temperature

Table 2. Temperature Coefficients of the Elastic Coefficients for EDT in 10^{-6}/°c.

$T(s_{ik})$		$T(s_{ik})$		$T(s_{ik})$		$T(s_{ik})$	
$T(s_{11})$	290	$T(s_{13})$	−2280	$T(s_{55})$	−280	$T(s_{25})$	−730
$T(s_{22})$	640	$T(s_{23})$	−55	$T(s_{66})$	320	$T(s_{35})$	2220
$T(s_{33})$	−95	$T(s_{44})$	260	$T(s_{15})$	−85	$T(s_{46})$	−28600
$T(s_{12})$	150						

Table 3. Piezoelectric Coefficients for EDT in 10^{-8} E.S.U. dyne^{-1}

d_{ik}	Mason	Jaffe	New values	d_{ik}	Mason	Jaffe	New values
d_{14}	23·5		−30·4	d_{23}	31	−36·9±3	−34·0
d_{16}	37		−36·6	d_{25}	14	−55·2±6	−53·8
d_{21}	34	+33·9±3	+30·3	d_{34}	37·5		−50·9
d_{22}	−20	+ 5·4±1·5	+ 6·6	d_{36}	50		−55·1

---

* The measurements of capacitance of various specimens were made by A. C. Lynch.

coefficients $T(s_{ik})$ of the elastic coefficients, which are accurate to within about 10%. The temperature coefficient for s_{46} has an unusually high negative value. Table 3 contains values of the piezoelectric coefficients, which are accurate to within about 3%. It also includes values first given by Mason (1947) and by Jaffe (1948); Jaffe's measurements were made by an electrostatic method. The new values quoted for 20° c. are practically identical with those recently published (Bechmann and Lynch 1949), but the values for d_{14} and d_{36} are improved. Some of the values of the temperature coefficients for the piezoelectric coefficients $T(d_{ik})$ and the values for the combinations $T(d_{22}-d_{16})$, $T(d_{16}-d_{34})$, $T(d_{22}-d_{34})$ are given in Table 4. The error in these values is less than 10%.

Table 4. Temperature Coefficients of Piezoelectric Coefficients for EDT in $10^{-4}/°$c.

$T(d_{ik})$		$T(d_{ik})$		$T(d_{ik})$	
$T(d_{14})$	− 7·3	$T(d_{23})$	−47	$T(d_{22}-d_{34})$	−25
		$T(d_{25})$	−10	$T(d_{16}-d_{34})$	−48
$T(d_{21})$	−18·5			$T(d_{22}-d_{16})$	−21
		$T(d_{36})$	−15·2		

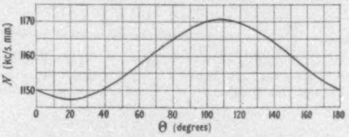

Figure 2. Variation of frequency constant with orientation for shear vibrating square plates of ethylene diamine tartrate rotated about the Y axis.

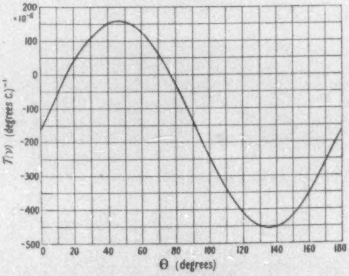

Figure 3. Variation of temperature coefficient of frequency for shear vibrating square plates of ethylene diamine tartrate rotated about the Y axis.

The values are based on the value for the density (see *Analytical Chemist* 1948) $\rho=1·538$ gm. cm^{-3} and the coefficients of linear expansion according to Mason's values: $a_{11}=0$, $a_{22}=20·3$, $a_{33}=80$, $a_{13}=-32\times10^{-6}/°$c. The values for the permittivities are required only in the correction terms of equations (2) and (14), and the values $\epsilon_{11}=5$, $\epsilon_{22}=8·2$, $\epsilon_{33}=6$, $\epsilon_{13}=0·65$ were used. The temperature coefficients are average values in the range of about 20 to 50° c.

Some interesting special cases may be derived from these values:

(i) *Square plates rotated about the Y axis, vibrating in contour shear mode.*

The frequency constant $N=\nu l$ (equation (8)) is shown as a function of the angle Θ in Figure 2; the temperature coefficient of frequency is given in Figure 3. At the angles $\Theta=17°$ and $77°$ the temperature coefficient of frequency is zero (Bechmann 1949). Although the temperature coefficients $T(s_{44})$ and $T(s_{66})$ have the same sign, the zero points are caused by the high negative value of $T(s_{46})$ which balances the values $T(s_{44})$ and $T(s_{66})$ at these angles. The coefficient of inductance $L_0=L/t$ derived from equation (12), where $L=1/4\pi^2\nu^2C_k$, is given in Figure 4, as function of the angle Θ. Finally, Figure 5 shows the temperature coefficient of L which is zero for $\Theta=13°$ and $136°$. All these curves have been calculated from the values given above. The factor a in equation (8) has the observed values for $\Theta=0°$: $a=0{\cdot}882$; $\Theta=77°$: $a=0{\cdot}898$; $\Theta=90°$: $a=0{\cdot}894$.

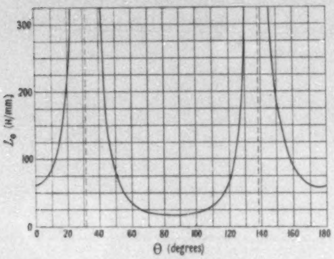

Figure 4. Variation of inductance coefficient for shear vibrating square plates of ethylene diamine tartrate rotated about the Y axis.

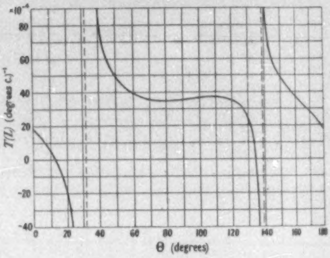

Figure 5. Variation of temperature coefficient of inductance for shear vibrating square plates of ethylene diamine tartrate rotated about the Y axis.

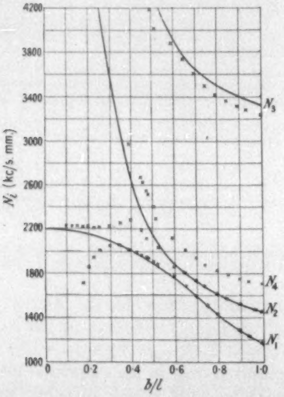

Figure 6. Variation of frequency constants with breadth–length ratio for Y cut plates of ethylene diamine tartrate.

(ii) ***Plate perpendicular to the Y axis.***

The calculated and measured frequency constants $N_i (i=1,2,3)$ of the three vibrations of a plate perpendicular to the Y axis as mentioned before in §4, are given in Figure 6 as a function of the breadth–length ratio, the reduced dimension being perpendicular to the X axis. This calculation was made in the same way as recently for quartz plates (Bechmann 1942). The curves are plotted from calculated results and crosses refer to observed values. For very small values of b/l, N_1 alone remains finite, as this represents the longitudinal vibration of a narrow bar. As the frequency for the longitudinal mode of a small bar is approximately

$$\nu = \frac{1}{2l}\sqrt{\left(\frac{1}{\rho s}\right)}$$

and that for the second flexural mode

$$\nu = \frac{\kappa^2}{4\pi\sqrt{3}}\,\frac{b}{l^2}\sqrt{\left(\frac{1}{\rho s}\right)},$$

both frequencies coincide when $b/l=0{\cdot}21$, as $\kappa=7{\cdot}20$ (Mason 1942) for this ratio. When the longitudinal mode is coupled through the shear mode to the second flexural mode, the coupling effect shown in Figure 6 at about this ratio occurs. This effect is already known in quartz bars. However, it is not included in the calculation for N as shown in Figure 6. N_3 represents the coupled mode, given by the breadth of the plate, and N_4 is unidentified, but this vibration may be related to mode 2 described by Ekstein (1944) since d_{21} and d_{23} have opposite signs.

ACKNOWLEDGMENTS

The author wishes to thank Miss S. Rodwell for assistance in measurements and calculations.

Acknowledgment is made to the Engineer-in-Chief of the General Post Office for permission to make use of the information contained in this paper.

REFERENCES

BECHMANN, R., 1940, *Hochfrequenztech. u. Elektroakust.*, **56,** 14; 1941, *Z. Phys.*, **117,** 180; 1942, *Ibid.*, **118,** 515, **120,** 107; 1949, *Nature, Lond.*, **164,** 190.

BECHMANN, R., and LYNCH, A. C., 1949, *Nature, Lond.*, **163,** 915.

CADY, W. G., 1946, *Piezoelectricity* (New York : McGraw-Hill).

EKSTEIN, H., 1944, *Phys. Rev.*, **66,** 108.

HIGHT, S. C., and WILLARD, G. W., 1937, *Proc. Inst. Radio Engrs.*, **25,** 549.

HOLMAN, W. F., 1909, *Ann. Phys., Lpz.*, **29,** 160.

JAFFE, H., 1948, *Phys. Rev.*, **73,** 1467.

LYNCH, A. C., 1950, *Proc. Phys. Soc.* B, **63,** 323.

MÄHLY, H., and TRÖSCH, A., 1947, *Helv. Phys. Acta*, **20,** 253.

MASON, W. P., 1942, *Electromechanical Transducers* (New York : D. van Nostrand); 1946, *Phys. Rev.*, **70,** 705; 1947, *Proc. Inst. Radio Engrs.*, **35,** 1005.

MEYER, G., 1937, *Ph.D. Thesis*, Göttingen.

SPITZER, F., 1938, *Ph.D. Thesis*, Göttingen.

TAMARU, T., 1905, *Phys. Z.*, **6,** 379.

1948, *Analytical Chemist*, **20,** 491.

Some Measurements of the Resistivity of Good Insulators

By N. W. RAMSEY
Radiotherapy Department, Charing Cross Hospital

Communicated by J. E. Roberts; MS. received 25*th July* 1949, *and in amended form* 3*rd January* 1950.

ABSTRACT. Measurements of the resistivity of good insulators were carried out by measuring the loss of charge on a condenser. A knowledge of the dimensions of the insulator is not required. It was found that the insulation resistances of amber, alkathene, distrene and Perspex increase with time over a period of weeks, the final values being considerably higher than previously published figures. There is no significant difference between the values for the first three materials. The leakage time necessary for reasonable accuracy is indicated.

§1. INTRODUCTION AND EXPERIMENTAL PROCEDURE

From experience in Radiological Physics, doubts of previously accepted values had arisen in view of the performance of the type of condenser ionization chamber used in measurements.

Observations were taken of the insulation resistance of the insulators of some condenser ionization chambers of the type used for the measurement of intracavitary x-ray dosage in radiotherapy (Farmer 1945). A cross section of the cylindrical chambers used is seen in the Figure. The insulators under test (see list below) were coated with graphite inside and outside before assembly, in order to improve contact with the electrodes and to eliminate stray capacities.

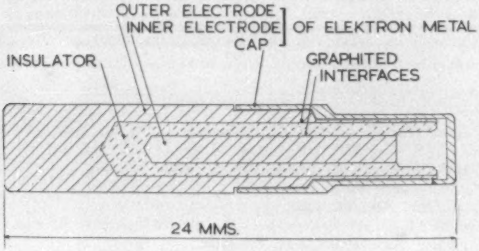

Condenser ionization chamber.

Natural amber, two samples.

Alkathene, samples 1 and 2: normal grade 20 alkathene; sample 3: grade 20 made in presence of small percentage of carbon monoxide. All three samples were supplied by Imperial Chemical Industries Ltd.

Distrene, one sample: commercial brand of polystyrene, supplied by BX Plastics Ltd.

Perspex, one sample: unplasticized Perspex acrylic rod (methyl methacrylate monomer), supplied by Imperial Chemical Industries Ltd.

The condensers, after being charged, were kept in a desiccator and the loss in charge over periods varying from a few days to several months was measured with a valve electrometer of the type devised by Farmer for use with small ionization chambers (Farmer 1942).

The potential gradient across the insulators was about 130 volts/mm. when the condensers were freshly charged, except in the case of the Perspex insulators, when the gradient was about 100 volts/mm. During the leakage periods the decrease in potential gradient was up to 50% for Perspex and up to about 20% for the other insulators.

§2. CALCULATION OF RESULTS

Treating the specimen for which the resistivity is to be found as a condenser in parallel with a high resistance, the voltage across the condenser at any time after the condenser was charged is given by

$$V_t = V_0 \exp(-t/CR),$$

where V_0 is the voltage to which the condenser was initially charged, V_t the voltage across the condenser after a leakage time t, C the capacity of the condenser and R the leakage resistance of the condenser.

For a rectangular block of insulation, the resistance between one pair of opposite faces is $R = sd/A$, where s is the resistivity, d the distance of separation between the two faces and A the area of these faces.

The capacity between the same pair of opposite faces is $C = KA/4\pi d$, where K is the dielectric constant.

The product $CR = \frac{KA}{4\pi d} \cdot \frac{sd}{A} = \frac{Ks}{4\pi}$.

Since the last expression is independent of the dimensions of the insulator, it can be used to replace CR for a condenser of any shape. Substituting in the formula for the voltage drop due to leakage, we have

$$V_t = V_0 \exp(-4\pi t/Ks),$$

from which we find the resistivity

$$s = \frac{4\pi t}{K \ln(V_0/V_t)}.$$

Thus all that is needed in order to find the resistivity is a measurement of the voltage across the condenser before and after the leakage period, and a knowledge of t the leakage time and K the dielectric constant. Tedious and possibly inaccurate measurements of insulator dimensions can thus be avoided. It is interesting to note that since the voltage loss of the condenser is independent of its dimensions, no improvement to shorten the long leakage periods can be effected by altering the shape of the insulator.

§3. ACCURACY OF RESULTS

The dielectric constant K can be obtained from published tables with more than sufficient accuracy. The leakage time is also known with ample accuracy, since the leakage periods used were of the order of days or months and could be timed to the nearest hour if necessary. The main cause of error was a variation in the calibration of the valve electrometer between the beginning and end of a leakage period, sometimes an interval of several months. For this reason the accuracy is often low, particularly where the drop in potential on a condenser is small, but the final results are probably not in error by more than a factor of 3 or 4.

The leakage period necessary to obtain a reasonably large drop in potential on a condenser can readily be estimated if the time constant of the condenser is known. The capacity of a typical condenser is about 3 pF. and the resistance of a specimen having a resistivity of 10^{21} ohm cm. is about 7×10^{19} ohm, so that the time constant in this case is $2{\cdot}1 \times 10^{8}$ seconds which amounts to 2,430 days or between 6 and 7 years.

§ 4. RESULTS

The results are set out in Table 1. It will be noticed that in general the measured values of resistivity rose during the early stages of the experiments, no further significant increase being detected after a period of approximately 100 days. This rise in resistivity might be attributed either to a long-term dielectric absorption, or to the removal of moisture present initially on the surface of the insulators, as all the condensers were freshly made at the beginning of the experiments.

Table 1

Material	(1)	(2)	(3)	Material	(1)	(2)	(3)
Amber :	5	5	0·61	Alkathene :	1	1	1·9
Sample 1	730	620	14	Sample 3	6	5	2·0
	867	137	14		33	19	5·0
	1023	156	8·1		716	620	14
	1066	43	22		853	137	55
	1248	182	9·6		1009	156	14
					1234	182	20
Amber :	3	3	0·34				
Sample 2	7	4	0·31	Distrene	5	5	1·0
	14	7	2·62		28	23	3·6
	96	35	0·75		47	19	2·2
	161	65	8·2		730	620	7·6
					867	137	18
Alkathene :	5	5	1·5		1023	156	15
Sample 1	28	23	10		1248	182	13
	730	620	23				
	867	137	46	Perspex	1	1	0·016
	1023	156	14		2	1	0·023
	1248	182	19		7	5	0·086
					15	8	0·73
Alkathene :	1	1	0·06		34	19	0·34
Sample 2	2	1	0·26		717	620	2·3
	7	5	8·8		854	137	1·4
	15	8	4·7		1010	156	1·6
	34	19	2·3		1053	43	2·0
	717	620	7·1		1235	182	1·9
	854	137	5·3				
	1010	156	8·0				
	1053	43	9·4				
	1235	182	7·4				

(1) Time from start of test (days); (2) leakage period over which loss of charge was measured (days); (3) resistivity in ohm cm. $\times 10^{20}$.

Further tests were made on two batches, each of six condensers, with amber insulators, one batch being kept in air, and the other in a desiccator. No significant difference between the final values of the resistivity for the two groups of insulators was found, beyond that attributable to variations from one specimen to another, and experimental error. All the specimens showed a final resistivity between 10^{19} and 10^{21} ohm cm. Thus it would appear that the rise in resistivity is not due to the drying of the insulator surfaces.

It must be emphasized that the results obtained give low limits for the resistivities, because no correction has been made for the loss of charge due to leakage, if any, over the end surface of the insulators, nor for the ionization produced in the air volume of the associated ionization chambers by stray penetrating radiation. Taking the ionization produced by the latter as 10 ions/cm^3/sec., the loss of charge due to this effect is estimated at not more than 1% of the loss due to insulation leakage in any of the condensers.

Some examples of previously published figures are given in Table 2.

Table 2

Material	Volume resistivity	Reference
Amber	5×10^{18} ohm cm. at 22° c.	*Handbook of Chemistry and Physics* 1944.
Distrene (Polystyrene)	10^{20} ohm cm.	Wearmouth and Cozens 1942.
Alkathene (Polyethylene)	3×10^{17} ohm cm.	I.C.I. 1945.
Perspex (Polymethyl-methacrylate)	$>10^{15}$ ohm cm. at 20° c.	I.C.I. 1944.

§ 5. DISCUSSION OF RESULTS

It will be seen that the magnitudes of the resistivities found are, in most cases, higher than figures previously published by a factor of the order of 10^4. No attempt has been made to carry out the measurement by a direct current method for the purpose of comparsion. In § 3 it is shown that a condenser having a dielectric with a resistivity of 10^{21} ohm cm. has a time constant of 2,430 days or 6 to 7 years. It is common experience that condenser ionization chambers in normal use have a time constant considerably greater than 0·24 day, which is the value corresponding to a dielectric having a resistivity of 10^{17} ohm cm.

The results quoted in Table 2 for alkathene and Perspex were obtained by measurement of the direct current through a specimen, after an electrification period of 1 minute. The fact that these figures are so much smaller than those in Table 1 might well be taken as additional evidence that the current through an insulator decreases with time after the application of voltage.

It appears that, for electrometer work, amber is no better than the newer insulating materials; from a practical point of view the latter are more readily obtainable, and easier to fabricate. However, for applications in which the insulation is subjected to irradiation by X-rays, amber is far superior to the synthetic materials in that it will withstand a greater amount of X-radiation before the resistivity is appreciably lowered.*

---

* It is hoped to publish some information on this later.

The reason for the existence of any current flow in good insulators has for a long time been the subject of speculation. It is very often attributed to the presence of impurities, in particular, small amounts of moisture. The flow of current through the specimens tested was of the order of 110 ions/cm^3/sec., when the resistivity had reached its final level, and it is conceivable that the initial rise in resistivity might be caused by the gradual dissipation by electrolysis of minute traces of moisture in the specimen. It is not obvious on this assumption, however, why the conduction current should attain an approximately steady value after the initial period of increase. This might be expected in those specimens maintained in normal moist air, but not in those which were kept dry.

A possible explanation of the existence of this final steady current is the production of ionization in the insulators by penetrating radiation. Some support for this theory can be found in the fact that the final values of conduction current are of the same order in three of the materials tested, amber, alkathene and distrene, and only a factor of 10 higher than this in Perspex. Taking rough values for the densities of air and the insulators as 0·001 and 1 gm/cm^3 respectively, and neglecting differences between their atomic numbers, it would be expected that something like 10,000 ions/cm^3/sec. would be produced in the insulators, by penetrating radiation, if the corresponding figure for air is 10 ions/cm^3/sec. as assumed above. With the potential gradients used in the tests of 130 volts/mm. or so, a large measure of ionic recombination would be expected, but the figure for the flow of current of 110 ions/cm^3/sec. quoted above could reasonably be attributed to this cause.

ACKNOWLEDGMENT

I am indebted to Professor J. E. Roberts of the Barnato-Joel Laboratories, Middlesex Hospital, where these measurements were mostly carried out, for his continuing interest and encouragement during long periods of waiting.

REFERENCES

FARMER, F. T., 1942, *Proc. Phys. Soc.*, **54,** 435; 1945, *Brit. J. Radiology*, **18,** 148.

Handbook of Chemistry and Physics, 1944, 28th Edition (Cleveland, Ohio: Chemical Rubber Publishing Co.).

IMPERIAL CHEMICAL INDUSTRIES, 1944, *Plastics Technical Bulletin*, No. 10; 1945, *Ibid.*, No. 13.

WEARMOUTH, W. G., and COZENS, E. G., 1942, *Electronic Engng.*, **14,** 667.

A Radio Meteorological Investigation in the South Island of New Zealand

By B. MILNES* and R. S. UNWIN
Departments of Scientific and Industrial Research, United Kingdom and New Zealand, respectively.

Communicated by R. L. Smith-Rose; MS. received 15th June 1949, *and in amended form 2nd February* 1950

ABSTRACT. A Föhn wind blowing off-shore produces super-refraction at radio frequencies. This results in the guiding of very high frequency radio waves beyond the horizon in a radio duct close to the sea surface. The problems involved and the experimental techniques adopted in a long term investigation of this phenomenon are described, and selected data are discussed. Field observations are presented in the form of isopleths of the relevant meteorological quantities and of modified refractive index over the area under investigation, together with contours of radio field strength for wavelengths of 300 cm., 60 cm., 10 cm. and 3 cm., corresponding to the particular meteorological situations described.

It is found that with off-shore winds of strength up to force 6 radio ducts of about 100 m. height are formed and the field strength everywhere beyond the horizon is much increased. In the duct itself, at ranges up to 200 km. from the coast, field strengths approximately equal to the free space level are obtained on wavelengths of 10 cm. and 3 cm., and up to 10 or 20 db. below this level on a wavelength of 60 cm. The duct is not sufficiently high to trap radiation at a wavelength of 300 cm. With stronger winds turbulence limits the duct height to 20 m. and radiation of wavelength above 10 cm. is no longer trapped. The presence of a local sea breeze underneath the off-shore drift has little effect on propagation normal to the coastline.

§ 1. INTRODUCTION

(i) *The Phenomenon of Super-refraction*

When a warm dry wind blows over a relatively cool sea, steep gradients of temperature and humidity occur in the lower atmosphere. Such conditions produce an abnormally great lapse rate of refractive index with consequent super-refraction of radio waves. Super-refraction results in a concentration of energy at low levels in a so-called radio duct and this causes the field strength beyond the horizon to be very much increased. The structure and properties of radio ducts were intensively studied during the war and the state of knowledge of the whole subject up to 1946 has been summarized in the Report of the Physical Society and Royal Meteorological Society Conference (1946) and the Report of the Committee on Propagation, N.D.R.C. (1946).

The extent and intensity of an advection duct depend upon the initial temperature difference between the air and the sea, the moisture content of the air before it reaches the sea, and the wind speed and direction at various heights. Further, for a given set of conditions the amount of energy trapped in a radio duct falls off rapidly with decrease in frequency below a critical frequency which is the cut-off of the lowest frequency mode of the duct. Moreover the duct is defined in terms of the distribution of refractive index of the air which can be calculated from a knowledge of the temperature, humidity and pressure of the air (Englund, Crawford and Mumford 1935). Theories have been developed so that, knowing the distribution of refractive index in the lower troposphere, the amount of energy trapped within the duct may be calculated. Booker and Walkinshaw (1946) have developed a waveguide theory to provide approximate solutions to the problem of calculating the field distribution inside and above the duct, and Price (1948) has described methods based on ray tracing to achieve the same ends. J. E. Freehafer working at the Massachusetts Institute of Technology (U.S.A.) has also developed the ray-tracing technique. Experiments made in many parts of the world (Katzin, Bauchman and Binnian 1947, Megaw 1946, Smith-Rose and Stickland 1946) have provided data with which to check these theories, but, especially in the case of coastal super-refraction, the meteorological data have usually been too meagre to permit of reliable correlation with the radio observations, or to provide satisfactory checks on the current theories of diffusion as applied to an air mass passing off-shore.

---

* Now at Telecommunications Research Establishment, Ministry of Supply, Malvern.

The 'Canterbury Project' was initiated jointly by the Telecommunications Research Establishment, Ministry of Supply, and the Departments of Scientific and Industrial Research, United Kingdom and New Zealand, with some material assistance from the United States of America, to study the whole problem and develop if possible a suitable forecasting technique for the onset, intensity and duration of super-refractive conditions.

This paper is confined to a description of the experimental techniques adopted to obtain the necessary meteorological and radio data, and a discussion of selected results which are typical of the super-refractive conditions experienced.

(ii) *Selection of Site for an Investigation*

In planning an experimental investigation of the problem a number of aspects must be considered. It is necessary to make detailed radio field strength and meteorological observations over a wide area both within and beyond the horizon and within and above the radio duct. To correlate radio and meteorological data ideally an instantaneous picture is required over the whole area, but to trace the modification of an air mass passing off-shore a number of measurements following each other in time and space are desirable. These conflicting aspects can be resolved if a steady meteorological situation can be found, where measurements over a comparatively short period of time (say two hours), will give a reliable picture of the radio propagation conditions and the modification of the air mass. The problem can be further reduced to two dimensions where an air mass moves off-shore perpendicular to a long straight coastline. In choosing a site irregularities of the land surface should be as few as possible, there should be no obstructions off the coast, and, of course, suitable weather conditions (i.e. the off-shore movement of homogeneous air) should be frequent.

This wide set of conditions is almost ideally satisfied in mid-Canterbury on the east coast of the South Island of New Zealand (Figure 1). In this region the prevailing weather is westerly, and the well-known north-west wind of Canterbury blows frequently all the year round, lasting several days at a time. It is especially warm and dry during most of the year, due to the Föhn effect produced by the Southern Alps, which extend up to an average height of about 2,000 metres approximately at right angles to the prevailing wind direction. The Canterbury Plains are about 60 kilometres wide at Ashburton, which was chosen as the Headquarters area for the investigation, with a gentle almost uniform slope towards the sea, free from hills and other major obstructions. To seaward the area is clear of islands. With the wind development at right angles to the coastline this region forms an almost ideal natural laboratory for investigating the formation of radio ducts off-shore with accompanying super-refraction at very high frequencies. The map (Figure 1) shows the line along which observations were made.

(iii) *Measurements Required*

From the foregoing it will be clear that detailed measurements of temperature, humidity, wind speed and direction of an air mass passing off-shore are required over land and sea, out to a considerable distance from the coast. A series of vertical soundings up to 600 m. or so should be made over a limited time interval simultaneously at various points along the line of operations. Under steady conditions the data obtained will yield information showing the modification of an air mass passing off-shore, and give the distribution of modified refractive index* over the sea showing the radio duct in full. For the development of a forecasting technique for super-refraction, continuous records of pressure, temperature, humidity and wind speed and direction over land are required, as well as synoptic charts of the whole area round New Zealand.

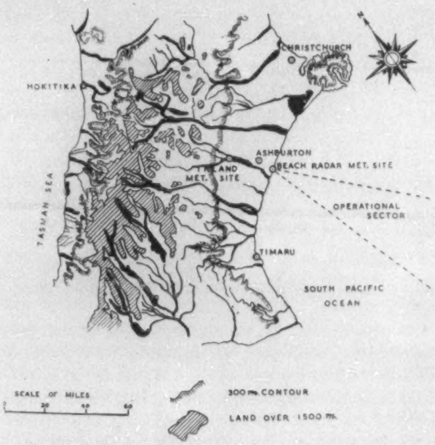

Figure 1. Sketch map of Canterbury and Westland, showing area of operations.

Super-refraction is most marked at microwave frequencies, but for a thorough investigation simultaneous measurements distributed over a wide frequency band from say 100 Mc/s. up to 10,000 Mc/s. should be made. Receivers at the selected frequencies must be placed at or near the coastline, preferably at different heights above sea level, and at the same time as the meteorological measurements are being made, observations of the signal strength from transmitters situated at various heights within and above the duct at selected ranges from the coast are required. These observations should be sufficiently closely spaced to provide a complete picture of the distribution of field strength within and above the duct out to the maximum range covered.

---

* The curvature of a ray relative to the surface of the earth, at a height h, is given by $(d\mu/dh)+(1/a)$, where a is the radius of the earth, therefore by adding the term h/a to the ordinary refractive index μ we obtain a fictitious refractive index which automatically takes account of the earth's curvature in any calculations of ray paths. Since the refractive index of air normally exceeds unity by only a few parts in 10^6 a more convenient unit (the Munit) is obtained by multiplying this excess by 10^6. Thus we have modified refractive index $M=10^6(\mu-1+h/a)$.

§ 2. EXPERIMENTAL PROCEDURE

(i) *General*

In order to meet the requirements stated in § 1 (iii), the only practical possibility was to use aircraft to obtain the necessary rapid coverage. Over the sea the aircraft observations were supplemented by observations from a trawler, and over land by observations from three mobile sounding stations. The sounding trucks and the trawler were fitted with wired sonde equipment whereby rapid and frequent soundings could be made up to heights of between 150 and 600 m. depending on the wind conditions.

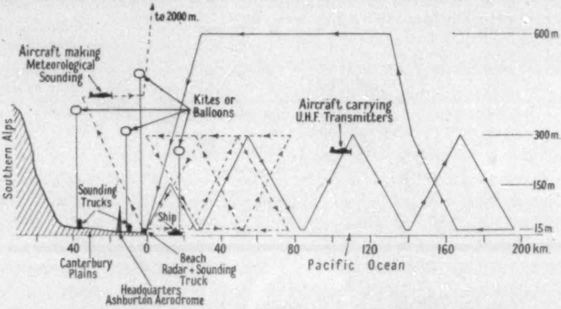

Figure 2. Cross section of area of operations, showing participating units.

The aircraft carried, in addition to meteorological instruments, transmitters operating on wavelengths of 300 cm., 60 cm., 10 cm. and 3 cm., and the signals from these transmitters were measured by the appropriate receivers situated at the coast. 10 cm. and 3 cm. receivers were located at heights of 8 m. and 26 m. above mean sea level, this duplication of receivers enabling any variation of trapping with height of source to be studied. The 300 cm. and 60 cm. receivers were at heights of 11 m. and 27 m. respectively. A higher receiving site would have been desirable near the top of, or just above, the average duct height experienced, but this, unfortunately, was not available. Horizontal polarization was used on all wavelengths.

Standard meteorological instruments provided a continuous record of surface temperature, pressure, humidity and wind speed and direction at stations at the coast, 15 km. inland and 38 km. inland along the line of observations.

Figure 2 depicts a cross section of the area looking from the south, and shows the general arrangement of the experiment. The Headquarters at Ashburton Aerodrome was in radio-telephone or land-line communication with all observing posts, and one or two persons controlled all observations from there. Land soundings were usually started one to three hours earlier than an aircraft flight to check the homogeneity of the air mass. If two aircraft were used simultaneously, only one provided signals for radio measurements, and the other, making meteorological soundings only, concentrated on the region up to 60 or 70 km. from the coast where the modification of the air mass is most rapid. For the same reason the ship usually remained within 30 km. from the coast, so that the very sharp gradients occurring in this region could be examined in detail, but it made periodical trips out to 150 km. from the coastline for measurement of sea temperature.

It will be seen from Figure 2 that, with the three sounding posts on land, the trawler off the coast, and the numerous ascents and descents of both aircraft up to 300 m. or higher, a wealth of meteorological and radio data could be obtained in the space of about two hours. On most occasions isopleths of temperature, humidity, modified refractive index and field strength on all four wavelengths could be drawn over the whole area.

Through the courtesy of the New Zealand Meteorological Office radiosonde ascents were made when desired from Hokitika on the West Coast. These provided data on the properties of the air mass before it crossed the mountain chain of the Southern Alps and, when compared with its properties on the eastern side, could yield valuable information on the Föhn effect, the cause of the warmth and dryness of the north-west wind in Canterbury.

(ii) *Meteorological Equipment*

The main requirement of the meteorological equipment was that it should have a rapid response to small changes in temperature and humidity since it was the gradients of these quantities with height that were the primary consideration; in addition the equipment had to be rugged and simple in operation for use in the field and on board ship or aircraft.

(*a*) *Aircraft installation.*

The aircraft installation consisted of a 'spirit in glass' wet and dry bulb psychrometer. Temperatures could be read to ± 0·2° F., giving a maximum possible error in modified refractive index of ± 1·3 Munits at 50° F. and ± 2 Munits at 80° F. The lag of the instrument was 8 seconds at an airspeed of 185 km/hr. since the rate of ascent and descent of the aircraft did not exceed 40 metres per minute, this lag introduced only a second order error except in the sharpest gradients. These sharp gradients were usually found close to the sea surface, so that when the finish of a descent and the start of a subsequent ascent were close together in range, errors due to lag could be smoothed out when necessary. Height was measured by an aneroid or radio altimeter, with a probable error between +6 and −3 m. in the first hundred metres. Height differences could be relied on to ± 5 m. or better.

The psychrometer was read every 15 to 30 seconds, corresponding to a height interval of 10 to 20 metres depending on the sharpness of the gradients encountered; airspeeds were also noted. Altitude was logged by the navigator every 30 seconds.

(*b*) *Wired sonde equipment.*

The wired sonde equipment used in the sounding trucks and trawler followed the technique developed by P. A. Anderson, G. L. Barker, K. E. Fitzsimmons and S. I. Stephenson at Washington State College (U.S.A.). Temperature measurement could be relied on to ± 1° F. or better, and relative humidity to

±3% in widely varying conditions such as occurred in a sounding through a sea breeze into a dry north-west wind. This gave a possible error in modified refractive index of ±3 Munits at 50° F. and ±8 Munits at 80° F., but in a more normal situation, with smaller gradients of humidity, the error would be less than half this amount.

Detailed measurements of wind gradient over the land were made with a small cup-type anemometer hoisted aloft by kite or balloon. This wind information was supplemented by frequent wind-finding runs made at the Headquarters site using standard pilot balloon and theodolite technique.

In winds of strength up to force 3 on the Beaufort scale the equipment (sonde elements or anemometer) was hoisted by balloon, in winds of force 3 to 5 by Seypang kite and balloon combination, and in stronger winds by the kite alone.

(iii) *Radio Equipment*

Since the signals to be measured were from a moving source, an airborne transmitter, it was essential to use pulse transmission in order to provide range information.

The four transmitters in the aircraft were triggered by signals received from one of the 10 cm. ground stations, and the signal strength of the returned pulses from these transmitters was measured at the ground stations by visual observation on an 'A' scope display, i.e. amplitude–range display. On the 300 cm. and 60 cm. receivers a comparator pulse was injected from a signal generator in parallel with the incoming radio signal. This comparator pulse was maintained at the same amplitude as the signal received from the aircraft by manual control of the calibrated signal generator attenuator, from which the signal strength could be read directly in microvolts or in decibels above some arbitrary value. On the microwave receivers, where the signals varied more rapidly, the amplitude was estimated directly against a series of horizontal lines engraved on the face of the display tube.

The signal strength was observed synchronously on all six receivers every ten seconds throughout an aircraft flight, i.e. a reading was obtained at average height intervals of 6 m. on each inclined run. Usually the aircraft made about eight ascents and descents between 300 m. and 15 m. out to a range of 180 km., as well as a level run for 100 km. at a height of 600 m. during one flight, hence a comprehensive picture of the radio field strength pattern was obtained over the whole area.

The level run towards or away from the ground stations at a height of 600 m. was made on almost every occasion primarily to enable a value of the 'free-space' signal strength for the various R.F. channels to be established for each operation. On this run the aircraft passed through a number of the normal interference lobes produced by reflection from the sea surface, and a $1/r^2$ attenuation curve could usually be fitted to the peaks of these lobes, when plotted, correct to one or two decibels. From this curve, by assuming a value of -1 for the reflection coefficient of the sea, the free-space signal at any range could easily be calculated. By obtaining a free-space signal level in this way it was not necessary to maintain an accurate check on the absolute sensitivity of the ground station receivers or the power output of the airborne transmitters. It is estimated that the signal strength observations on 300 cm. and 60 cm. are accurate to about 1 db. and on the 10 cm. and 3 cm. wavelengths to 2 or 3 db.

The transmitters used in the aircraft were modified airborne radar transmitters and all four antennae had wide coverage in the horizontal plane to reduce aspect effects. The 10 cm. receiver in the aircraft supplied triggering pulses to all four transmitters, locked in phase to the received pulses from the 10 cm. ground transmitter, and this link was such that it remained operative down to about 35 db. below the free-space signal at a range of 150 km.

The ground station receivers were of standard radar type, all receiver displays being locked in phase with the 10 cm. transmitter providing the triggering pulse. Manual control of the antennae and tuning was used on all the ground stations.

§ 3. DISCUSSION OF SELECTED DATA

Observations were begun in September 1946 and continued until the end of 1947, by which time 84 sets of observations had been obtained on 70 days. In addition, 13 sets of observations confined to the sea breeze structure and without radio data were obtained. A sufficient number of 'nor'westers' occurred throughout the whole period for the seasonal variations to be established, and the conditions encountered varied between wide limits. Owing to technical difficulties with the aircraft no observations were made at night.

It is not possible in the space of this paper to present more than a very small fraction of the total data collected, and for further information reference should be made to the complete record of observational data which is at present in course of publication in New Zealand.

In selecting the data for discussion a situation has been chosen in which the refractive index gradient is approximately standard, and two examples of north-westerly conditions have been included, one occurring in early spring and the other in early summer. With a light north-west wind a sea breeze often penetrates underneath the off-shore drift, and an example of this complication has also been included. The remaining situations have been selected because of some peculiarity markedly affecting radio propagation.

In spite of the many advantages of the mid-Canterbury Plains as a site for an investigation, on most occasions there was a sufficient change in the situation over the period covered by an aircraft flight to necessitate its being taken into account when interpreting the data. The effect was usually small, though quite distinct; but in complex situations such as occurred with a sea breeze or north-easterly drift under a 'nor'wester', some smoothing of the observations was necessary, or separate isopleths were required to show the situation at a later time.

The field strength contours for wavelengths of 60 cm. and 300 cm. can usually be drawn with very little difficulty, and present a reliable picture of the situation. The contours of field strength for 10 cm. and 3 cm., however, usually present some difficulty because of greater fluctuations in the observed values, and it is considered that, in many instances, the exact situation shown never existed as an instantaneous picture, but the contours give an indication of the amount of energy leaking from the duct. These points must be borne in mind when examining the data. The contours are in decibels on a scale such that the free-space radiation field at one metre from the transmitter is 150 db. (50 db. at 100 km.).

(i) *Nearly Standard Propagation*

The observations of 17th October 1947 reveal meteorological conditions giving rise to almost standard refractive index gradients (Figure 3), with no trapping of radio energy, and are included in this paper for comparison with the examples of anomalous conditions which cause super-refraction.

Conditions on this day resulted in the formation of an evaporation duct, about 5 m. in height and having 5 Munits inversion, out to a range of about 100 km. Above 5 m. the modified refractive index increased almost linearly with height to give a normal gradient (Figure 3). There was no trapping of energy on wavelengths of 300 cm., 60 cm. and 10 cm., or on 3 cm. where the source was above the duct. A small amount of trapping was noticed on the low-sited 3 cm. receiver on one run only, and this is shown by the dotted line in the figure.

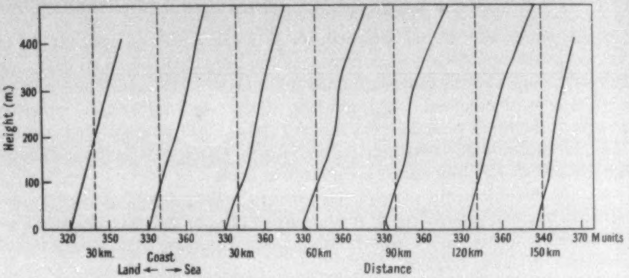

Figure 3. (*M*, *h*) curves at various ranges, 17th October 1947, 1130 hours, – – – $M=340$. [*M* at sea surface $=336$ approx.]

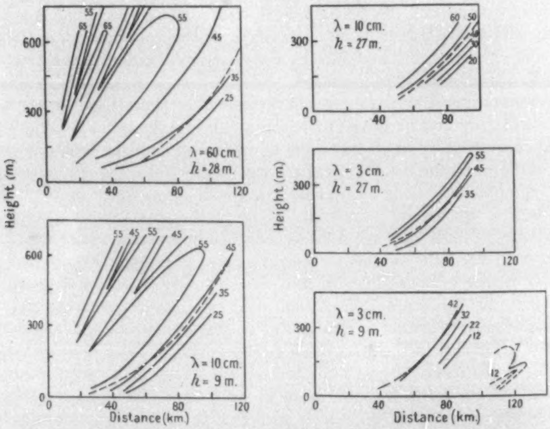

Figure 4. Field strength contours, 17th October 1947, – – – horizon line for a standard atmosphere.

The general appearance of the field strength contours (Figure 4) is seen to be the same on all wavelengths. The signal falls off very rapidly below the first interference lobe, i.e. below the horizon, and does not increase again as the sea surface is approached, indicating that the amount of super-refraction, if any, is negligible.

(ii) *An Early Spring 'Nor'wester'*

An example of a typical 'nor'wester' of early spring was that which occurred on 5th August 1947. The synoptic situation (Figure 5) shows an intense ridge of high pressure north of New Zealand extending across the North Tasman Sea and eastwards into the Pacific. The resulting gradient across New Zealand gave a north-west to north-north-west wind of force 3 to 6 blowing off-shore in mid-Canterbury throughout the day.

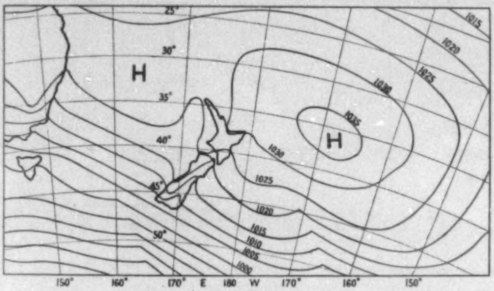

Figure 5. Isobars at 06 hours local time, 5th August 1947.

The potential temperature of the air mass in the early afternoon when the observations were made was about 70° F., and the specific humidity 4 to 4·5 gm/kg. The sea surface temperature varied between 46° F. close in-shore and 48° F. at about 70 km. from the coast, decreasing again beyond 120 km. to 46·5° F. The corresponding saturation values of specific humidity are 6·6 and 7·0 gm/kg. respectively. Thus the resulting temperature excess and humidity deficit between unmodified air and sea is 22 to 24° F. and between 2 and 3 gm/kg., sufficient to cause a marked advection duct off-shore.

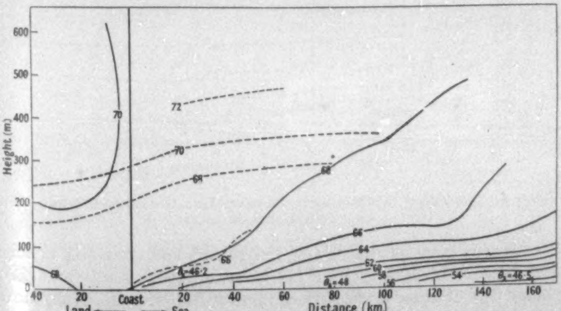

Figure 6. Isopleths of potential temperature (in degrees F.), *c.* 14 hours 5th August 1947, - - - - - situation at 15 hours.

The modification of the air mass off-shore is typical of a 'nor'wester' at this time of the year. The isopleths clearly depict the cooling and moistening of the air over the sea surface (Figures 6 and 7). However, the dotted lines showing the situation about an hour later than that represented by the full lines show that there is some inhomogeneity in the air mass crossing the coast during the period.

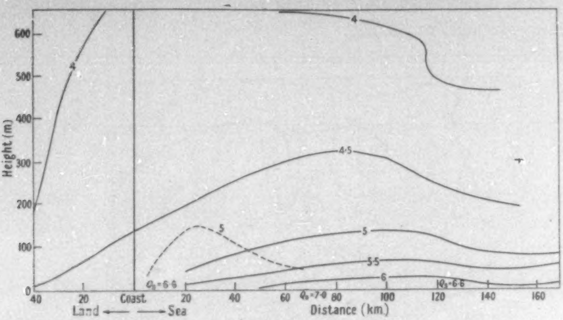

Figure 7. Isopleths of specific humidity (in gm/kg.), *c.* 14 hours, 5th August 1947, ----- situation at 15 hours.

The distribution of modified refractive index over the area shows a marked duct extending out to the maximum range covered, 160 km. from the coast (Figure 8). The small duct at the beach is due to the modification of the air by the land surface, largely caused by evaporation from the ground, a common feature of the Canterbury 'nor'wester' at this time of the year. The duct close in-shore is low and intense, gradually decreasing in intensity and increasing in height with increasing distance off-shore. The fall in sea temperature beyond 120 km. is accompanied by a decrease in the surface value of M by 4 units, hence the decrease in intensity of the duct is greater than it would be with constant sea surface temperature. The slight intensification of the duct at 160 km. is due either to the

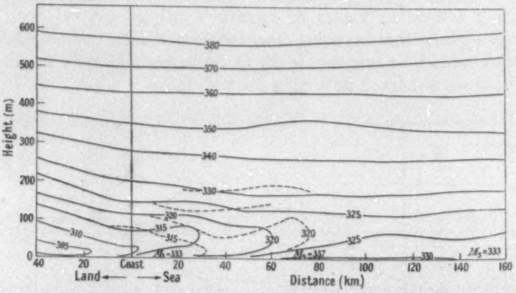

Figure 8. Isopleths of modified refractive index, *M*, *c.* 14 hours, 5th August 1947, ---- situation at 15 hours.

subsidence of warm upper air, or to inhomogeneity of the air mass. However, the height and intensity of the duct at all ranges, with a maximum height of approximately 100 m. beyond about 120 km. off-shore, is typical of a spring or summer 'nor'wester'. As would be expected, the change is most rapid close to the shore, the variation beyond 80 km. taking place very slowly. At 80 km. the height and intensity are 70 m. and 16 Munits, at 120 km., 90 m. and 11 Munits, at 160 km., 90 m. and 10 Munits (Figure 9).

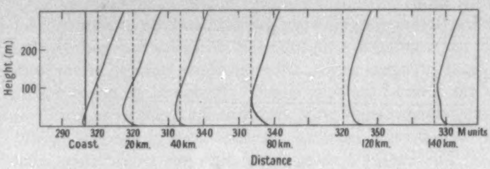

Figure 9. (M, h) curves at various ranges off-shore, *c.* 14 hours, 5th August 1947, ---- $M = 320$.

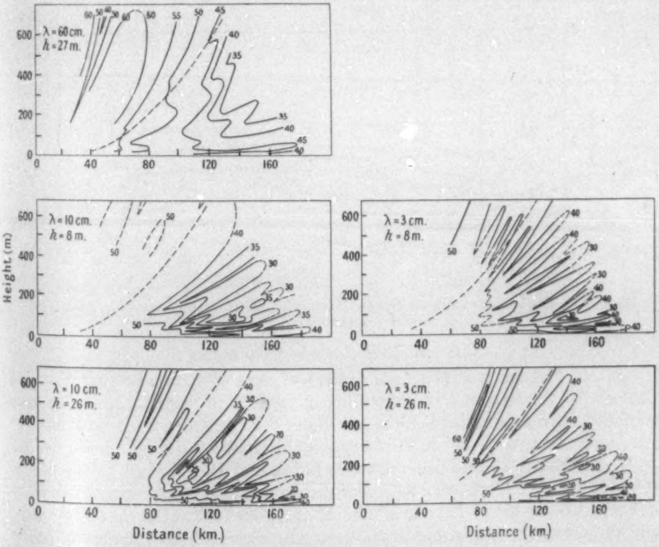

Figure 10. Field strength contours, *c.* 14 hours, 5th August 1947, ---- horizon line for a standard atmosphere.

Figure 10 shows the field strength contours obtained on this day on wavelengths of 60 cm., 10 cm. and 3 cm. The contours show that there is considerable trapping of energy in a narrow channel close to the sea surface on all three wavelengths. On 10 cm. and 3 cm. the strongest signal in the duct occurs between 15 and 25 m. from the surface and on 60 cm. between 25 and 45 m.

The amount of trapping increases with decrease in wavelength; at a range of 160 km. the peak signal in the duct is 4 db. below the free-space signal on 60 cm., 2 to 3 db. above the free-space value on 10 cm. and 6 or 7 db. above the free-space value on 3 cm.

The contours obtained from the high and low sited receivers on the same wavelength show a somewhat similar structure below the horizon line and give equal peak signals in the duct relative to the free-space value, within the limits of experimental error.

In the diffraction region, between the duct and the interference lobes, leakage from the duct has resulted in a complicated field pattern, especially for 10 cm. and 3 cm., with signal strengths which, although above normal, are nevertheless about 10 db. below the level of the duct signal. It should be noted that the contours are for one-way transmission only, therefore in considering radar coverage the difference in decibel value between one contour and the next would be double that shown. The energy leaking from the duct would then assume far less importance and could generally be neglected for practical purposes. The energy found within the duct constitutes the greater portion of the energy refracted out of the normal lobe pattern.

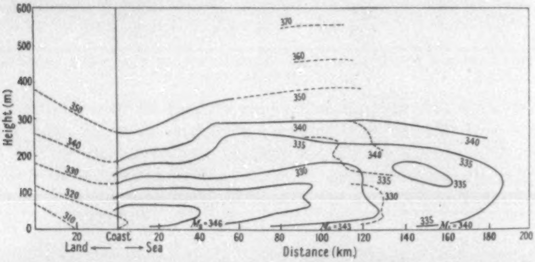

Figure 11. Isopleths of modified refractive index, *M*, *c.* 1130 local time, 3rd November 1947, – – – – situation *c.* 1215.

(iii) *An Early Summer 'Nor'wester'*

On 3rd November 1947 a 'nor'wester' of force 3–4 blew off-shore in mid-Canterbury throughout the day. The temperature excess, 16–22° F., and humidity deficit, average 3·5 gm/kg., were not very different from the values for 5th August, and we should therefore expect the resulting situation to be similar.

The isopleths of modified refractive index and the derived (M, h) curves (Figures 11 and 12) are essentially very similar to those of 5th August, the main differences being the much smaller modification over land at this time of the year, and the greater height of the duct due to the slightly greater humidity deficit and the more rapid modification of the air with the smaller wind velocity. At 80 km. the duct is about 90 m. in height with an intensity of 21 Munits; beyond this range it becomes higher but weaker due mainly to a decrease in sea temperature. At 150 km. it is 11 Munits to 150 m. and at 180 km. 7 Munits to 120 m.

The field-strength contours show that the amount of trapping on all wavelengths is much the same as on 5th August, except that the low level peak for 3 cm. is relatively weaker than that for 10 cm. This latter effect is possibly due to mutual interference between the greater number of propagation modes trapped by this higher duct for the 3 cm. wavelength. Again, owing probably to the greater height of the duct compared with the previous example, the low level peak at 160 km. off-shore for 10 cm. and 3 cm. is between 30 and 60 metres from the surface; for 60 cm. it lies between 45 and 75 m.—which is considerably higher in both cases than on 5th August.

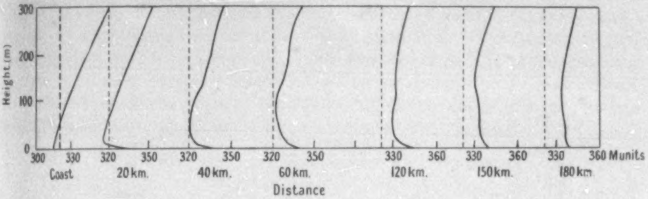

Figure 12. (M, h) curves at various ranges off-shore, *c.* 1130 local time, 3rd November 1947, ---- $M = 320$.

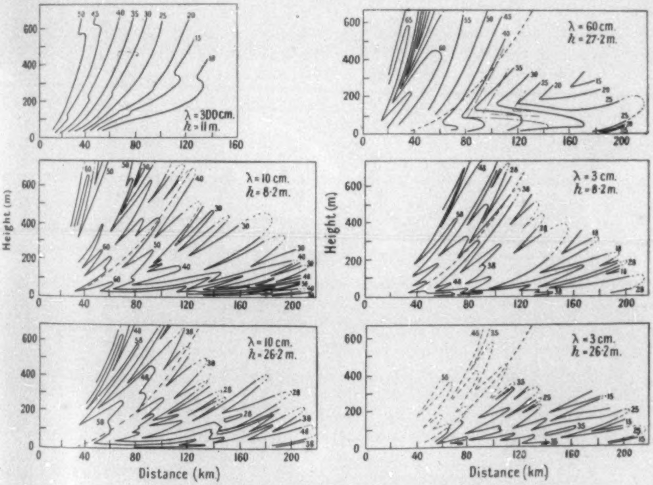

Figure 13. Field strength contours (in db.), *c.* 1130 local time, 3rd November 1947, ---- horizon line for a standard atmosphere.

The 60 cm. wavelength contours show a particularly simple structure and give a very clear picture of the guiding of energy by the duct round the surface of the earth when plotted on a curved earth diagram (Figure 14).

(iv) *Attenuation in the Duct*

Aircraft flights were made on several occasions at a constant height in the duct, to study the variation of signal strength in the duct with range. The results of such a flight on 21st October 1947, at a height of 45 m., are illustrated in Figures

15 and 16. There was a strong duct of 20 to 25 M units up to 60 m. in height out to the maximum range of observation, 160 km. This duct height, although insufficient to produce complete trapping at 60 cm., was great enough to cause

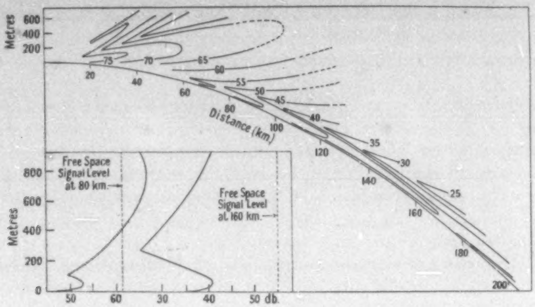

Figure 14. Field strength contours * for wavelength of 60 cm., 3rd November 1947. Inset : Height–gain curves derived from contours.

* The figures on the contours and in the abscissae of the inset are 10 db. high.

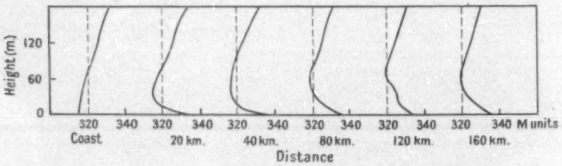

Figure 15. (M, h) curves at various ranges off-shore, 21st October 1947, 11 hours. ---- $M = 320$.

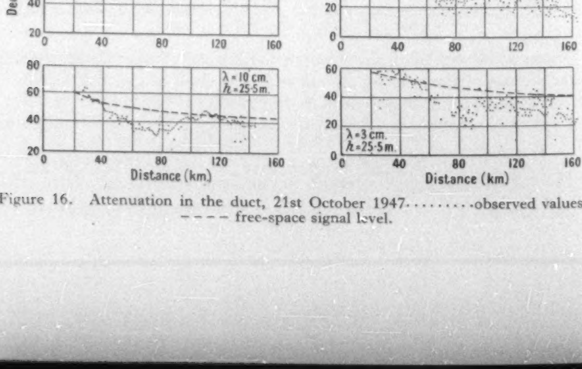

Figure 16. Attenuation in the duct, 21st October 1947 .... observed values, ---- free-space signal level.

considerable super-refraction at this wavelength and was sufficient for trapping to take place at wavelengths of 10 cm. and 3 cm. The 300 cm. and 60 cm. signals show a steady decrease with increasing range and are always below the free space signal value. Over the range of observations on the 60 cm. channel, 20–120 km., a $1/r^4$ law fits the observed values almost exactly.

For the wavelengths of 10 cm. and 3 cm. the signal oscillates slowly about the free-space value, all four channels showing somewhat similar fluctuations, with a region of weaker signal between about 60 km. and 90 km. The increase beyond this range may have been due to an increase in duct height causing the maximum signal to approach the height at which the aircraft was flying (45 m.). Alternatively, it may have been caused either by slow temporary fading, due to changed meteorological conditions, or by the presence of islands of strong and weak signal due to interference between two or more trapped modes within the duct. This latter possibility is unlikely in view of the fact that all four channels behave similarly, for it would be expected that different frequency or different height of source would change the position of such islands.

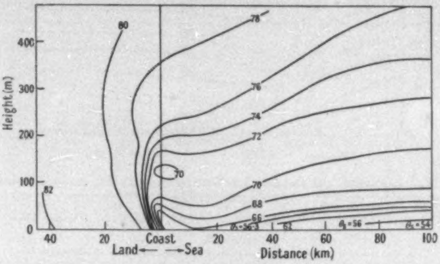

Figure 17. Isopleths of potential temperature (in degrees F.), *c.* 1430 local time, 8th December 1946.

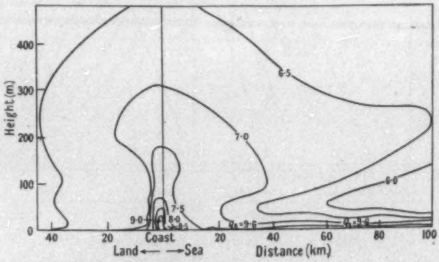

Figure 18. Isopleths of specific humidity (in gm/kg.), *c.* 1430 local time, 8th December 1946.

(v) *The Sea Breeze Complication in Summer*

In a light 'nor'west' situation, with a warm land surface, a sea breeze circulation at the coast frequently develops, and this may occur even in winter. A small-scale circulation is shown in Figures 17 and 18, the on-shore current of air being about 100 metres deep at the coast, the air above passing off-shore. The sea breeze did not penetrate more than about 10 km. inland on this day, 8th December 1946, the sea air being rapidly warmed by the ground and ascending to pass out to sea again in the off-shore drift above 100 to 120 m. The isopleths show the circulation extending about 15 kilometres seawards, but relatively moist air is carried above 100 m. out to more than 100 km., though the shape of the isopleths above 100 m. between 10 and 60 km. off-shore is open to question, as observations in that region were scanty.

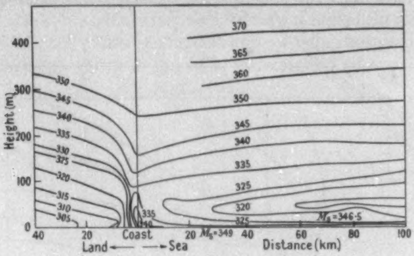

Figure 19. Isopleths * of modified refractive index, M, *c.* 1430 local time, 8th December 1946.

* The values assigned to the isopleths over the sea '325, 320, 325' *should read* '330, 325, 330'.

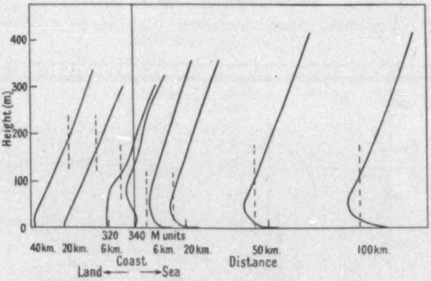

Figure 20. (M, h) curves, *c.* 1430 local time, 8th December 1946, - - - - $M=330$.

The chief feature as regards the distribution of modified refractive index (Figures 19 and 20) is the existence of an elevated duct at the beach, and a small duct, or very steep slope of the (M, h) curve over a limited height interval, to a variable distance inland depending on the penetration of the sea breeze. The effect on the duct over sea is negligible beyond about 20 km. off-shore; at less than this range the effect of the sea breeze is to increase the height of the duct until it reaches a maximum at the beach (in this case 80 m.), after which it rapidly loses height and intensity as we pass inland. The net effect on radiation propagated at right angles to the coastline is practically as though there were no sea breeze. However, radiation propagated along the coast could be markedly affected by the presence of the elevated inversion.

(vi) *Some peculiar Situations*

The remaining situations have been selected because of some peculiarity in the meteorological situation which has a pronounced effect on propagation.

(a) Low duct.

On 23rd October 1947, a strong (force 6 to force 8) and gusty 'nor'wester' was blowing off-shore throughout the day. Although the temperature excess, 16–22° F., and humidity deficit, varying between 2 and 4·5 gm/kg., were ample for a strong duct to form off-shore, there was apparently so much turbulence near the surface of the sea that sufficiently sharp gradients were not maintained to give an inversion in the (M, h) curve above a height of about 15 m. The result was an intense low level duct up to a maximum height of 18 m. out to the full range covered, 160 km. from the coast (Figure 21). The relative effect on propagation at the different wavelengths is striking (Figure 22). At 300 cm. the effect is negligible, and at 60 cm. only very slight. Both lower sited microwave channels are effectively trapped, though the trapping at 3 cm. is not as great as would be expected when compared with 10 cm. This is possibly due to the greater scattering of the shorter wavelength energy at the rough sea surface.

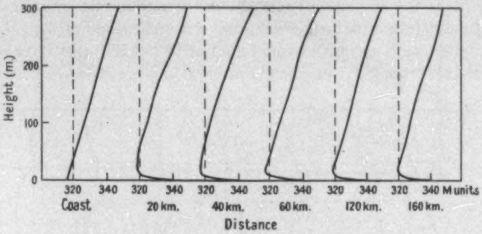

Figure 21. (M, h) curves at various ranges off-shore, 23rd October 1947, – – – – $M=320$.

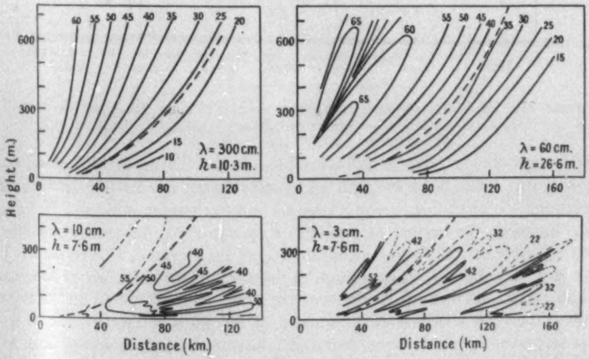

Figure 22. Field strength contours, 23rd October 1947, – – – – horizon line for a standard atmosphere.

(b) Surface-based duct changing to elevated duct.

A day or two before 4th September 1947, a vigorous depression passed to the south of New Zealand, the associated cold front being followed by a strong south-westerly flow over the South Island. An anticyclone in the central Tasman reinforced this flow until the appearance of a small but vigorous depression in the South Tasman rapidly turned the isobars to the north-west across the South Island on the early morning of 4th September. This depression moved rapidly eastwards, the 'north-wester' steadily pushing further off-shore during the day. The result was a warm current of air moving off-shore establishing itself over cooler fully modified southerly air. At the time of the observations (around 16 hours), the 'nor'wester' had pushed about 60 km. off-shore at the surface, though it was at least 160 km. from the coast at a height of 300 m. Under these conditions a simple surface duct was formed off-shore as far out as 60 km. but beyond this range the air immediately above the surface up to an increasingly greater height was fully modified, producing a normal slope of the (M, h) curve at the lower levels, with a sharp elevated duct of 10 to 12 Munits intensity above. This elevated duct extended over a height interval of 60 or 70 m., centred at 150 m. at 100 km. off-shore, 180 m. at 120 km. off-shore, and 220 m. at 140 km. off-shore (Figure 23). The field strength contours (Figure 24) in this situation are interesting. Considerable energy is trapped on wavelengths of 60 cm., 10 cm. and 3 cm., but when the normal M gradient is encountered this energy is diverted upwards, but is entirely kept beneath the top of the elevated M inversion. The result is a very marked concentration of energy (up to 12 db. above free-space level on 10 cm. and 8 db. above on 3 cm.) in a narrow track within and under the elevated duct. A relatively small amount of energy is refracted back to lower levels on wavelengths of 10 cm. and 3 cm., but nowhere does energy leak away above the duct beyond 60 km. or so from the coast.

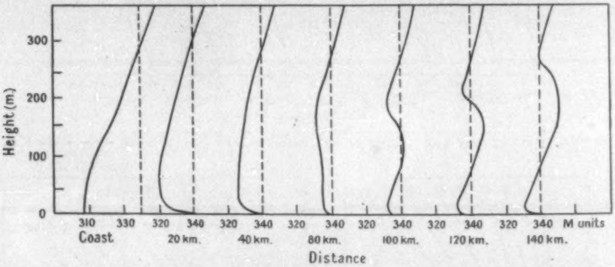

Figure 23. (M, h) curves at various ranges off-shore, *c.* 16 hours, 4th September 1947, ---- $M = 340$.

(c) Weak duct passing into strong duct.

On 6th October 1947, there was a light north-west wind. The air mass had a temperature excess of some 22° F. above the sea surface, and a humidity deficit of about 2 gm/kg. close in-shore, falling to about 1 gm/kg. beyond 180 km. due to reduced sea temperature at this range. The result was a fairly high duct (100 m.), of medium strength, the M inversion being 15 Munits out to 100 km. off-shore, at which range it weakened considerably, due largely to the change in surface temperature mentioned above. Beyond 120 km. there was considerable subsidence of warm dry air, and this caused the duct to increase in strength once more

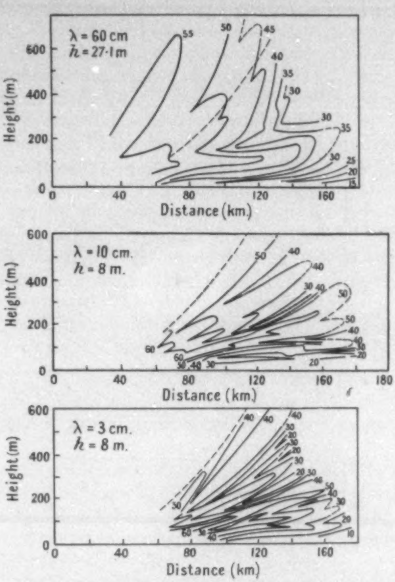

Figure 24. Field strength contours, *c.* 16 hours, 4th September 1947, - - - - horizon line for a standard atmosphere.

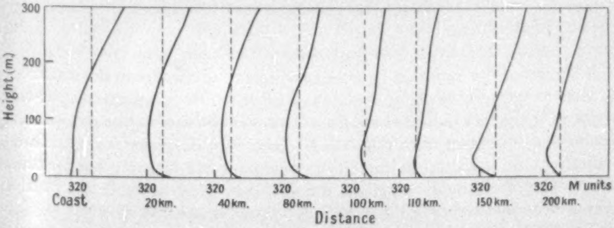

Figure 25. (M, h) curves at various ranges off-shore, 6th October 1947, - - - - $M = 330$.

(Figure 25). The effect of this refractive index structure is clearly shown by the contours of field strength (Figure 26). On all three wavelengths shown, 60 cm., 10 cm., 3 cm., there is considerable trapping of energy in the lower levels out to a range of 100 km., after which leakage is very pronounced as the duct weakens and the refractive index gradient diverts the energy upwards. Beyond 120 km., as the duct becomes stronger again, the contours indicate renewed trapping of energy close to the surface. The effect is least on the 3 cm. wavelength as a much greater proportion of energy is trapped by the intense part of the duct which is always present immediately above the surface.

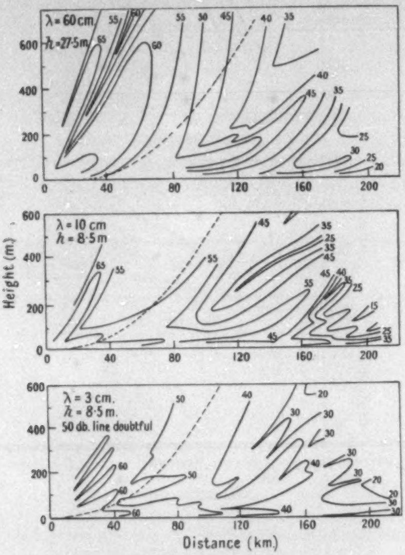

Figure 26. Field strength contours, 6th October 1947,
– – – – horizon line for a standard atmosphere.

§ 4. CONCLUSIONS

A survey of the data that have been obtained allows us to draw some general conclusions concerning the phenomenon of duct formation and super-refraction produced by Föhn winds over the Canterbury Bight during the day-time. These conclusions are drawn from inspection of the data only and are therefore largely qualitative; no statistical or theoretical treatment has hitherto been attempted in New Zealand, although a certain amount has been carried out at the Telecommunications Research Establishment (Macfarlane 1948).

The Canterbury 'north-wester' has a temperature excess over the sea surface temperature of 10 to 20° F. in winter and up to 30° F. in summer; it has a humidity deficit relative to saturated air at the sea temperature of between 1 and 6 gm/kg. The resulting *M* deficit is usually between 15 and 30 Munits and an *M* inversion of this magnitude is formed immediately off the coast. The height of the inversion, i.e. the duct height, increases rapidly to about 30 m. in the first 10 or 20 km.

from the coast where the Föhn air characteristics are quickly modified by the relatively cool sea. The duct then rises more slowly to between 90 and 130 m. at a range of 60 to 120 km. off-shore as eddy diffusion carries the effects of the surface modification to greater heights. Associated with the increase in height of the duct is a slight decrease in intensity since the *M* inversion takes place at a higher value of *M*. Beyond 120 km. the duct tends to weaken and diminish in height slowly but this tendency is complicated by variations in sea temperature changing the surface value of *M*. At ranges of 160 to 220 km. the (M, h) curve is characterized by an inversion of about 5 Munits at the surface (up to 10 or 15 m.) and a nearly constant value above up to about 150 m.

The height of the duct in the first 60 km. off-shore appears to have a rough dependence on wind velocity, the greater the wind speed the lower the duct at a given range. This effect is not very clearly marked and does not extend over very wide limits, and for practical purposes can probably be neglected except when turbulence is excessive. In winds of strength above force 6 turbulence is usually so great that steep gradients of temperature and humidity are not maintained over large height intervals and the resulting duct, although intense, remains low (<20 m.) out to at least 160 km. from the coast.

The effect of the ducts usually encountered in a 'north-west' situation in daytime on radio propagation at various wavelengths is as follows:

(i) Radiation on wavelengths of 10 cm. and 3 cm. is strongly trapped in the duct to give a maximum signal at a height of 15 to 30 m. of strength ± 10 db. relative to free-space signal level up to ranges of 200 km. from the coast.

(ii) Radiation on a wavelength of 60 cm. is usually trapped to give a maximum signal at heights between 30 m. and 90 m. This signal is usually 5 to 10 db. below free-space level at a range of 100 km. and 15 to 20 db. below at a range of 200 km. There is no trapping on this wavelength when the duct height is less than about 50 m.

(iii) Radiation on a wavelength of 300 cm. suffers only partial trapping of the first propagation mode and no peak in signal strength is found in the duct.

Field strength in the diffraction region below the horizon is considerably increased by leakage from the duct. For 10 cm. and 3 cm. the field pattern in this region has a very complicated structure but seldom results in a signal strength as great as that found in the duct.

The duct has negligible effect on propagation at angles of elevation exceeding ¼°.

The presence of a local sea breeze beneath the off-shore drift increases the height of the duct locally but has very little effect on propagation at right angles to the coastline.

To sum up, the degree of trapping on microwave frequencies (3,000 Mc/s. and above) appears to vary only a little over quite a wide range of conditions. The practical result of this is that an approximate quantitative forecast of super-refraction conditions at these frequencies in a 'north-westerly' situation in Canterbury, or in other parts of the world where similar weather situations exist, may not be very difficult. Full analysis, however, especially of the meteorological data, is a task of considerable complexity, and will not be completed for a year or two.

ACKNOWLEDGMENTS

This investigation was carried out as part of the research programme of the Departments of Scientific and Industrial Research, United Kingdom and New Zealand, by whose permission this account is published.

The authors wish to acknowledge the contributions of the many members of these Departments who took part in the field observations and in the preliminary analysis work in New Zealand, and in particular the contribution of Dr. F. E. S. Alexander of Raffles College, Singapore, formerly with the Radio Development Laboratory of the Department of Scientific and Industrial Research, New Zealand, who was responsible for the initial organization of the project.

REFERENCES

Booker, H. G., and Walkinshaw, W., 1946, *Meteorological Factors in Radio Wave Propagation* (London : The Physical Society), p. 80.

Englund, C. R., Crawford, A. B., and Mumford, W. W., 1935, *Bell Syst. Tech. J.*, **14**, 369.

Katzin, M., Bauchman, R. W., and Binnian, W., 1947, *Proc. Inst. Radio Engrs., N.Y.*, **35**, 891.

Macfarlane, G. G., 1948, *Proc. Phys. Soc.*, **61**, 48.

Megaw, E. C. S., 1946, *J. Instn. Elect. Engrs.*, **93** (Pt. III A), 79.

Price, W. L., 1948, *Proc. Phys. Soc.*, **61**, 59.

Smith-Rose, R. L., and Stickland, A. C., 1946, *Meteorological Factors in Radio Wave Propagation* (London : The Physical Society), p. 18.

Report of the Physical Society and Royal Meteorological Society Conference, 1946, *Meteorological Factors in Radio Wave Propagation* (London : The Physical Society).

Summary Technical Report of the Committee on Propagation, N.D.R.C., 1946 (New York : The Academic Press Inc.).

Ionospheric Cross-Modulation: Techniques of Measurement

By C. C. NEWTON, F. J. HYDE and H. G. FOSTER
Department of Electrical Engineering, The University of Birmingham

Communicated by L. G. H. Huxley; MS. received 20th March 1950

ABSTRACT. This paper describes the techniques developed at Birmingham University to measure the amplitude and phase of the ionospheric cross-modulation observed in the test transmissions which are described in detail elsewhere. The devices which were developed and the techniques of observation employed allowed trustworthy measurements to be made with comparative ease.

§ 1. INTRODUCTION

This paper describes in detail the chief techniques that were developed by a team of observers at Birmingham for the systematic investigation of ionospheric cross-modulation (radio wave interaction).

An account of the results of this investigation has already appeared elsewhere (Huxley 1950), but no systematic description of the experimental techniques employed has been published hitherto.

As described elsewhere (Huxley, Foster and Newton 1948, Ratcliffe and Shaw 1948, Huxley 1950) the technical problem is to measure the depth of transferred modulation T_ω which is impressed at an audio frequency $\omega/2\pi$ on a radio carrier wave (the wanted wave) during its passage through the ionosphere. The modulation T_ω is in fact transferred to the previously unmodulated wanted wave within a region of the ionosphere which is irradiated by a second radio wave (the disturbing wave) which is already modulated with the tone of frequency $\omega/2\pi$ when transmitted; that is to say, cross modulation takes place from the modulated disturbing wave to the unmodulated wanted carrier wave.

Since the modulation depths T_ω are small and in practice of the order of a few per cent, special techniques were required to measure them accurately.

It was also of importance, for reasons described in the references already given, to measure the phase of the modulation T_ω relative to the modulation M_ω of the same frequency on the direct ground wave received at the point of observation from the disturbing transmitter. The retardation in phase of T_ω relative to M_ω at the same point of observation is denoted in what follows by χ_ω.

§2. MEASUREMENT OF PERCENTAGE DEPTH OF TRANSFERRED MODULATION T_ω

Figure 1 is a block diagram of the system used to measure the modulation T_ω and the phase retardation χ_ω at any frequency between 50 c/s. and 2,000 c/s.

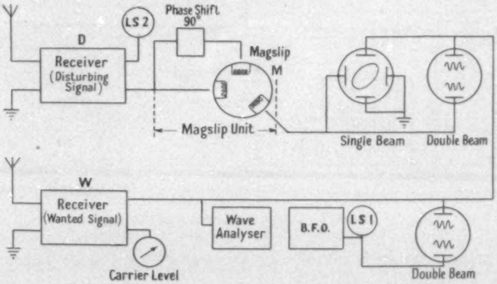

Figure 1. Block diagram of receiving system.

D and W are a pair of commercial communications receivers, tuned respectively to the disturbing and wanted waves. In each receiver the detector and audio output stages are modified. In D the detector load was changed in order that the modulation depth of 80% on the disturbing wave could be handled without distortion. The original detector and output stages of W were replaced by those shown (Figure 2) together with a built-in valve voltmeter to give the strength of the carrier of the wanted wave. The output stages in both D and W are cathode followers.

Consider the audio-frequency output from W. This is fed in parallel to a Marconi wave analyser (bandwidth 4 c/s.) and to one of the Y-terminals of a double-beam oscilloscope. To the other Y-terminal an audio-frequency voltage is applied from a beat-frequency oscillator (B.F.O., Figure 1) fitted with an output meter. Thus, with a linear time base, a pair of sinusoidal traces appears on the face of the tube.

The beat-frequency oscillator also excites a loudspeaker LS1 through an isolating amplifier, consequently the B.F.O. can be adjusted to give 'zero beat' with the tone from the loudspeaker LS2 driven by D. This is a convenient method of synchronizing the traces on the oscilloscope. The amplitudes of the two traces can be made identical by superimposing the traces and appropriately adjusting the output from the B.F.O.

The reading of the output meter of the B.F.O. provides, therefore, a relative measure of the audio signal output from W. Alternatively, the output from W may be measured directly by means of the wave analyser.

In order to obtain the absolute percentage value of the transposed modulation a preliminary overall calibration of the system is carried out by feeding into W a carrier modulated to known small percentages.

The factors by which it is necessary to multiply the B.F.O. readings or the wave analyser readings so that when they are divided by the readings of the carrier meter the absolute percentage modulations T_ω are obtained, were thus found for any modulation frequency $f = \omega/2\pi$. Under actual conditions of observation, with the normal strength of carrier, transferred modulations T_ω as small as 0·2% could be measured.

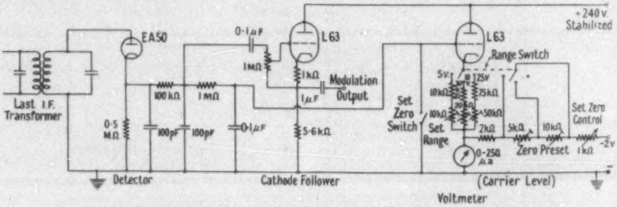

+240 V.
Stabilized
EA50
0·1 μF
L63
L63
Range Switch
1 MΩ
1 kΩ
Modulation
Output
1 μF
5 V.
125 V
10 kΩ
75 kΩ
20 kΩ
10 kΩ
50 kΩ
100 kΩ
1 MΩ
Last I.F.
Transformer
0·5 MΩ
100 pF
100 pF
0·1 μF
5·6 kΩ
Set
Zero
Switch
Set
Range
2 kΩ
5 kΩ
10 kΩ
Set Zero
Control
0-250 μa
Zero Preset
1 kΩ
-2 V
Detector
Cathode Follower
(Carrier Level)
Voltmeter

Figure 2. Detector and output units.

§ 3. MEASUREMENT OF RELATIVE PHASE RETARDATION

In order to determine the height of the mean centre of cross-modulation it is necessary to find the phase retardation of the transferred modulation at the receiver, relative to the modulation received on the ground wave from the disturbing transmitter.

The method used to measure this quantity at each frequency of $f = \omega/2\pi$ is indicated in Figure 1.

The output from the receiver D which is tuned to receive the disturbing wave excites the loudspeaker LS2, as mentioned above, but is also fed to the magslip unit. From the input voltage to this unit two alternating currents of equal amplitude but in phase quadrature are made to flow in the respective stators of a two-phase magslip. A rotating magnetic field of constant amplitude is thus excited within the magslip which induces in its rotor an electromotive force whose amplitude is independent of, but whose phase depends upon, the angular position of the rotor. The output voltage from the rotor is applied, through an amplifier, to one pair of deflecting plates of a single-beam oscilloscope. The transferred modulation T_ω from the receiver W is applied to the other pair of deflecting plates so that in general an elliptical trace appears on the face of the oscilloscope. However, by turning the rotor of the magslip the phase of the disturbing modulation from D can be continuously varied until the ellipse becomes a straight line, thus indicating phase equality of the signals. The corresponding position of the rotor is read on a scale and pointer. But in order to deduce the actual phase difference between T_ω and the disturbing modulation M_ω at the inputs to the receivers, it is necessary to know what scale reading corresponds to zero phase difference at each frequency $f=\omega/2\pi$. When this zero is known the actual phase shift is the difference between the scale reading required to give a linear trace on the oscilloscope, and the zero scale reading.

In order to find the appropriate zero at any frequency f it suffices merely to tune both receivers W and D to the disturbing wave. The rotor is turned until the trace on the oscilloscope indicates no phase difference, and the corresponding scale reading is the zero. This is done over the complete range of frequencies used in practice. A curve giving the 'zero phase' scale reading at any frequency is prepared. The advantage of this method of calibration lies in the fact that phase differences between T_ω and M_ω introduced by the circuits are automatically accounted for. In practice the calibration is done at the beginning of the set of test observations by using the disturbing wave and its modulation M_ω as a calibrating signal.

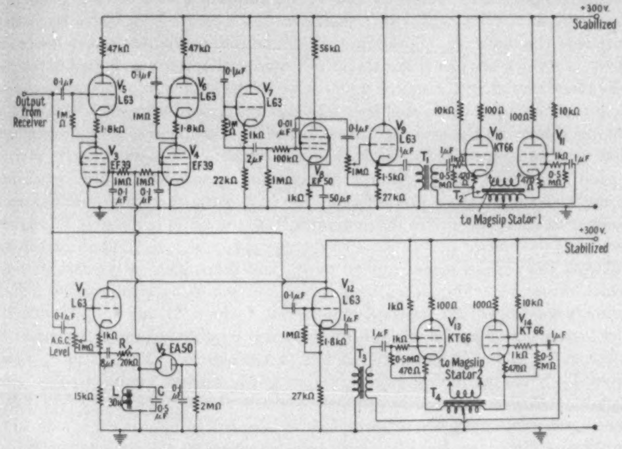
+300 V. Stabilized
47kΩ
47kΩ
56kΩ
0·1μF
Output from Receiver
V5 L63
V6 L63
V7 L63
1MΩ
1·8kΩ
V3 EF39
V4 EF39
0·01 μF
2μF
100kΩ
22kΩ
1kΩ
V8 EF50
50μF
V9 L63
1·5kΩ
27kΩ
T1
10kΩ
100Ω
V10 KT66
V11
T2
0·5 MΩ
to Magslip Stator 1
V1 L63
A.G.C. Level
R
20kΩ
8μF
V2 EA50
15kΩ
L 30H
C 0·5 μF
2MΩ
V12 L63
T3
V13 KT66
V14 KT66
470Ω
to Magslip Stator 2
T4

Figure 3. Magslip unit : detailed circuit.

It is found that as T_ω diminishes with increasing ω the elliptical display becomes masked by noise and it is preferable to phase-match a pair of sinusoidal traces using a double-beam oscilloscope with a linear time base, as shown in Figure 1.

§ 4. MAGSLIP UNIT: CIRCUIT DETAILS

The circuits incorporated in the magslip unit are shown in Figure 3.

In order to ensure that the rotating field within the magslip shall remain circular and not become elliptical as the frequency f is changed, it is necessary to keep the amplitudes of the currents in the stators equal at all frequencies f within the range used in practice.

The phase shift of 90° between the stator currents at all frequencies used was produced by means of a Miller integrator (V_8). Unfortunately, the amplitude of the output from the Miller integrator, with constant input, is inversely proportional to the frequency. To overcome this defect two procedures are obvious. A correcting network giving amplification proportional to the frequency with negligible phase shift must be introduced either before or after the integrator. In practice it was found preferable to place the network before the integrator, since in the alternative position serious hum was introduced.

The correcting network comprises valves V_1 to V_6 with their associated circuit components. Valves V_5 and V_6 are amplifiers with valves V_3 and V_4 in their cathode circuits to provide negative feedback controllable by the D.C. voltage output of the diode V_2. The input to V_2 is developed across a circuit resonant at 40 c/s., which lies just below the lowest modulation frequency used in practice. The tuned circuit L, C together with the series resistance R form a potentiometer such that the input to V_2 diminishes as the frequency increases. The negative control voltage on the grids of valves V_3 and V_4 thus decreases as the frequency rises, with consequent reduction in their A.C. resistances. Thus the gain of stages V_5 and V_6 increases in proportion to the frequency up to 1,000 c/s., after which there is slight departure from proportionality. It follows, therefore, that the signal, when it reaches the input to the integrator from the cathode follower V_7, has been amplified by a factor proportional to the signal frequency. There are now two voltages, the original signal applied to V_{12} and the voltage in quadrature with it which drives V_9. The valves V_9 and V_{12} are cathode followers which feed the primary windings of the identical step-up transformers T_1 and T_3. In order that the currents shall be the same in the primary windings of the transformers the input to the grid of V_9 is controlled by a potentiometer. The secondary voltage from T_1 drives the pair of cathode followers V_{10} and V_{11} in push-pull. These cathode followers are used to drive a current in the primary of the output step-down transformer T_2 whose secondary is coupled to one of the stators of the magslip. The other stator is driven from an identical circuit following V_{12}.

A rotating field is thus produced in the magslip which is effectively circular over the whole range of input frequencies employed.

§ 5. UNIFIED DISPLAY OF AMPLITUDE AND PHASE

With the system shown in Figure 1, amplitude and phase are found independently and thus require the presence of at least two observers. It was thought to be of interest and use to develop the system so that the amplitude–phase information is given on the face of a single oscilloscope in the form of an (r, θ) display. This object was achieved successfully by means of the system shown in Figure 4. This system is a replica of that given in Figure 1 but with the following additional units: a magslip M_2 and a switch unit S ganged to the original magslip M_1, a rectifier unit R and a single-beam cathode-ray oscilloscope. The transferred modulation T_ω from the receiver W is fed into the rotor of M_2 and induces voltages in its stators whose amplitudes are proportional to $\cos\theta$ and $\sin\theta$, where θ is the angular position of the rotor. These voltages are rectified and applied to the respective pairs of deflecting electrodes of the single beam oscilloscope, and produce a radial deflection of the spot proportional to T_ω in the direction θ. However, in order to obtain radial deflections for all directions other than those in a single quadrant it is necessary to introduce a switch unit to ensure that the

X and Y components of the displacement of the spot change sign with $\cos\theta$ and $\sin\theta$. It follows, therefore, that by suitable alignment of the rotors of M_1 and M_2, the phase setting of M_1 can be translated into the θ-deflection of the cathode-ray spot. Thus a complete (r, θ) representation of amplitude and phase is achieved. As the frequency rises T_ω diminishes, and the phase retardation χ_ω increases, consequently the spot on the cathode-ray oscilloscope follows a spiral path.

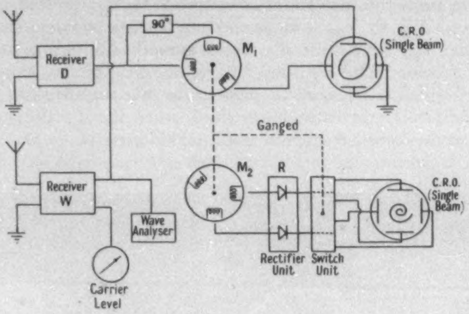
90°
C.R.O
(Single Beam)
Receiver D
M₁
Ganged
Receiver W
M₂
R
C.R.O.
(Single Beam)
Wave Analyser
Rectifier Unit
Switch Unit
Carrier Level

Figure 4. Block diagram of (r, θ) display unit.

§6. SECOND MAGSLIP, RECTIFIER AND SWITCH UNITS: CIRCUIT DETAILS

In addition to the circuits already mentioned, those shown in Figure 5 are used in the unified display.

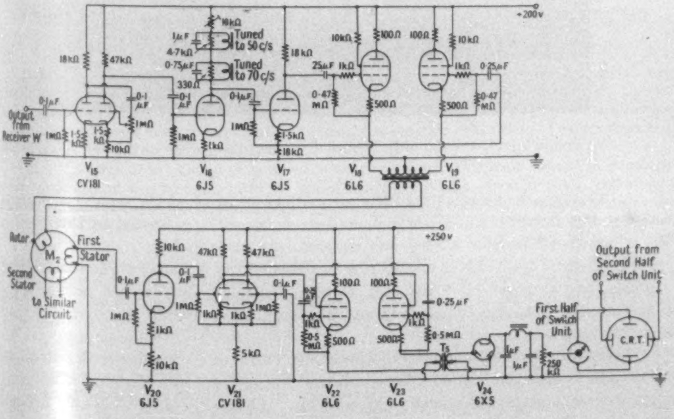
+200v
10kΩ
1µF
Tuned to 50 c/s
4·7kΩ
0·75µF
Tuned to 70 c/s
330Ω
18kΩ
47kΩ
0·1µF
0·1 µF
1MΩ
Output from Receiver W
1MΩ
1·5 kΩ
1·5 kΩ
10kΩ
0·1 µF
1MΩ
1kΩ
0·1µF
1MΩ
18kΩ
1·5kΩ
18kΩ
10kΩ
100Ω
100Ω
10kΩ
25µF
1kΩ
1kΩ
0·25µF
0·47 MΩ
500Ω
500Ω
0·47 MΩ
V₁₅ CV181
V₁₆ 6J5
V₁₇ 6J5
V₁₈ 6L6
V₁₉ 6L6
Rotor
M₂
First Stator
Second Stator
to Similar Circuit
+250v
10kΩ
47kΩ
47kΩ
0·1µF
0·1 µF
1MΩ
1kΩ
10kΩ
1MΩ
1kΩ
1kΩ
1MΩ
5kΩ
0·1µF
0·5 µF
100Ω
100Ω
0·25µF
1kΩ
1kΩ
0·5 MΩ
500Ω
500Ω
0·5MΩ
Ts
1µF
1µF
250 kΩ
First Half of Switch Unit
Output from Second Half of Switch Unit
C.R.T.
V₂₀ 6J5
V₂₁ CV181
V₂₂ 6L6
V₂₃ 6L6
V₂₄ 6X5

Figure 5. Circuit details of second magslip and rectifier units.

The amplifier, consisting of valves V_{15} and V_{19} and associated components, which is used to feed the output of receiver W into the rotor of magslip M_2, is similar in general principles to those circuits previously discussed in relation to magslip M_1. However, because of the reduced response at low frequencies of the various transformers used, it was found necessary to introduce a correcting network in order to maintain linearity between the input signal applied to the system and the subsequent D.C. voltage output from the rectifier unit. This network is shown in the anode circuit of valve V_{16}.

The output from the first stator of magslip M_2 is amplified in the circuit containing valves V_{20} to V_{23}, and applied by means of transformer T_5 to a bi-phase rectifier V_{24}, the output of which is smoothed in normal manner by the low-pass filter shown. The resulting D.C. voltage is developed across the 250 kΩ potentiometer, which is adjusted in practice to give an adequate deflection of the spot on the face of the cathode-ray tube, when the signal output from the receiver W is at the lowest frequency used in the tests.

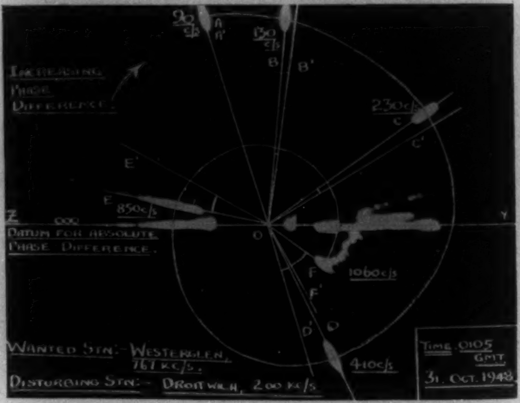

Figure 6. Photograph of (r, θ) display of ionospheric cross-modulation.

In this way, the amplitude of the D.C. voltage output of the system is proportional to the amplitude of the transferred modulation T_ω accepted by the receiver W, at any fixed angular setting θ of the rotor of magslip M_2.

The output from the second stator of magslip M_2 is fed to an identical set of circuits, and thus we have two D.C. signals whose amplitudes are each proportional to the transferred modulation T_ω, and individually to $\cos\theta$ and $\sin\theta$ respectively.

However, since the polarity of these D.C. voltages is positive with respect to earth, and is independent of θ, a switch unit in the form of a simple commutator is ganged to the rotors of magslips M_1 and M_2. One D.C. voltage, passing through one half of the switch unit, is applied to the X deflector plates of the cathode-ray tube and the other voltage similarly to the Y deflector plates. The ganging of the switch unit to the rotors of magslips M_1 and M_2 is arranged in such a way that the spot on the face of the display tube appears in the same quadrant as the angular setting of the rotors.

The performance of the system may be judged from Figure 6 which is a photographic record of an actual test transmission. In addition to the actual amplitude–phase polar record, the phase error is corrected at each frequency and the true phase angle is indicated in each case by a radial line.

It was found in practice that the straightforward technique described in §§2 and 3 was simpler to use and more flexible.

ACKNOWLEDGMENTS

The authors have pleasure in acknowledging their appreciation of the invaluable assistance given by the Engineering Research Department of the B.B.C. in providing transmission and to Messrs. H. L. Kirke and R. A. Rowden, the observers at Tatsfield and Caversham and the engineers at the transmitters in particular.

They are also indebted to Professor A. Tustin for encouragement.

They finally wish to record their appreciation of the general guidance throughout the work given by Dr. L. G. H. Huxley who suggested some of the techniques which the authors were able to develop.

REFERENCES

Huxley, L. G. H., 1950, *Proc. Roy. Soc.* A, **200,** 486.
Huxley, L. G. H., Foster, H. G., and Newton, C. C., 1948, *Proc. Phys. Soc.*, **61,** 134.
Ratcliffe, J. A., and Shaw, I. J., 1948, *Proc. Roy. Soc.* A, **193,** 311.

LETTERS TO THE EDITOR

The Measurement of Microwave Power at Wavelengths of 3 cm. and 10 cm.

Collard, Nicoll and Lines (1950) have recently pointed out that large discrepancies may occur in the measurement of microwave power at wavelengths below 3 cm. using thermistor milliwattmeters. In this note we wish to give a preliminary report of microwave power measurements recently carried out here on the absolute calibration of milliwattmeters for operation in the 3 cm. and 10 cm. wave bands.

The apparatus used in the measurements for both wavebands were similar in principle and consisted of a generator, either a pulse magnetron or a klystron (both capable of delivering mean powers of the order tens of watts into a matched load), connected to a waveguide run. The latter was terminated in a matched wedge constant flow calorimeter, and a waveguide Bethe single-hole directional coupler was inserted between the generator and calorimeter. Thus, if the power entering the calorimeter is determined and the fraction of the power abstracted by the directional coupler (coupling factor) is known, the absolute power delivered into a milliwattmeter matched to the low power guide of the directional coupler may be calculated. The coupling factors of the directional couplers were about 44 db., as determined by a piston attenuator of accurately known characteristics, and hence for a dissipation of 25 watts in the calorimeter the power delivered to the milliwattmeter was about 1 milliwatt in each case.

The milliwattmeters used in the experiments were :

(i) 10 *cm. band.* A thermistor head designed by R. C. Robbins at R.R.D.E.; a short description of this instrument has already been published (Street 1949).

(ii) 3 *cm. band.* A.S.R.E. thermistors, with ceramic protective tubes, incorporated into a T.R.E. design of waveguide thermistor mount.

(iii) 3 *cm. band.* Sperry type 821 barretter capsule in a type 82X mount (Montgomery 1947).

All the instruments were standardized by D.C., and the results of calibration are given in the following table :

Milliwattmeter type	(i)	(ii)	(iii)
Ratio of $\dfrac{\text{Absolute power}}{\text{Indicated power}}$	1·04	1·10	1·04*

* This result was obtained by comparing the power indications of instruments (ii) and (iii) at a level of 1 milliwatt of C.W. power in order to avoid the possibility of burn-out of the barretter by peak pulse power.

It is estimated that the accuracy of this method of calibration is within approximately 2 per cent. Further experiments showed that the reproducibility of milliwattmeter readings was 2–3 per cent for type (ii) milliwattmeters when different samples of thermistor were incorporated in the same mount. From these measurements it appears that there is no significant difference between the absolute power input and the powers indicated by milliwattmeters (i) and (iii). However, the readings of milliwattmeters of type (ii) may be in error by about −10 per cent. Further details of this work will be published at a later date.

Acknowledgment is made to the Chief Scientist, Ministry of Supply, for permission to publish. Thanks are also due to the Chief Superintendent, Radar Research and Development Establishment, for the provision of essential apparatus.

The University,
Nottingham.
1st June 1950.

R. Street.
P. D. Whitaker.

Collard, J., Nicoll, G. R., and Lines, A. W., 1950, *Proc. Phys. Soc.* B, **63,** 215.
Montgomery, C. G., 1947, *Technique of Microwave Measurements* (New York and London: McGraw-Hill), Chap. 3.
Street, R., 1949, *Proc. Instn. Elect. Engrs.*, **96,** Pt. II, 391.

Photoconductive Cells of Cadmium Selenide

Polycrystalline layers of CdSe have been produced by methods previously described (Schwarz 1948). These cells exhibit an appreciable sensitivity for electromagnetic radiation within a range starting from the X-ray region, covering the Schumann, ultra-violet and visible region and extending into the near infra-red. The spectral distribution of sensitivity at room temperature for the visible, near ultra-violet and infra-red is given in Figure 1 for different voltages across a cell with a sensitive area of 0·2 mm. × 10 mm. There is a sharp drop of sensitivity after the maximum at approximately 0·72 μ. The position of the maximum varies somewhat for different cells.

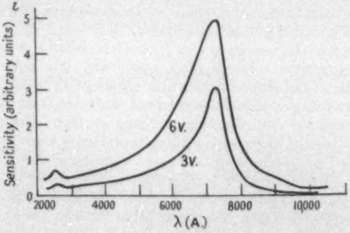

Figure 1.

The sensitivity of a cell with a sensitive area of 10 mm. × 0·2 mm. to the radiation of a tungsten filament lamp operated at a colour temperature of 2,850° K. has been measured by the National Physical Laboratory with the following results :

Illumination (lumens/m^2)	2·15	21·5	215
P.D. across cell (volts)	12	12	12
Cell current (μa.)	21·6	365	2800
Cell current per lumen (amp/lumen)	5·0	8·5	6·5

The dark current of the cell for a potential difference of 12 volts was less than 0·2 μa. The dark resistance of the cells can be varied within very wide limits and may be as high as 10^{10} ohms at room temperature.

The response of a cell to X-rays from a Cu anode for different electron currents I, voltages E and cell distances from the anode d are shown in Figures 2 and 3. The photocurrent i in microamps was measured for a field of 1,100 v/cm. across the cell.

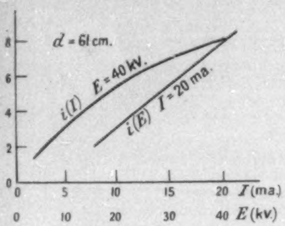

Figure 2.

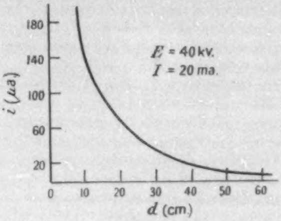

Figure 3.

Preliminary speed measurements indicate that cells with extremely high D.C. sensitivities are relatively slow, as would be expected. At a chopping frequency of 200 c/s. for the light from a tungsten lamp the output may drop to one third or one fourth of the D.C. value, but there seems to be a strong dependence of the speed on light intensity and applied voltage. As, on the other hand, it has been possible to minimize slow, secondary effects (fatigue and creep) to a very small fraction of the photocurrent, these cells should prove of great practical importance for D.C. measurements.

Contrary to the method for the production of photoconductive single crystals of CdS and CdSe (Frerichs 1946) the methods used here involve the application of oxygen and it has been found that all the properties of the cell are governed by the amount and form of oxygen present in the layer. It has been suggested (Schwarz 1949) that adsorption of oxygen on the grain boundaries is one essential condition for the production of photocells with a high quantum yield and the experiments on CdSe strongly support this view. This matter will be discussed in detail elsewhere.

I would like to thank Mr. C. G. Cannon, University of Reading, for help with measurements in the Schumann region, Mr. J. H. Pratt, Services Electronics Research Laboratories, Baldock, for speed measurements, and Hilger and Watts Ltd. for permission to publish this letter.

Hilger and Watts Ltd.
98 St. Pancras Way,
Camden Town, N.W. 1.
8th June 1950.

E. SCHWARZ.

FRERICHS, R., 1946, *Naturwissenschaften*, **33**, 281.
SCHWARZ, E., 1948, *Nature, Lond.*, **162**, 614; 1949, *Proc. Phys. Soc.* A, **62**, 530.

REVIEWS OF BOOKS

Gas Tables, by JOSEPH H. KEENAN and JOSEPH KAYE. Pp. x+238. 2nd Edition. (New York: John Wiley and Sons, Inc.; London: Chapman and Hall, Ltd., 1948). 30*s*. (Published in 1945 under the title *Thermodynamic Properties of Air, including Polytropic Functions*.)

These tables are intended to do for the engineer using air or similar gases what the Steam Tables do for the steam engineer. By assuming air, or the products of combustion, to be gases which obey the law $pV = \boldsymbol{R}T$, the tables are greatly simplified, for the enthalpy and internal energy are then functions of one variable only, and the ratio of volumes at two temperatures along an adiabatic is the same whatever adiabatic is selected. Instead, therefore, of a table of double entry as used in steam engineering, a table of single entry can give volume ratio and the fundamental thermal properties. The error so introduced is discussed on pages 203 to 204.

The tables are a revision of *Thermodynamic Properties of Air* by the same authors. The thermal properties are based on spectroscopic data, using absolute zero as the zero for energies, and adopting the latest values for the gas constant, the velocity of light and the value of the international joule in absolute units.

The tables, 64 in number, are designed to cover the conditions and to give directly the quantities needed for turbine calculations and for jet design work. They include a table for air, others for products with various quantities of excess air, for hydrogen, hydrocarbons, carbon monoxide and argon. Other tables deal with conditions along a Rayleigh line or a Fanno line, with different values of the polytropic index, and yet others are purely mathmatical tables (log N, and fractional powers). The whole collection should be of great value to technologists in this field.

J. H. A.

A Manual of Vacuum Practice, by L. H. MARTIN and R. D. HILL. Pp. 82+34, Appendix. 1st Edition. (Melbourne: University Press, 1947; British Agents: Cambridge University Press.) 10*s*. 6*d*.

This little volume is probably the best of the manuals and handbooks on vacuum technique which have been offered to us. It omits the detailed discussion of kinetic theory principles which can be found in the standard textbooks on the subject and presents them in a form immediately useful for the calculation of vacuum systems. The theory underlying the various types of pump and gauge is sketched and profuse references to papers and textbooks are given (95 in all).

In chapter 1, the kinetic theory formulae relating to molecular flow etc. are given, with some examples of how to calculate the types of pump, sizes of piping etc. required in actual vacuum systems, including consideration of what happens when a burst of gas is released. Chapter 2 describes the various types of pressure gauge and includes a note on the difficulties and errors in the use of the ionization gauge which have recently come into prominence. Chapter 3 is devoted to pumps and the characteristics of a number of modern rotary and diffusion pumps are illustrated. The importance of keeping water out of oil diffusion pumps—an important practical point—is mentioned. The final chapter is on vacuum plumbing; various types of rubber-sealed valves are described, also the Wilson seal for transmitting motion into a vacuum system, dimensions for various shaft sizes being given. Leak finding is discussed, including the use of the palladium ionization gauge.

The 18 appendices contain information about the properties of various substances used in vacuum work, including getters. There are also descriptions of the manufacture of copper-to-glass sales and wire seals through glass and silica.

No misprints of any importance were detected in the book, which can be recommended to students of physics and those engaged in the " vacuum consuming " industry.

M. D. ARMITAGE.

Tables of Sines and Cosines to Fifteen Decimal Places at Hundredths of a Degree, NATIONAL BUREAU OF STANDARDS, APPLIED MATHEMATICS LABORATORY. Pp. viii+95. (Washington: U.S. Government Printing Office, 1949.) $0.40.

Of the three systems for measuring angles (the radian, the degree with sexagesimal sub-division and the degree with decimal subdivision), sometimes one and sometimes another is the favourite of the table maker. For many years, when 8 or less figures were wanted, the degree, minute and second were much better catered for than were the others, though now they are all properly tabulated at convenient intervals in easily accessible volumes.

When we turn to many-figure tables, however, the position is somewhat different, and it appears that there has been no table in degrees and decimals for more than 10 figures since the pioneer work of Briggs, in 1633. He gave 15 decimals, at intervals of 0·01°, and his work has now been repeated by the Mathematical Tables Project. They have recalculated the values at each degree, using 25 decimals, have sub-tabulated to obtain the values at 0·01° and then sub-tabulated these. This gave a draft to 18 decimal places, which was checked by differencing, and then rounded off and checked again by differencing. It would appear that the volume is printed from this typescript by a photographic method, thus avoiding the possibility of errors by compositors. There is no suggestion that the final table has been read against Briggs's table, in which the only known error is at 16·49°.

Linear interpolation in these tables can be relied on everywhere for 8 decimals, and second differences suffice for full accuracy. These differences are tabulated opposite every entry, and the coefficients required in Everett's formula are given in a supplementary table. Inverse interpolation can be effected either by taking arc sin x from tables of that quantity, and then converting to degrees, or by any of three methods explained in the Introduction to the present tables.

There is a supplementary table of $\sin x$ to 30 decimals, at intervals of 1°. This was computed by Herrmann, who gave also a table of tangents ; for the present volume, his values have been checked by the relation $\cos x \tan x = \sin x$ and by the formula

$$\sin 1^\circ (1 + 2\Sigma_1^{89} \sin x^\circ) = 1 + \cos 1^\circ .$$

The tables are bound in stiff paper, and owners will probably think it worth while to have them properly bound.

J. H. A.

Surface Tension and the Spreading of Liquids, by R. S. BURDON. Pp. xiv+92. Cambridge Monographs on Physics. 2nd Edition. (Cambridge: University Press, 1949.) 12*s*. 6*d*.

The first appearance of Dr. Burdon's book on Surface Tension in 1940, as one volume of the series of Cambridge Physical Tracts, was a healthy reminder that in one branch at least of classical physics considerable progress is still taking place, and that the spirit of novelty is far from dead. In the original monograph we were reminded of many points of interest which are frequently glossed over in the standard treatises on the general properties of matter ; and it must have been with considerable surprise that many readers learnt of the scantiness of our exact knowledge of such an apparently straightforward matter as the surface tension of mercury. All this was very much to the good, as it necessarily stimulated interest in a branch of physics which is an admirable subject of research for many of those to whom the elaborate and expensive apparatus associated with some other branches of physics is quite prohibitive.

Now, in the second edition, we have a complete revision of the original book, attractively presented in a cloth binding, albeit at a somewhat increased price. The chapter on the measurement of surface tension has been expanded to include some account of the measurement of small differences in tension. Greater attention is given in the new edition to the effects of adsorption and surface contamination ; and progress is noted in the exact measurement of the surface tension of mercury. On the subject of the spreading of liquids on solid and liquid surfaces, Dr. Burdon's account, which forms a large part of the book, is the most comprehensive up-to-date treatment which is available to the English reader. This section, like others, has been fully revised and now includes a short section on the effect of surface films in inhibiting evaporation from water. The section on angles of contact has been expanded to include reference to the newer methods of measurement, and Bate's observation of a 90° angle of contact between glass and carefully prepared mercury is recorded in the appropriate section. It is perhaps only right to say, however, that our knowledge of the angles of contact of liquid metals is still very scanty, and that real progress is possible only when the less subjective methods of observation are applied under conditions in which the degree of surface contamination is properly controlled.

Altogether, Dr. Burdon's book is a valuable contribution to the literature of what is still, unfortunately, known as classical physics, and in its new edition should be of even greater value both to the University student and to the industrial physicist who is concerned with the practical solution of the problem of wetting. G. D. YARNOLD.

Elements of Aerodynamics of Supersonic Flows, by A. FERRI. Pp. x + 434. 1st Edition. (New York: The Macmillan Co., 1949.) 50*s*.

The aerodynamic theory of supersonic flow is receiving so much attention at the present time and being developed so rapidly that any book purporting to be up to date when written is inevitably no longer so by the time it gets published. Through no fault of the author this is to some extent true in this particular case as, during the past two years, many important advances have been made which are not even mentioned in the book. In this connection readers in this country will note with some surprise the unfortunate lack of references to recent British work. However, the book as a whole is a valuable addition to the literature on the aerodynamics of supersonic flows and makes a useful introduction to the subject. It discusses in detail the fundamental principles involved and the assumptions made in the development of the theory. The various problems considered are treated in a manner that is easily understood, and the material is presented clearly and concisely. In the main the book is written from the engineer's point of view rather than that of the mathematician, and it should be of great value to aeronautical engineers and designers who are concerned mainly with practical applications of the theory of supersonic flow.

Chapter 1 considers in general the basic equations of the flow and the physical nature of the phenomena associated with bodies moving faster than sound. In the following four chapters the theory of two-dimensional flow for small disturbances, the theory of shock waves and the theory of characteristics for rotational as well as irrotational flow are discussed.

Chaptef 6 deals with the techniques used for measuring the physical quantities associated with supersonic flow, and a brief account is given of the principles involved in the use of the interferometric, the shadowgraph, and the schlieren methods for investigating density variations.

Various applications of the theories developed in the earlier chapters are given in Chapter 7. Pressure distributions on supersonic profiles of different shapes are determined and comparisons are made between theoretical and experimental results. The influence of viscosity, which is neglected in the theory, and effects due to the presence of boundary layers are also discussed. This chapter concludes with an account of the Buseman biplane and the basic ideas of its design.

The problems which arise in the design of effusors and diffusors are discussed in some detail in Chapters 8 and 9. Numerical examples are included to illustrate the methods of design described.

After giving an outline of the theory of supersonic flow in three dimensions in Chapter 10, the author proceeds to discuss in the next three chapters problems connected mainly with axially symmetric flow and particularly those associated with flow past bodies of revolution. Numerical examples are given of some of the cases considered, and these should form a useful guide to the application of the theory to the calculation of actual flows.

The last two chapters deal with the determination of the pressure distributions and aerodynamic forces on wings of various plan forms.

Tables which are useful in supersonic flow investigations are included at the end of the book, the value $\gamma = 1{\cdot}40$ being assumed. W. P. JONES.

CONTENTS FOR SECTION A

PAGE

Prof. G. I. Finch. The Sliding Surface (34th Guthrie Lecture) 785

Dr. P. Torkington. The Planar Vibrations of Tetra-chloro-ethylene: an Example of a Complete Normal Coordinate Analysis 804

Miss A. J. Buzeman. The Electronic Structure and the Bond Lengths of Ovalene. 827

Dr. H. Kuhn and Mr. G. K. Woodgate. Hyperfine Structure and Nuclear Spin of Yttrium, ${}^{89}_{39}$Y 830

Dr. J. R. Holt and Mr. C. T. Young. The Angular Distribution of Protons from the Reaction ^{27}Al (d, p) ^{28}Al 833

Mr. R. W. Parsons and Mr. C. H. Collie. Photodisintegration of the Heavy Elements 839

Dr. S. C. Curran, Mr. A. L. Cockroft and Mr. G. M. Insch. Gamma and Beta Ray Spectroscopy with Proportional Counters in Magnetic Fields . . 845

Dr. H. Lawton and Dr. K. H. Stewart. Magnetization Curves for Polycrystalline Ferromagnetics 848

Mr. D. A. Richards. Magnetite Inclusions in Mica 852

Dr. V. Appapillai and Prof. A. W. Mailvaganam. Transition Effect of Extensive and Local Penetrating Cosmic-Ray Showers in Colombo 856

Mr. Alladi Ramakrishnan. A Note on the Size–Frequency Distribution of Penetrating Showers 861

Mr. D. Broadbent, Dr. E. W. Kellermann and Mr. M. A. Hakeem. The Density Spectrum and Structure of Extensive Cosmic-Ray Air Showers at Sea Level 864

Mr. S. L. Martin, Dr. E. H. S. Burhop, Mr. C. B. Alcock and Dr. R. L. F. Boyd. The Scattering of Neutrons by Deuterons 884

Dr. F. C. Barker. Schwinger Potential in Nuclear Forces 898

Mr. D. V. Osborne. The Rotation of Liquid Helium II 909

Letters to the Editor:

Dr. M. Blackman and Mr. V. F. G. Tull. On the Inner Potential of Metals. 913

Mr. L. E. Beghian, Mr. M. A. Grace and Dr. H. Halban. The ^{11}B (α, n) ^{14}N Reaction 913

Mr. R. W. Parsons, Mr. D. J. Lees and Mr. C. H. Collie. The Photo Threshold of ^{208}Pb 915

Mr. E. W. Titterton. The Photodisintegrations ^{6}Li$(\gamma D)^{4}$He and ^{7}Li$(\gamma T)^{4}$He 915

Prof. M. A. Catalán and Mr. R. Velasco. Unequal g-Values for the Different Magnetic Levels of an Atomic Energy Level 917

Mr. H. D. Rathgeber. The Semi-Diurnal Variations of Atmospheric Pressure and of Cosmic-Ray Intensity 920

Mr. C. D. Mee. The Mechanism of Colloid Agglomeration in the Formation of Bitter Patterns 922

Contents for Section B 923

Abstracts for Section B 923

ABSTRACTS FOR SECTION A

The Sliding Surface (34th Guthrie Lecture), by G. I. Finch.

The Planar Vibrations of Tetra-chloro-ethylene: an Example of a Complete Normal Coordinate Analysis, by P. Torkington.

ABSTRACT. A normal coordinate analysis of the planar vibrations of tetra-chloroethylene is carried out. For the B_{1g}, B_{2u} and B_{3u} modes the analysis is complete, including the calculation of the coefficients in the transformation to normal coordinates, the components in the displacements, the directions of the displacement vectors and the distribution of the potential energy, as well as the force constants, for a range of solutions; in each case, two alternative assignments are employed. For the A_g vibrations, several ranges of possible solutions are obtained. Curves are given in every case, and corrections for variable structural parameters calculated for selected solutions. The results for the various symmetry classes are discussed and correlated, and the most likely set of force constants in the valence-force potential function deduced. Details of the method of analysis are given.

The Electronic Structure and the Bond Lengths of Ovalene, by A. J. Buzeman.

ABSTRACT. The method of molecular orbitals has been applied to find the bond orders and the bond lengths of ovalene $C_{32}H_{14}$.

A comparison with the preliminary experimental values of Donaldson and Robertson shows general agreement.

Hyperfine Structure and Nuclear Spin of Yttrium, $^{89}_{39}Y$, by H. Kuhn and G. K. Woodgate.

ABSTRACT. By the use of a liquid-air-cooled hollow-cathode tube with very low current densities it was possible to resolve hyperfine structure in the arc spectrum of yttrium. The value of the nuclear spin was found to be $I=\frac{1}{2}$ and the sign of the magnetic moment to be negative. This agrees with recent results of Crawford and Olson, who determined the nuclear spin from the intensity ratio of a hyperfine-structure doublet in the second spark spectrum of yttrium.

The Angular Distribution of Protons from the Reaction $^{27}Al(d, p)^{28}Al$, by J. R. Holt and C. T. Young.

ABSTRACT. Experiments are described in which a differential ionization chamber was used in the measurement of angular distributions of disintegration particles. Results are given for seven groups of protons from the (d, p) reaction with aluminium in which deuterons having energies of 4·6, 5·8 and 7·5 Mev. were used. The distribution curves are of complicated form, with a general tendency for the protons to be emitted in the forward direction.

Photodisintegration of the Heavy Elements, by R. W. Parsons and C. H. Collie.

ABSTRACT. The photo thresholds for the emission of neutrons by the following elements have been determined. The threshold in Mv. is given in the brackets following the symbol: Pt (6·1±0·1); Au (8·1±0·1); Hg (6·6±0·2); Tl (7·3±0·25); Pb (6·9±0·1); Bi (7·2±0·1); Th (6·0±0·15); U (5·8±0·15).

The neutrons were detected by the Szilard and Chalmers method of chemical concentration and the γ-rays obtained from a small betatron. Rough values of the total cross sections can be estimated from the results.

Gamma and Beta Ray Spectroscopy with Proportional Counters in Magnetic Fields, by S. C. Curran, A. L. Cockroft and G. M. Insch.

ABSTRACT. Proportional counters operating in a ' condensing ' type of magnetic field can be used as β- or γ-ray spectrometers up to at least 2 Mev. Results for P32 and annihilation γ-radiation are given.

Magnetization Curves for Polycrystalline Ferromagnetics, by H. Lawton and K. H. Stewart.

ABSTRACT. Recently described developments have led to greatly improved agreement between theory and experiment for the magnetization curves of single crystals of iron and iron–silicon in the region where magnetization proceeds by rotation of domain vectors against the action of magnetocrystalline forces, i.e. in the range 10–500 oersteds. On the basis of the assumption that in polycrystalline material the magnetization is approximately uniform from grain to grain, which is rendered plausible by consideration of internal demagnetizing effects, a method is developed for deriving the magnetization curves of such material by averaging the fields required to produce a given magnetization in the different constituent grains, rather than by averaging the magnetizations produced in the different grains by a given field. The application of this method to specimens with known distributions of grain orientations is shown to give results in fair agreement with experiment.

Magnetite Inclusions in Mica, by D. A. Richards.

ABSTRACT. The paper describes the investigation of the orientation of magnetite inclusions in mica using electron diffraction by transmission through composite films. The diffraction pattern obtained indicates that the magnetite is a single crystal with its (111) planes parallel to the cleavage plane of mica and one of the face diagonals parallel to the *b* axis of mica. The technique for preparing the thin films is described in some detail.

Transition Effect of Extensive and Local Penetrating Cosmic-Ray Showers in Colombo, by V. Appapillai and A. W. Mailvaganam.

ABSTRACT. An account is given of the experiments on the transition effects of local and extensive penetrating cosmic-ray showers at Colombo (geomagnetic latitude 4° S.). A comparison of the present results with those reported for higher latitudes indicates that there is no observable latitude effect of the local penetrating showers. Contrary to the findings of Broadbent and Jánossy, the transition effect of the extensive showers in paraffin appears comparable in magnitude with the effect in lead.

A Note on the Size–Frequency Distribution of Penetrating Showers, by Alladi Ramakrishnan.

ABSTRACT. Heitler and Jánossy have calculated the probability that n mesons are produced due to nucleon–nucleon collisions by a fast nucleon in its passage through matter of a given thickness. In this note the results of Heitler and Jánossy are obtained by the direct method of writing the integro-differential equations of the problem using the Markoff nature of the process.

The Density Spectrum and Structure of Extensive Cosmic-Ray Air Showers at Sea Level, by D. Broadbent, E. W. Kellermann and M. A. Hakeem.

ABSTRACT. Showers have been examined in the density range 5–500 particles/m^2 using two trays of Geiger counters 5 m. apart, the discharges of individual counters being recorded using neon lamps. The observed showers are compared with a theoretical analysis based on the usual assumptions that the incident densities are uniform over the extent of the apparatus and distributed according to the spectrum $N(x)=Bx^{-\gamma}$ per hr. per m^2. The comparison shows (i) that in the density range examined the above spectrum applies only for a vanishingly small area of observation, with $\gamma=1{\cdot}425\pm0{\cdot}022$, $B=620$, and with no evidence for a change of γ with density, and (ii) that for the separation of 5 m. employed, the density can *not* be regarded as uniform over the extent of the apparatus. It is shown that this second conclusion is capable of explaining many of the differences found between the results of other authors obtained on the assumption of uniformity of density: in particular, it is concluded that there is yet no significant evidence for a change of γ with altitude.

The Scattering of Neutrons by Deuterons, by S. L. Martin, E. H. S. Burhop, C. B. Alcock and R. L. F. Boyd.

ABSTRACT. The photographic plate method has been used to investigate the angular distribution of deuterons recoiling after neutron impact. The deuteron recoils were produced in a thin target of heavy wax placed in contact with a C2 Ilford nuclear emulsion.

For neutrons of energy 2·6–3·1 MEV., produced in the d–d reaction, 2,000 deuteron recoils were measured. Owing to the short range of the recoils produced when neutrons of low energy are scattered through small angles, the technique is only applicable to the study of the angular distribution in the range 90°–180° in the centre-of-mass system. For angles between 120° and 180° the results of the present work are in satisfactory agreement with those of previous experimenters using different methods, and they agree with the theoretical form of the distribution calculated by Buckingham and Massey on the assumption of ordinary forces between nucleons. This agreement is not decisive, however, since in this region the calculated distributions for ordinary and exchange forces do not lie far apart. For smaller scattering angles where a decisive test could have been made, the method is too inaccurate.

For neutrons of energy from 4·0 to 6·0 MEV. and from 6·0 to 9·0 MEV., obtained from a Ra–Be source, the angular distribution over a much larger range of scattering angle has been obtained from the measurement of 1,200 deuteron recoils. The angular distribution for neutrons scattered through angles near 180° appears to be rather steeper than for slower neutrons; but the ratio of the differential cross section at 90° to that at 180° is found to be about 0·35–0·40, of the same order as for neutrons in the lower energy range.

Measurements of 1,000 proton recoils from the d–d neutrons showed an angular distribution for neutron scattering angles between 90° and 180° that was constant within the limits of the statistical error.

Schwinger Potential in Nuclear Forces, by F. C. Barker.

ABSTRACT. The properties of the potential derived from the mixed pseudoscalar–vector meson field are investigated and compared with the experimental data on the two-nucleon system. An attempt has been made to use methods which are more accurate than those formerly applied to this problem, and some of these may be useful in calculations with other potentials. It is found that agreement with experiment cannot be obtained for any choice of meson masses and coupling constants.

The Rotation of Liquid Helium II, by D. V. Osborne.

ABSTRACT. An experiment is described in which the free surface of rotating liquid helium II is studied. It is shown that the results, which are the same as for any ordinary liquid, are not in accordance with the hypothesis that the superfluid component remains stationary. On this basis an estimate of the critical velocity for superfluidity is made and is compared with previous determinations.